Západočeská univerzita v Plzni
Fakulta aplikovaných věd

Molekulární motory a Maxwellův démon

Ing. Milada Krejčová

Disertační práce
k získání akademického titulu doktor
v oboru Aplikované mechaniky

Školitel: doc. Dr. RNDr. Miroslav Holeček
Katedra Mechaniky

Plzeň 2021

University of West Bohemia in Pilsen
Faculty of Applied Sciences

Molecular motors and Maxwell's demon

Ing. Milada Krejčová

Disertation thesis
to obtain academic title doctor
in the field of the Applied mechanics

Supervisor: doc. Dr. RNDr. Miroslav Holeček
Department of Mechanics

Pilsen 2021

Acknowledgements

I was supported by the project LO1506 of the Czech Ministry of Education, Youth and Sports, SGS-2013-036, SGS-2016-038, SGS-2016-059, SGS-2019-002. I also want to thank my supervisors doc. Dr. RNDr. Miroslav Holeček and prof. Ing. Josef Rosenberg, DrSc. for their guidance and advice. Moreover, I want to thank dr. hab. Przemysław Chełminiak and prof. dr hab. Michał Kurzyński for their help with the demon during my stay in Poznan, Poland, via the Erasmus+ programme.

Affidavit

I affirm that this dissertation thesis represents my own written work and used no sources and aids other than those indicated. All passages quoted from publications or paraphrased from these sources are appropriately cited and attributed.

Date	Signature

Abstract

My presented dissertation thesis aims to show possibilities and the usage of statistical physics in biomechanics, especially for modelling a muscle on a molecular level (myosin II molecular motor) and its connection to the so-called Maxwell's demon. In the model, I use the Fokker-Planck equation with the Wang-Peskin-Elston algorithm for solving partial differential equations, which approximates the Markovian chain in the spatial variable. I compare The WPE algorithm to the corresponding analytical solution in two cases - the stationary Fokker-Plank equation and the diffusion equation. Then, I create a three-state model depending on ATP concentration and simulate the myosin head behaviour. The most important results are the molecular motor's velocity and simulation of measurement, which imitates Maxwell's demon's behaviour. The measurement procedure calculates the production of relative entropy and mutual information. All source codes are written in MATLAB software.

Key words

statistical physics, Maxwell's demon, theory of information, thermodynamics, biomechanics, molecular motors, Fokker-Planck equation, WPE algorithm, three-state model, condensation of states, myosin head velocity, simulation of measurement.

Contents

List of Figures

List of Tables

Part I

Introduction

Chapter 1

Introduction

The topic of the presented thesis concerns muscle mechanics at the microscopic level. The head of myosin II is the main object of the thesis. Myosin is a member of a superfamily of linear molecular motors [35, 78]. Its main task is muscle contraction. Myosin filaments create a thick muscle filament [3].

These molecular motors belong among nano-systems. Thus, the myosin head executes Brownian motion – it undergoes thermal fluctuations [82]. These neverending fluctuations produce unpredictable movement.

A biological system modelling requires some assumptions and simplifications. Concerning muscle modelling, some pure mechanical models exist. Hill's model is the most well-known one or its enhancement called Huxley's model [107] or Hai-Murphy's model [81].

These models are based on classical mechanics and omit thermal fluctuations and random character of the environment as if they were macro-systems. At the nanoscale, however, the system behaves differently due to random thermal fluctuations. Thus, it is essential to include them in the model of myosin. It is the reason for using a statistical description of the myosin head movement.

The statistical description used in the thesis combines a mechanical approach and a chemical one (see Figure 1.1). In my model, effective potentials describe the mechanical aspects of behaviour. The chemical features are characterised by transition rates between discrete states of the head and the form of the effective potentials as well [44]. Many authors, e.g. [16, 136], use this statistical description of the myosin dynamics. Cited authors use a system with an even number of myosin states (especially two). These articles inspire my model, but it works with three states for the myosin head description (like in [27]). On the contrary, my model does not primarily aim to study mechanical properties, like in these papers. It mainly analyses information-theoretical aspects.

In reality, myosin functionality belongs to physiological processes. Myosin consumes ATP (adenosine triphosphate) molecule and converts its energy to mechanical work with producing ADP (adenosine diphosphate) molecule. The movement of myosin is regulated in many ways, such as phosphorylation, autoinhibition, divalent cations, or actin-linked regulation [37]. The whole process is very complex and depends on the type of muscle where the studied myosin is [84]. In my dissertation thesis, I focus on skeletal muscles and the influence of ATP concentration.

In 2016, a dissertation thesis was defended at the Department of Mechanics Faculty of Applied sciences, which is focused on modelling muscles as well [139]. However, that thesis is more devoted

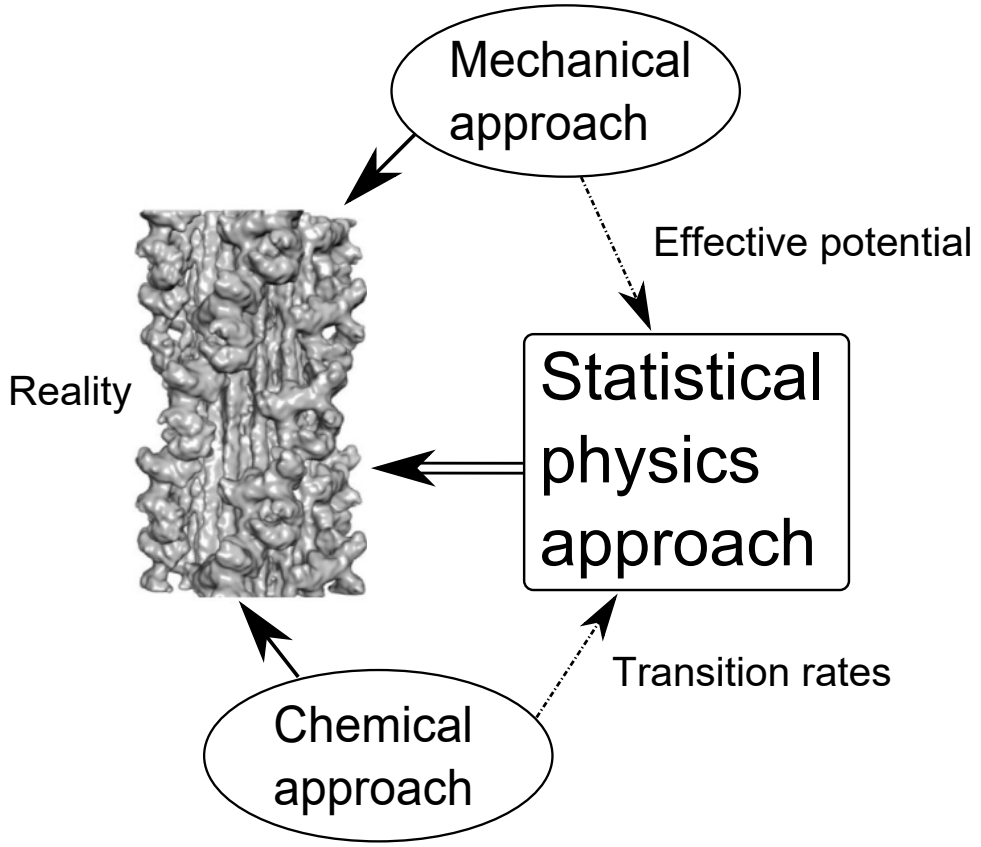

Figure 1.1: Reality and its possible approaches to describe it. The figure of a real muscle filament is taken from [135]. It is tarantula (spider) thick muscle filament under 3D cryo-electron microscope. The statistical physics approach is connected to mechanical approach (via effective potentials) and to chemical approach (via transition rates of chemical reactions).

to pure biomechanical modelling (three filament model of cross-bridge) than mine, where I omit the presence of the titin filament in the model.

The idea of Maxwell's demon inspired my thesis. This metaphorical "being" represents an effective controlling process at the molecular level. Information is the keyword in this topic [72]. In physics, Shannon's meaning of entropy quantifies information. Similarly, in my work, I focus on the connection among mechano-chemical processes, information fluxes, and gains corresponding to their control.

The work has several parts. The first part is a summary of the recent state-of-art. In Chapter 2 is the biological background. The chapter describes molecular motors, especially myosin II and their significance to muscle contractions. As an impressive illustration, there is a narrative of the latest achievements in Nobel prices given in studying nanomachines.

In Chapter 3, there is a rapid overview of the statistical and information theory. Several sections have a key role in the rest of the thesis. They are

- 3.4.3 – describing the Fokker-Planck equation using for the myosin head movement description,
- 3.4.4 – describing information which is a quite important physical quantity for Maxwell's demon concept,

- 3.4.4 – describing Maxwell's demon itself and its history and recent progress in this field.

The second part is about the main objectives and crucial hypotheses of the thesis.

In the third part, the methodology used in the model is described. Chapter 5 contains an analytical solution of simplified versions of the Fokker-Planck equation. It serves as an initial verification of the model. The chapter is closely connected to Chapter 10. Chapter 6 is devoted to the used algorithm for the Fokker-Planck equation's spatial solution. It is not an original algorithm. The procedure was taken from [132]. Chapter 7 focuses on a description of the three-state model originally used by [27]. However, this approach to the myosin head was applied to a different set of equations, not to the Fokker-Planck one used here.

Chapter 8 describes the condensation of the states. It is here due to myosin data were found only for more states models, especially, five-state one. The procedure is not original. Ref. [136] used it to condensate the five states model to receive two states model. However, the procedure to obtain the three states model was not clear. The biggest issue was how to deal with a one-way transition between two states and how to condensate the original states properly. For these reasons, the procedure can be considered as a new result. Chapter 9 describes the method of numerical measurement prediction. The measurement is simulated by a random number generator and using the central limit theorem [142]. Thus, it uses Gaussian distribution. This method produces relative information and mutual information.

The fourth part focuses on the results of the model. Chapter 10 describes a comparison between the analytical and numerical solution provided by the WPE algorithm. Chapter 11 deals with the non-normalised probability density is changed by different boundary conditions. Chapter 12 uses the condensation of states method to include the ATP concentration into the three-state model. The included dependences have integrated Arrhenius equations [84], which is often used in physical chemistry [31]. Crucial chapters for the thesis follow this chapter. Chapter 13 contains the results of the model mechanical property – velocity. The next one (Chapter 14) deals with the numerical simulation of measurement techniques which is described in Chapter 9.

The fifth part contains the thesis's benefits, a recommendation for the following work, a conclusion and its summary. The subsequent chapters are resumes in different languages (Czech, English and German), my published papers and bibliography sources used for this thesis.

The last part, the Appendix, deals with topics that are not suitable to the text itself, but there are essential for a better understanding of problems around the thesis field. There is a chapter referring to thermodynamic potentials, a chapter about balance types and a chapter about potentials used to input the Fokker-Planck equation.

Chapter 2

Biological background

The thesis outlines the biological background of the nanomachines to create a basic overview. These nanomachines are called molecular motors due to their ability to convert mechanical energy to work – movement. Sometimes, researches consider the movement as a deterministic one. However, there is also a source of stochastic movement. It is the Brownian motion.

The field of molecular motors is growing very fast. It is proved by the list of Nobel prize in Chemistry [121]. Since 2015, when my work on this topic has begun, two Nobel prizes awarded to scientists whose works touch molecular motors.

The first came in 2016 for the creation of a synthetic molecular motor. The short version of the Nobel prize committee declaration sounds to Jean-Pierre Sauvage, Sir J. Fraser Stoddart, and Bernard L. Feringa "for the design and synthesis of molecular machines" [121].

Jean-Pierre Sauvage had founded the basics of creating a synthetic molecular motor. In 1983, he developed a way how to control molecules. Figure 2.1 shows the description of the control mechanism.

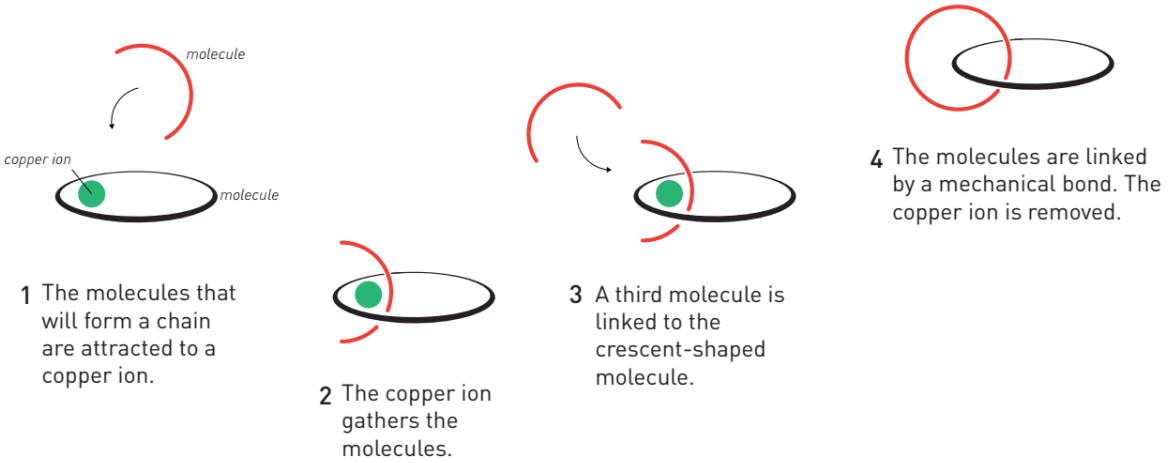

Figure 2.1: Jean-Pierre Sauvage's way of control molecules. Adapted from [122]

The next winner from this year, Sir J. Fraser Stoddart, came with a molecular elevator in 2004 [122], see Figure 2.2.

The last winner (Bernard L. Feringa) has constructed a nano-car (molecular car), see Figure 2.3

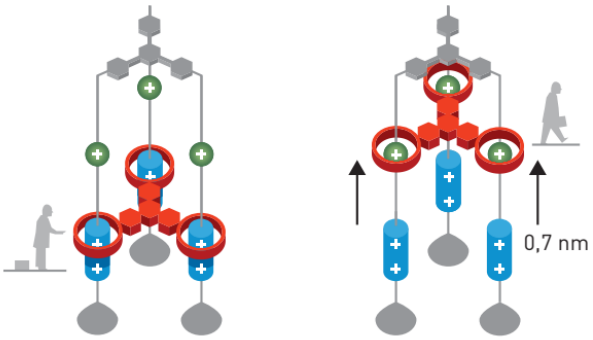

Figure 2.2: J. Fraser Stoddart's molecular elevator. Adapted from [122]

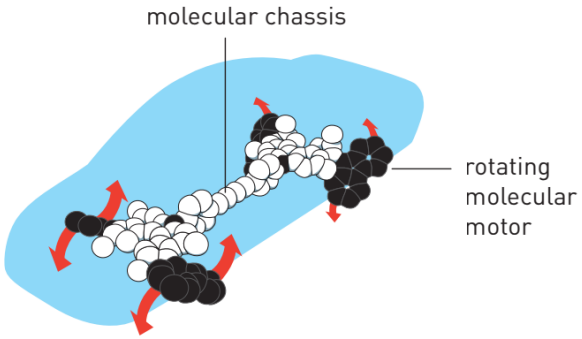

Figure 2.3: Bernard L. Feringa's molecular car. Adapted from [122]

The second prize related to molecular motor came one year later, in 2017. Molecular motors themselves were not the winning topic. Nevertheless, it allows a more detail way of studying them. The award was for the developing of cryo-electron microscope [123].

In that year, Jacques Dubochet, Joachim Frank and Richard Henderson won the Nobel prize "for developing cryo-electron microscopy for the high-resolution structure determination of biomolecules in solution." [124]

Three significant steps summarise the progress on the cryo-electron microscope. The first one was Henderson resolution increasing of an electron microscope. The electron microscope requires a vacuum, where the aqueous solution evaporates and changes the properties of the sample [123].

A way how to prevent water vaporisation was an idea of Dubochet. He came with a method of water vitrification. It means the method can change water to a kind of glass – to an amorphous structure. It provides uniform background to visualisation [123].

The last part of the Nobel prize 2017 in Chemistry was for 3D structure analysis. There are several randomly oriented samples with a similar structure, which a computer analyses and produces the 3D structure [123].

The development in the field goes very fast. The resolution of obtained Figures increases rapidly, see Figure 2.4.

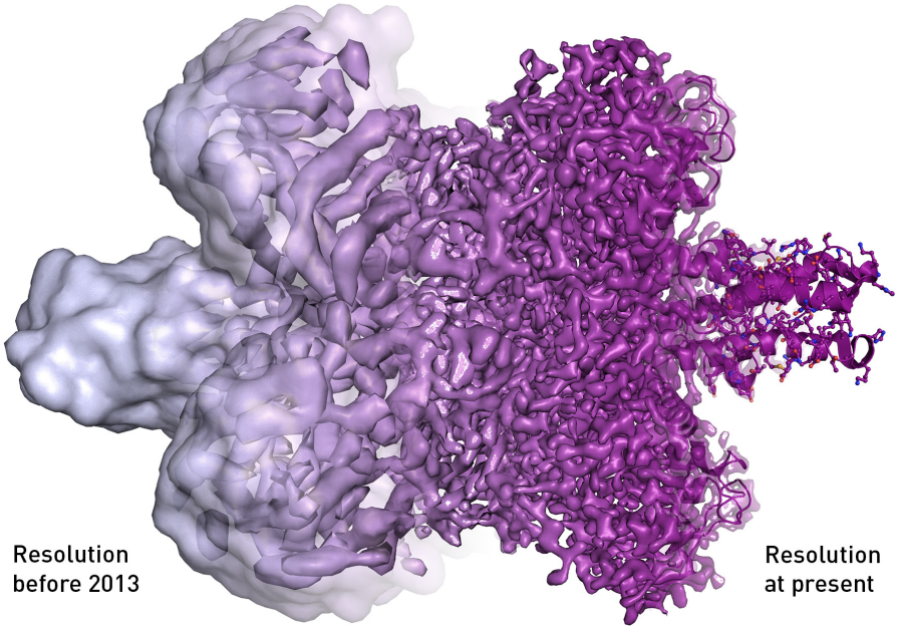

Figure 2.4: Protein image resolution before 2013 and after 2013. Adapted from [123]

2.1 Molecular motors

Molecular motors have many functions in a biological system. They convert energy to create mechanical work, like motors well-known from an ordinary human's daily life. Some of the molecular motors' performance affects the macroscale. As an example can serve muscle contraction. In this case, many molecular motors (myosins II) join together to contract a muscle. Other motors function can be observed indirectly (for example, poorly working cytoplasmic dynein can cause several serious diseases – see Section 2.2.2) or not at all.

There are three sets of molecular motors. The first set is called linear due to its movement along a filament. The second set is rotary. It is moving along its axis. The last set is called revolution motors [35].

This division to the sets is not the only possibility, how to divide them. Sometimes the third set is called nucleic acids motor proteins [60], or it is neglected at all [5].

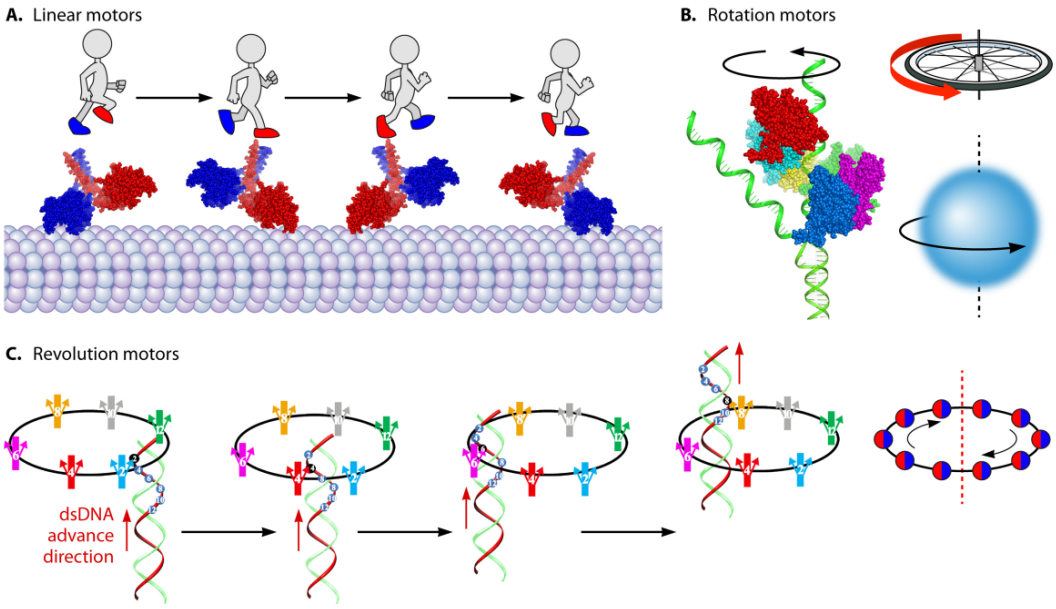

Figure 2.5: Different sets of molecular motors. Human walk is an equivalent to a linear motor. Rotation motor move like planetary rotation or like o wheel. Revolution motor move similary to the Moon around Earth. Adapted from [35].

2.1.1 Linear motors

Linear motors can be divided into two massive groups according to their movement on a filament (the type of filament depends on the specific kind of the motor). One of these groups is called processive. It means the motor has two stalks, and every time at least one is connected to the filament. Sometimes motors from this group are called walking due to their similar movement to a human walk, see Figure 2.5. The movement can also be the "inchworm" type. Figure 2.6 shows both types of movement.

The second group is called non-processive. The rest of the motors, which does not fit the first group, belongs to this second group. An example of the non-processive motor is myosin II, see Section 2.3.

More information about linear motors is in Section 2.2.

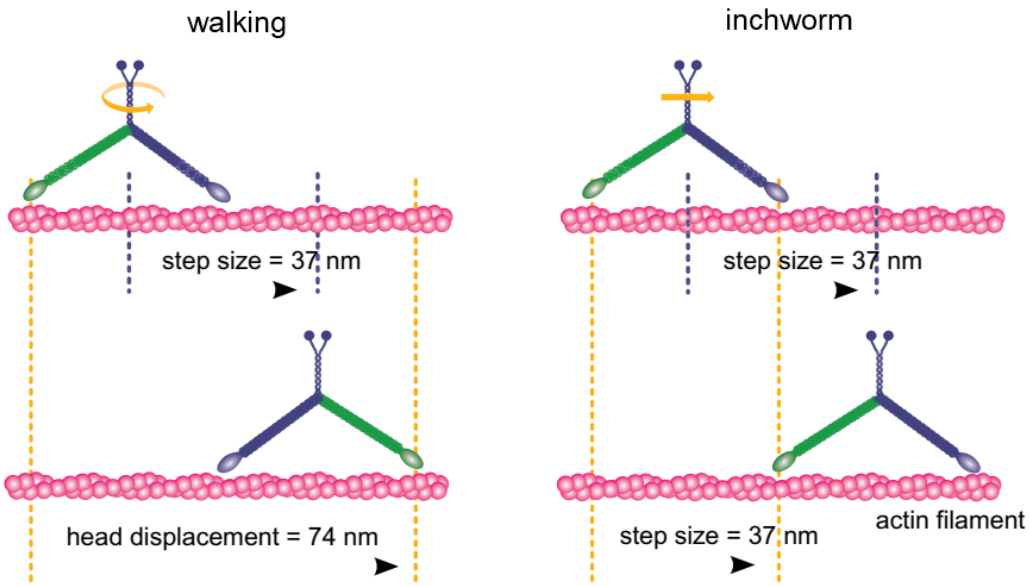

Figure 2.6: Linear molecular motors movements. On the Figure is molecular motor myosin V with its walking style of movement at the left side of the Figure and with its inchworm style at the right side, respectively. Adapted from [5].

2.1.2 Rotation motors

F_0F_1-ase, helicases, and flagella are representatives of rotation motors [35]. The F_0F_1-ase serves to the synthesis of ATP [60]. Bigger attention is to F_1 part [96]. Its movement is shown in Figure 2.7. The step requiring energy is not the synthesis of ATP from ADP and inorganic phosphate, but the binding of ADP and the phosphate to the enzyme which produces the ATP [96]. In other words, there is needed energy for storing.

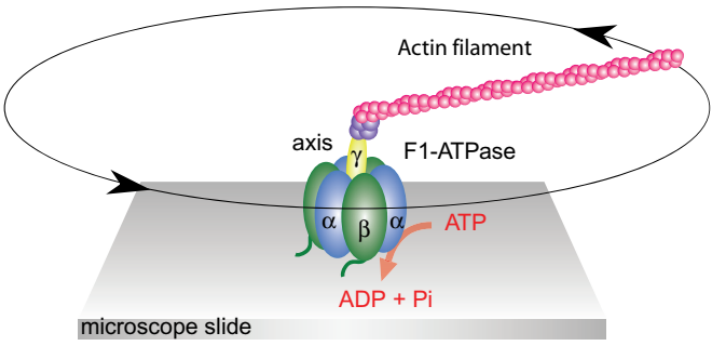

Figure 2.7: F_1-ase (part of F_0F_1ase) molecular motors movements. The actin filament goes around γ-axis. Adapted from [5].

2.1.3 Revolution motors

This group was established in 2013 [35], aside from the rotation motor. In that year, Guo and his team found out that these motors do not rotate. The second difference is in the size of a channel inside the motor. Rotation motors have a smaller (<2 nm), revolution motors have a

more extensive (>4 nm) channel.

Revolution motors are related to DNA (deoxyribonucleic acid). It "translocate DNA along the helix through unidirectional revolution, resulting in a thermodynamic edge over-rotation motors involving double-stranded DNA translocation" [35].

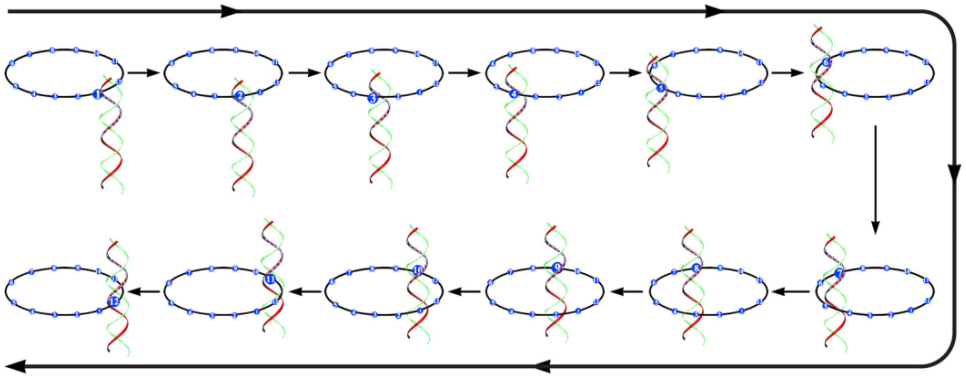

Figure 2.8: Revolution motors movements along the 12 subunits of the connector channel. Adapted from [35].

2.2 Linear Molecular Motors

Three superfamilies of linear molecular motor exist – kinesins, dyneins, and myosins. Each of these superfamilies divides itself into classes and further into types [78].

2.2.1 Kinesin

In this superfamily, 14 subclasses of kinesins exist, which share amino acid sequence homology. They are mainly involved in mediating transport and primarily going from the (-) end to the (+) end of the microtubule. Two kinds of kinesin classes are exceptions to these rules. kinesin-13 can enhance the depolymerisation of microtubule ends due to not having motor activity. Kinesin-14, on the other hand, has motor activity, but it moves reversibly to other kinesins, thus from the (+) end to the (-) end and serves during mitosis [78].

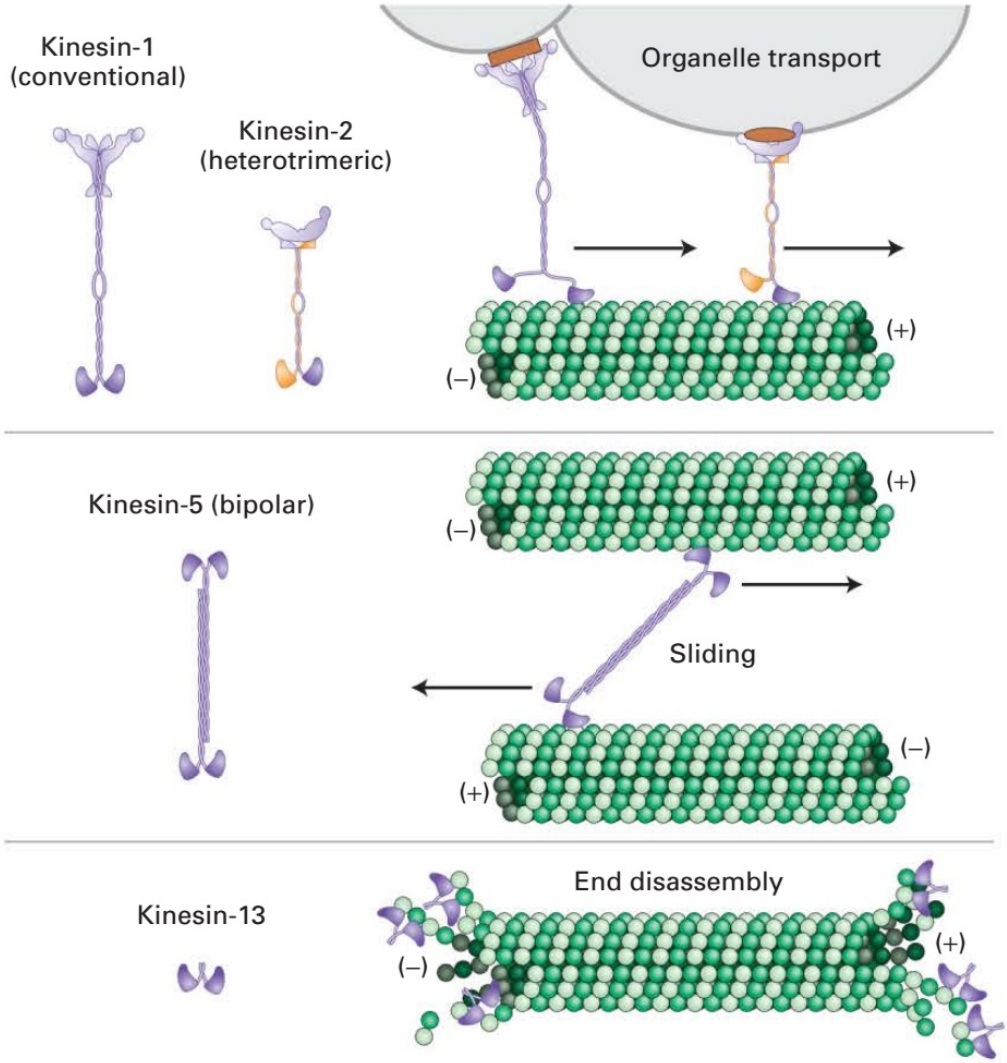

Figure 2.9: Some motors from the kinesin superfamily and their purpose. Kinesin-1 and kinesin-2 ensure organelle transport, kinesin-5 pushes two microtubules apart and kinesin-13 enhances the microtubule depolymerization. Adapted from [78].

Usually, a kinesin consists of two heads linked with a tail by a stalk [78]. These heads are used in the same way as humans use their feet for walking. Thus, at least one kinesin head connects to the filament (to a microtubule). Kinesins are usually part of the molecular motors group called the processive motors, with some dyneins and myosin-V.

The tail served as storage for a cargo (organelle) during its transport. Nevertheless, from this rule are some exception too. Evolution developed kinesins to serve various purposes. Thus, it was impossible to keep the same shape. Some kinesins could have four heads (two pairs on each side) and none tail, or have just two connected heads, see Figure 2.9.

The most common kinesin is kinesin-1, which ensures organelles transport. It is a dimer of two heavy chains, each associated with a light chain, with a total molecular weight of about 380 kDa. The molecule comprises a pair of globular head domains connected by a short flexible linker domain to a long central stalk and terminating in a pair of small globular tail domains associated with the light chains. Each domain carries out a particular function: the head domain binds microtubules and ATP and is responsible for the motor activity of kinesin; the stalk domain involves in dimerisation through a coiled-coil interaction of two heavy chains; the tail domain is responsible for binding to receptors on the membranes of cargoes [78]. Recent discovery shows this conventional kinesin behaves unconventionally; it slips against each other [79].

The example of the subclass, which ensures non-typical movement among other kinesins, is the kinesin-5. Its purpose is to slide between two microtubules. The movement is to their (+) ends. Due to this, it requires to be bipolar two sets of motor's heads, see Figure 2.9.

The last example of the kinesin subclass is kinesin-13. It is shown in Figure 2.9 as the last one. This member was originally identified "in screens for motors involved in spindle function" [88]. The main role of kinesin-13 is the depolymerisation of the microtubule.

2.2.2 Dynein

A large amount of dyneins with different purposes exists. Some of them are in neurons, some in the cilia and flagella and some inside eukaryotic cells [55]. The last group is called the cytoplasmic dynein. Properties of the cytoplasmic dynein are varying among diverse organism where the dynein exits. For example, bovine cytoplasmic dynein has different properties than porcine one [1, 126] or human one [56].

Dyneins, in general, are huge dimer molecules (>0.5 MDa[1]) [78]. Cytoplasmic dynein is a dimer with a size of approximately 1.2 MDa [55]. There are several different components – the stalk, the motor domain and the tail domain. All these components are a few tens of nanometers long, see Figure 2.10.

The microtubules bounding domain (microtubule BD) and coils create the stalk. The motor domain consists of 6 AAA motor domains where the motor's fuel (ATP) can attach to the dynein. For example, if the ATP binds to the AAA1 domain, the stalk unbounds from the microtubule. Thus, the electrostatic force is broken [75].

Cytoplasmic dynein moves vesicles (cargo) along microtubule in a processive way [55]. On the other hand, dynein usually cannot carry cargo alone. There are necessary the other proteins like e.g. dynactin which create with dynein one complex [14], see Figure 2.11. The next possibility

[1]Dalton (Da) is another name (Non-SI) for the unified atomic mass unit. Scientists in biochemistry and molecular biology often use it. Although, it was never approved by the Conférence Général des Poids et Mesures [19]

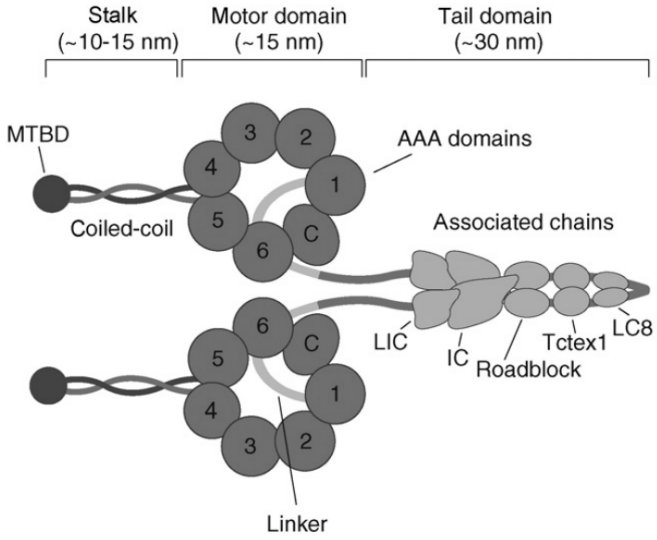

Figure 2.10: Dynein structure. Adapted from [34]

.

is that several dyneins join together [105]. Thus, dynein is a cooperative molecular motor. The cooperation helps dyneins effectiveness of the "tug-of-war" against stronger kinesin [100].

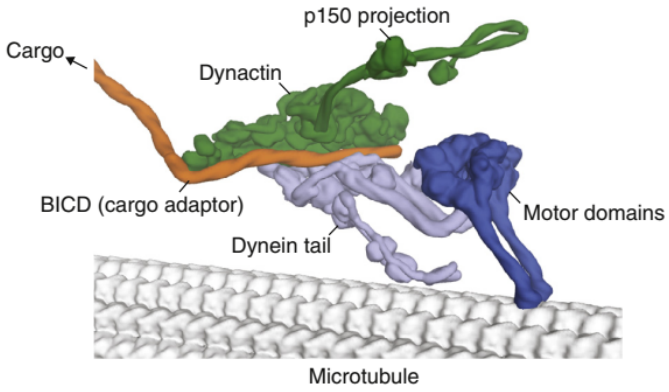

Figure 2.11: Different proteins helping dynein. Adapted from [14]

.

Cytoplasmic dynein mechanical cycle is drawn in Figure 2.12. In the initial state, the dynein stalk is attached to the microtubule. The ATP provides energy to unbound from the microtubule. The stalk is released. During ATP hydrolysis to ADP, the stalk provides the power stroke and moves to the next bounding domain to the microtubule's (-) end (the retrograde motor). The last step is tail priming (and moving with the cargo).

The most impressive property of the cytoplasmic dynein is the so-called catch-bond effect. It allows increasing of the stall force. In other words, dynein can walk with a higher load, see Figure 2.13.

If cytoplasmic dynein does not work correctly, it can cause some serious diseases like Parkinson, Alzheimer, ALS (Amyotrophic lateral sclerosis), or Glaucoma [55].

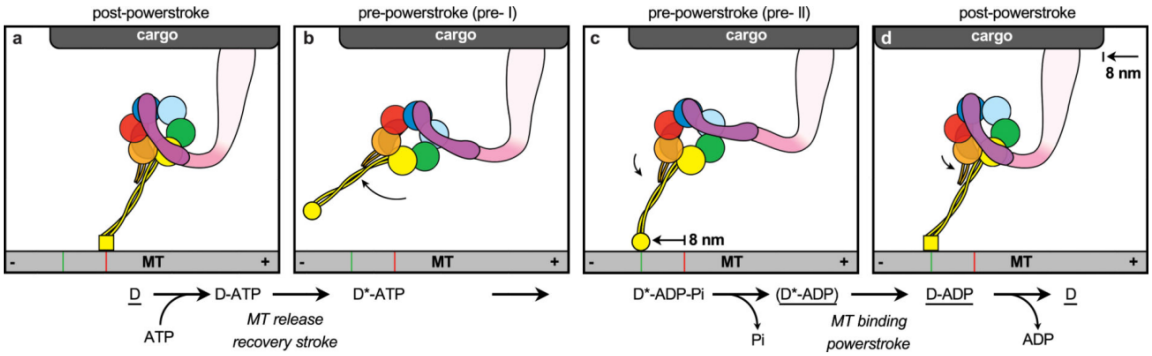

Figure 2.12: Scheme of the dynein mechanochemical cycle. High affinity is in the underline states. D and D denotes post-power stroke and pre-power stroke states, respectively. Adapted from [76]*

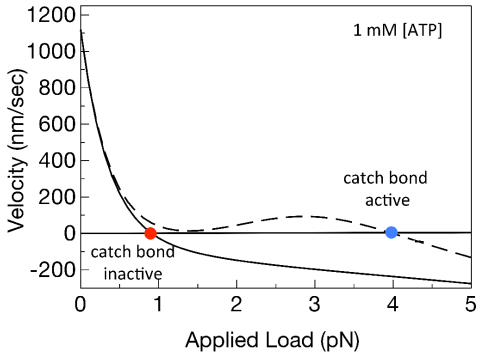

Figure 2.13: Influence of the catch bond effect. Adapted from [53]

2.2.3 Myosin

Motors from the myosin superfamily usually contain six polypeptides – two identical high-molecular-weight polypeptides (myosin heavy chains) and four light chains. One myosin can contain more than one type of light chain [18].

In an alternative division, myosins have a globular head, flexible neck and a long tail. The tail depends on the myosin type, but generally, the tails bind specific cargoes [78]. It is similar to previous superfamilies.

The myosin superfamily properties are extensive. There are more than 20 classes to categorize [18]. For example, myosin I is involved in endocytosis (transport organelles through cell membrane [130]), myosin II causes muscles contraction, myosin V is quite similar with its functionality to kinesins – it is processive and transports cargo along a filament [78], myosin VI goes "backwards" [18]. A small overview of myosin functions is in Table 2.1.

Because of an already huge number of myosin classes, a limitation for a new class of myosin exists. It says: "To prevent a premature inflation in the number of newly described myosin classes due to the discovery of divergent myosins in the newly sequenced genome, it was proposed to establish new myosin classes only in cases where putative class members derive from at least two reasonably distantly related genera .... Myosins known from only a single genus are considered "orphan" myosins" [18]. The structure is on Figure 2.15.

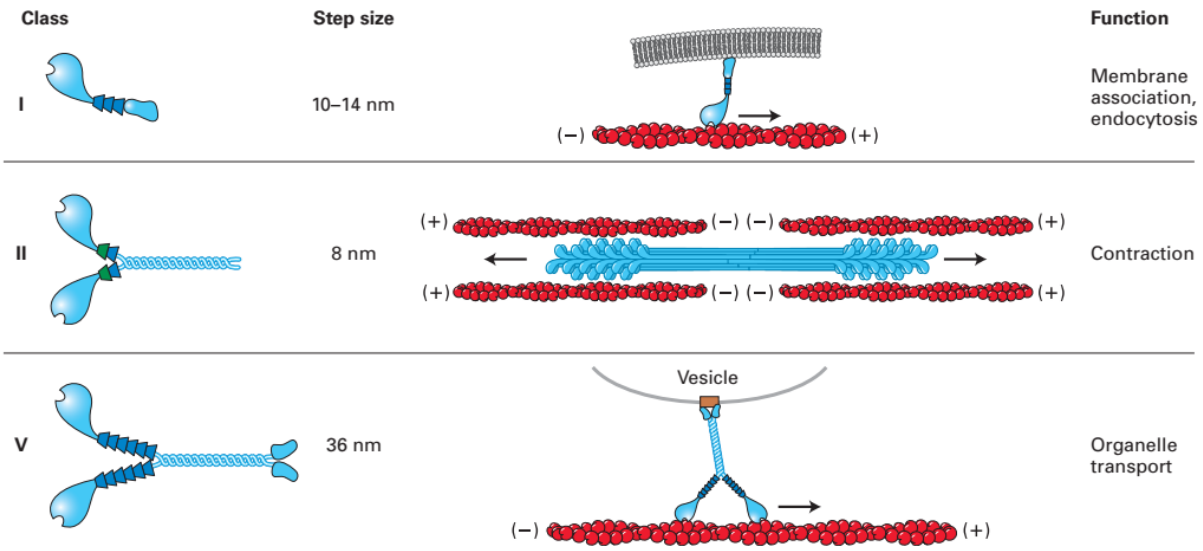

Figure 2.14: Common classses of myosins and their properties. Adapted from [78]

.

Table 2.1: Different classes of myosin and their functions – examples. Inspired by [18].

Function	Myosin class
Tension generation	I, II, VII, VIII
Endocytosis	I, II, VI, VII, X
Signal transduction	I, III, V, VI, VII, IX, X, XV, XVI
Organelle movement/localization	V, VII, XI, VII

The evolution history of myosins is very long. The origin of myosins can be tracked to early eukaryotes. It is presumed they had different groups in their era [104]:

- similar to present class I,
- with domain features – now found in classes V, XI,
- with MyTH4/FERM tail domain – classes IV, VII, X, XII, XIV, XV, XXII.

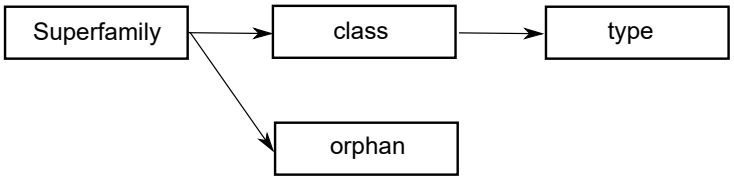

Figure 2.15: Myosin superfamily structure.

2.3 Muscle contraction and myosin II

Every muscle is created by myosin II (in the next text is denoted only as myosin – it was discovered as the first one [78]) and by actin filaments at the nanoscale, see Figure 2.16. It is necessary to go deep into the muscle structure through a bundle of muscle fibre, multinucleated muscle cell, myofibril and sarcomere to find these filaments, see Figure 2.17. The distance between two myosin heads connected to actin's binding site is 36 nm [99]. Each myosin head can perform 3 – 4 pN [30, 41]. The power-stroke distance is around 2 – 8 nm [44].

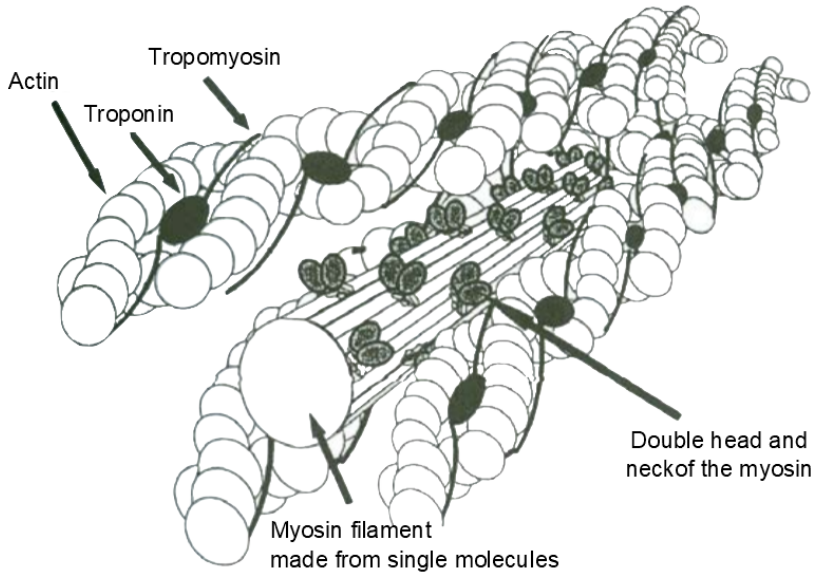

Figure 2.16: Schematic actin-myosin complex. Adapted from [107].

The structure of the (mammalian) skeletal muscle is strictly hierarchal. It is possible to see the basic structure of the muscle with a bare eye – its thick filaments (myosins), see Figure 2.18 and thin (actins) filaments. In the case of a smooth muscle, the filaments do not have a precise orientation. They are organised randomly – with an influence of the precise type of smooth muscle.

The widely accepted theory of muscle contraction is called the cross-bridge hypothesis. The myosin attached to the actin filament creates a so-called cross-bridge, and by a rowing movement, it can create muscle contraction [101]. It is necessary for at least 20 myosin heads working together to produce continuous sliding [117]. Experiments show that one molecule of ATP (fuel) consumption provides energy enough to several myosin cycles [57, 58].

There are several ways how to divide the cross-bridge (continuous) cycle into a discrete cycle. The complex myosin movement is usually simplified to a 6-state kinetic model [44] as follows – a molecule of ATP bounds on the myosin head (step 1). The ATP hydrolyses into ADP (adenosine diphosphate) and free P (phosphorus). It is step 2. The hydrolysis provides energy to bound to actin (step 3), where the atom of phosphorus is released (step 4). The ADP molecule relaxes from myosin (step 5), and it is replaced by a new ATP molecule (step 6). Then myosin unbinds itself from actin, and the cycle is complete (step 1).

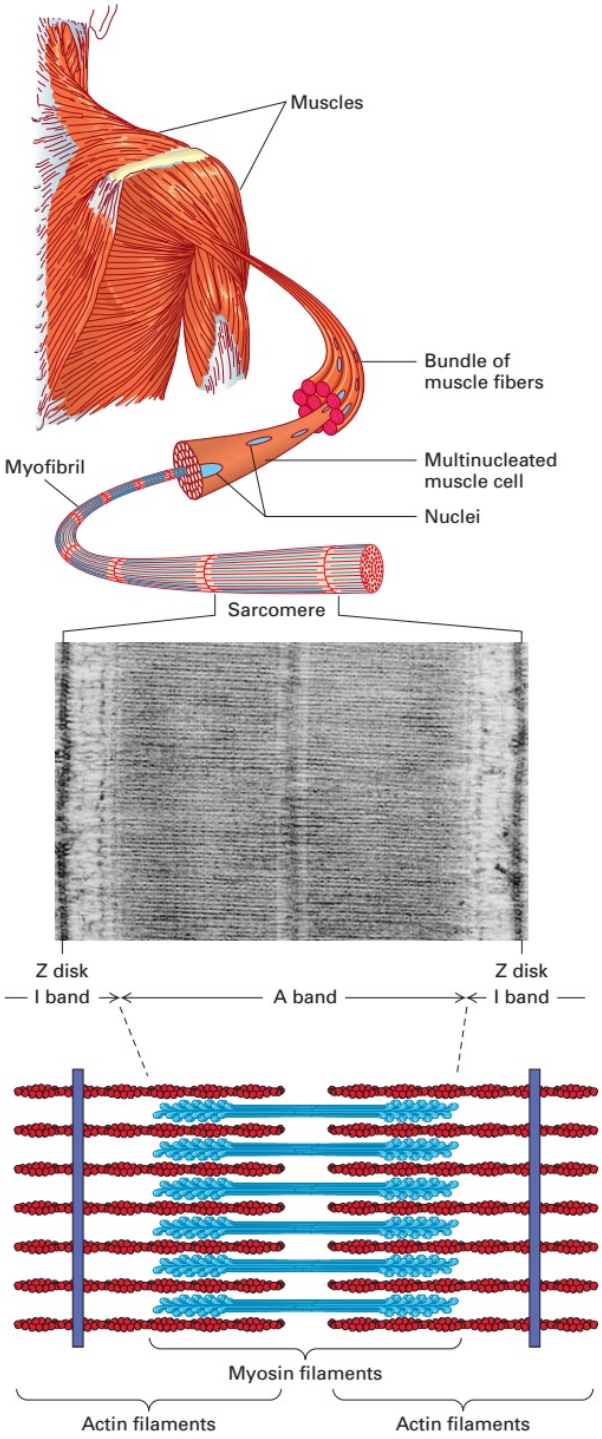

Figure 2.17: Skeletal muscle and its elements to the molecular level – from muscle fibre to myosin-actin complex. Bundles of muscle fibres create every muscle. Every fibre is created by repeating myofibril units made by sarcomeres. A sarcomere is bounded by a Z disk surrounded by an I band. Between two I bands is A band created by actin and myosin filaments. Adapted from [78].

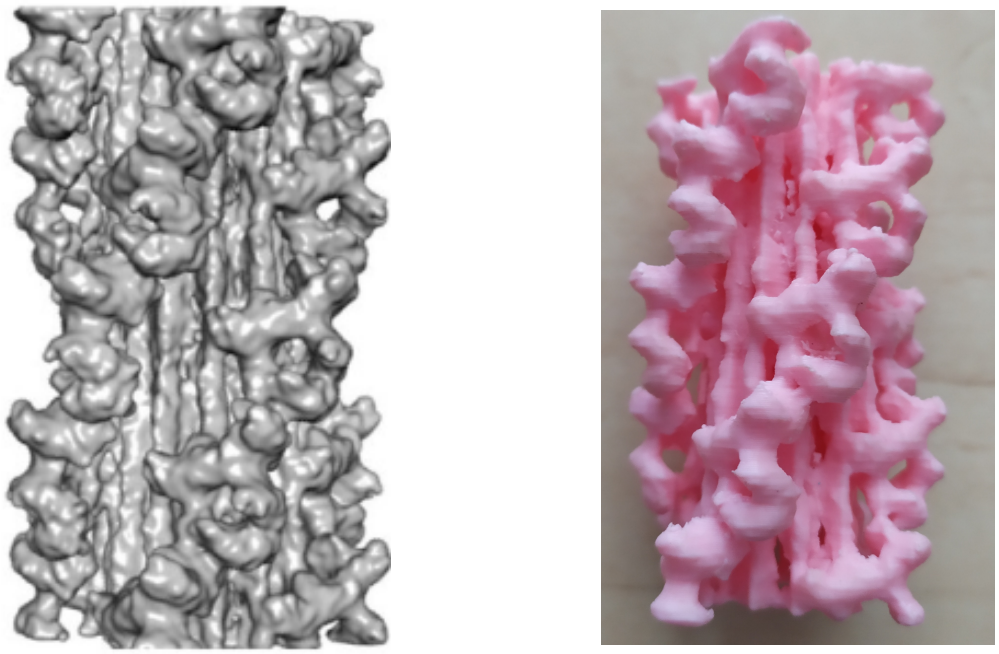

Figure 2.18: Tarantula thick filament. On left side it is a 3D image with resolution 1.3 nm. Adapted from [135]. On the right side it its 3D printout. Data was provided by Roger Craig and Shixin Yang from Department of Cell and Developmental Biology, University of Massachusetts Medical School, USA. It was printed by Jan Heczko from Department of Mechanics, Faculty of Applied Sciences, University of West Bohemia, Czech Republic.

A little different description is in [78]. There is a written 5-state myosin cycle. It assumes as the first step, the myosin head is released from the actin filament, and the head binds ATP. In the second step, the ATP hydrolyses to ADP and P. It causes the myosin head rotation. Then, the myosin head is bent to the actin filament. In the fourth step, there is the "power-stroke", when the phosphorus atom is released, elastic energy straightens myosin and moves actin filament to the left. In the last step, the ADP molecule is released, a new ATP molecule binds to the myosin, and the head is free from actin. The fifth step ends at the same configuration as the first one. So, it can consider as a 4-state myosin cycle.

The movement of myosin can be more simplified to 3-state cycle ([25, 27, 128]) or even to 2-state cycle ([16]). The 2-state cycle is only bound and unbound states. This description does not provide any deeper knowledge about the contraction controlled by Ca^{2+} [2]. The 3-state model is used further for its ability to describe muscle contraction. It recognises the unbound state, the weakly-bound state and the post-power stroke state. More details about the 3-state model are in Chapter 7.

The description of the myosin cycle by a numerical means has two different approaches. The more common one is by classical Hill and Huxley models [39, 40, 45], but they do not consider surrounding influence. Different mathematical model has to be used to do so, see Chapter 3 and its sections 3.4.2 and 3.4.3, especially.

Myosin molecular motor can undergo a load and still works, although there is a limitation. At loads bigger than the stall force, the myosin could no longer support the continuous forward motion, resulting in the actin filament is effectively pulled backwards [22].

Chapter 3

Statistical and information theory background

Statistical physics describes the whole ensembles of systems, where our computation abilities are not sufficient to handle every member of the ensemble or a random parameter is present in the description. Statistical physics covers a description of large systems or, on the other hand, small systems (meso-, micro-). These small systems are essential for this theses due to the connectivity of statistical physics and molecular motors. Here, I use distributions with a meaning of probability density of myosin head presence. It is a way how to describe a statistical ensemble.

Nowadays, statistical physics has two parts – classical (equilibrium) and non-equilibrium. These groups correspond with the division of thermodynamics. In classical statistical physics, the temperature is well defined, and the whole system is in thermal equilibrium (with the same temperature in whole volume [61]). In non-equilibrium statistical physics, the temperature of the whole system cannot be defined. Sometimes, it is possible to be close to an equilibrium. It means the temperature exists only in a small vicinity of a point [61]. Statistical physics explains thermodynamics [94].

3.1 Statistical physics

Statistical physics studies systems where it is impossible to study the individual behaviour of every particle precisely. It can be for different reasons

- number of particles is too high to handle it by today's computation methods
- random effects

It may seem more straightforward to simplify its reducing number of particles and neglect the random effects, but this has no sense. Without these effects, it is impossible to obtain valid data, and for example, water cannot freeze without random effects [15].

3.1.1 Relation between thermodynamics and statistical physics

The connection between thermodynamics and statistical physics was established by Ludwig Boltzmann in 1872 [94]. In this year, he published his H-theorem [11] where he tried to derivate the second law of thermodynamics from the laws of mechanics.

He came with a result [68]

$$-k_B \frac{\mathrm{dH}}{\mathrm{d}t} = \frac{\mathrm{d}S}{\mathrm{d}t} \tag{3.1}$$

where k_B is Boltzmann constant, H is a function for a dilute gas comprised of spherical particles[1]

$$\mathrm{H} = \sum_i f_i \ln f_i \delta\vec{x}\delta\vec{\mathfrak{p}} \tag{3.2}$$

with statistical distribution f of the ensemble, position $\vec{x}$ and momentum $\vec{\mathfrak{p}}$.

Variable S in equation (3.1) is thermodynamic entropy.

Boltzmann claimed (see Section 3.2.2) based on knowledge of the second law of thermodynamics

$$\frac{\mathrm{dH}}{\mathrm{d}t} \leq 0. \tag{3.3}$$

The equality is valid only in an equilibrium state [68]. It is not the only benefit of Boltzmann's work on H-theorem. He showed the Maxwell-Boltzmann distribution is the only distribution that stays invariant during molecular collisions [94].

Based on the work of Boltzmann, who established the fundamentals of statistical physics (or sometimes called statistical mechanics) [94], thermodynamic potentials (see Appendix A), are connectors between statistical physics and thermodynamics. The connector can be Ensemble theory and its partition function. See Section 3.3.

Sometimes, thermodynamics is noted as a macroscopic counterpart of statistical physics [15].

[1] Boltzmann's H-function is identical to Shannon entropy[68]

3.2 Equilibrium thermodynamics

Equilibrium (or classical) thermodynamics is more used than non-equilibrium thermodynamics nowadays. It describes a more significant part of all thermodynamics phenomena[95]. It was developed in the 18th and 19th century by observing heat engines.

The most fundamental postulate of the equilibrium thermodynamics is sometimes called the zeroth law of thermodynamics. It describes what the equilibrium and thermodynamic variables (function) are.

In Ref. [114], there is a possible formulation of the law:

Zeroth law "If a system is left isolated for a sufficiently long time from any environment and any external system, it will reach a state with no further macroscopic changes. Such a state is said to be in an equilibrium state. ..."

3.2.1 First law of thermodynamics

First law of thermodynamics is kind of conservation of energy law [95]. The mathematical description of the law is [61]

$$\mathrm{d}U = \mathrm{d}Q + \mathrm{d}W \tag{3.4}$$

where $\mathrm{d}U$ is differential of inner energy, $\mathrm{d}Q$ differential of accepted heat and $\mathrm{d}W$ is differential of accepted work[2].

This law set the heat as a form of energy. Before general acceptance of thermodynamics' first law, the heat was considered an indestructible fluid-like substance without mass, called caloric. The caloric measured was calories [61].

3.2.2 Second law of thermodynamics

The second thermodynamics law does not have such a clear expression as the first (and the zeroth) one. It has many versions mostly equivalent – with some reasonable assumptions [59].

William Thomson (Lord Kelvin)
It is impossible to derive mechanical effect from any portion of matter by cooling it below the coldest surrounding objects' temperature through an inanimate material agency.[125]

Later, the law was reformulated by McClare in 1970 for a microscopic version of the second law [52]:

C. W. F. McClare
"It is impossible to devise an engine, of any size whatever, which, acting in a cycle which takes a time t, shall produce no effect other than the extraction of energies, which have equilibrated with each other in a time less than t, from a reservoir at one temperature and the conversion of these energies into a form in which they would remain stored for longer than t; either at a higher temperature or in a population-inversion." [87]

[2]The sing '+' prior the term $\mathrm{d}W$ is sometimes change to the sign '-', which means in that case it is considered produced work[95].

3.2.3 Third law of thermodynamics

Sometimes it is called the Nernst–Planck theorem [114]. It says a limitation to the entropy:

"The entropy of a system approaches a constant value as the temperature approaches zero." [59]

From this statement usually comes out, the temperature cannot be negative [114]. It is not always true [98]. Some systems break it. These systems are in localised spin systems [12].

3.3 Ensemble theory

In classical statistical physics, the ensemble theory describes large systems often. It provides a way to categorised problems into simple groups. Three kinds of ensembles exist, the microcanonical, the canonical and the grand canonical ensembles, respectively [94]. The microcanonical ensemble describes a simple closed system, where all system options have the same probability. The second one, the canonical, allows a close system to have some options with higher or lower probabilities. The last one, the grand canonical ensemble, provides a way to treat an open system, where interaction with surroundings is allowed. For example, this ensemble is valid for a chemical reaction description, which is out of the thesis's scope.

3.3.1 The Microcanonical ensemble

The most elementary one is the Microcanonical ensemble. It assumes that every microstate of the isolated system in thermal equilibrium occurs with the same probability p_m. It means

$$p_m = \frac{1}{g} = const., \tag{3.5}$$

where g is called the statistical weight. The approach is not quite applicable in an open system case, but it is handy for deriving the other canonical ensembles [142].

3.3.2 The Canonical ensemble

The second one is called The (Gibbs) Canonical ensemble. It describes a closed isothermal system in the surrounding characterised by a thermostat. For most purposes, the thermostat's precise nature is not very relevant [94], but it needs to be defined. Ref. [142] defines the thermostat as a macroscopic component with a much larger number of degrees of freedom than the system. The thermostat has a constant volume and can exchange only thermal energy with the system, not particles.

For using the Canonical ensemble for N identical particles with total energy E, the system has to fulfil two simple conditions, which are obvious from the thermostat definition.

$$\left.\begin{array}{l} \sum_r n_r E_r = E = NU \\ \sum_r n_r = N \end{array}\right\} \tag{3.6}$$

These conditions say the total product of the number of particles n_r with their energy E_r is total energy E which also expresses the product of all particles N and the mean energy U.

Then the probability of the given particle r is determined by a relation

$$p_r = Z^{-1} \exp(-\beta E_r), \tag{3.7}$$

where β^{-1} is the product of Boltzmann constant k and temperature T. The parameter Z^{-1} has the meaning of a scaling factor to obey one of the axioms of probability which says total probability has to be equal 1. A mathematical expression for Z can be obtained from this condition

$$Z = \sum_r \exp(-\beta E_r). \tag{3.8}$$

A schematic visualisation of equation (3.7) is drawn in Figure 3.1. The energy of the state and the number of particles there determine the probability of the given state.

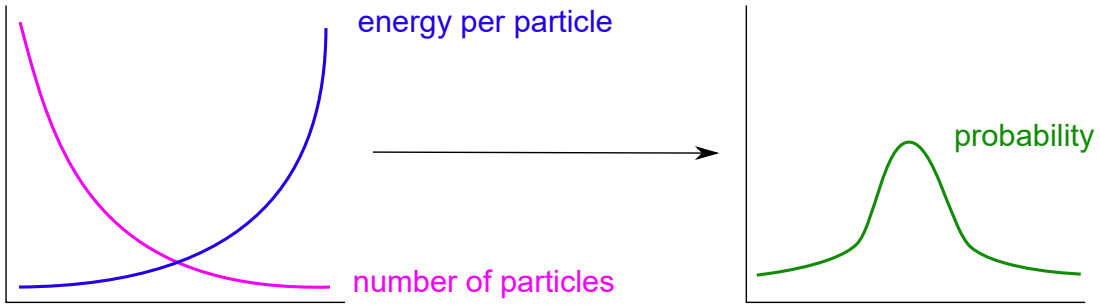

Figure 3.1: Schematic representation of the dependence probability density on energy and number of particles with a given energy. The biggest amount of particles is with the lowest energy, and only a few particles have the biggest energy. The probability is a normalised product of the number of particles and their energies. The scheme is scaleless.

The quantity Z has not only meaning of the scale factor but also can be used for a statistical expression of thermodynamic parameters (entropy S, Helmholtz free energy F_H and so on, see appendix A). Due to its wide use, the parameter Z has its own name, the partition function. Sometimes Z is also called the "sum-over-states" from German Zustandssumme [94]. It is worth stressing that in the case of degenerated energy levels (multiple states have the same energy), the partition function can be determined as

$$Z = \sum_s g_s \exp(-\beta E_s), \tag{3.9}$$

where g_s is the weight function of the given degenerated state s. Equation (3.9) is only computational simplification of the previous equation. There can be found a relationship between the maximum values of the index s and the index r

$$\max(s) \leq \max(r). \tag{3.10}$$

The equality sign is valid only in a case of $g_s \equiv 1$ for all s.

An example of a system with degenerated energy levels can be in biology myosin molecules involved in muscle contraction, see Section 2.3. In such cases, the thermostat can describe the aqueous solution in cells. Particles of the solution fluctuate with their energy (Brownian motion) and impact the myosin head. The impact can influence the movement of the head.

A knowledge of a parameter A expected value (or mean value) $\langle A \rangle$ is very important in statistics. It can be evaluated by a simple relation

$$\langle A \rangle = Z^{-1} \sum_r A_r \exp(-\beta E_r), \tag{3.11}$$

where A_r is a value of the parameter A with an energy E_r.

3.4 Non-equilibrium thermodynamics

In non-equilibrium statistical physics, fluctuations of the system have a significant role. The fluctuation is defined like the irregularity or stochasticity among the realisations, which are statistical by its nature (requirement of a data ensemble) and the uncertainty (given a part of the data up to a given time and it is impossible to predict precisely the remaining data or the data in the future) [114].

The main approaches for description are various fluctuation theorems and the Langevin equation; see Equation (3.29) with a direct connection to Jarzynski's theorem.

3.4.1 Fluctuation theorem

There is not only one fluctuation theorem. Their history began in 1993 [36], when Evans et al. [28] simulated shear of fluids. Two years later, Gallavotti and Cohen proved the fluctuation theorem rigorously for deterministic dynamics [33].

Jarzynski created one of the most important fluctuation theorems described further. It is developed and expanded in Refs. [43, 49, 50, 51, 110].

Jarzynski theorem

The Jarzynski theorem's base was founded in 1997 [48]. It comes from infinitely slow parameters change during its path γ between points $\mathcal{A}$ and $\mathcal{B}$ and from the assumption that total work W performed in such system is equal to the Helmholtz free energy difference ΔF_H (see Section A.4) between the initial and the final configuration

$$W = \Delta F_H \equiv F_H^{\mathcal{B}} - F_H^{\mathcal{A}}. \tag{3.12}$$

Equality comes from the work of spring definition. The spring with a rubber band has similar properties as a polymer (like myosin), see Figure 3.2. The spring has a known inside force F_{spring}. Thus,

$$W = \int F_{spring} \mathrm{d}\gamma. \tag{3.13}$$

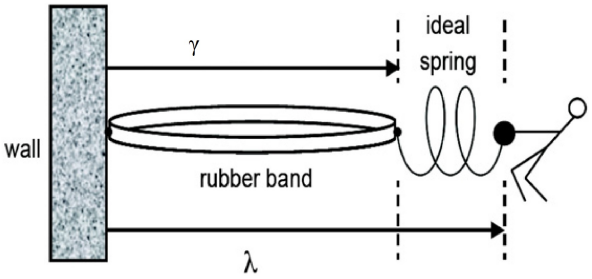

Figure 3.2: An ideal spring is connected with a rubber band. A being pulls the spring and the band, respectively along a path γ. Adapted from [10].

When the parameters change along γ at a finite rate, the W will depend on the microscopic initial condition of the system and reservoir, and its average will exceed ΔF_H

$$\langle W \rangle \geq \Delta F_H. \tag{3.14}$$

The difference $\langle W \rangle - \Delta F_H$ is equal to dissipation work W_{diss}.

Jarzynski has realised the following thing. He presumed that the system fulfils a canonical distribution for its initial conditions. Thus, the system has a Hamiltonian $\mathcal{H}_0$ and the beginning and $\mathcal{H}_1$ at the end. An ensemble of all possible trajectories z between point $\mathcal{A}$ and $\mathcal{B}$ describes a phase-space density f, which satisfies

$$f_0 = Z_0^{-1} \exp(-\beta \mathcal{H}_0). \tag{3.15}$$

Next, he presumed, the space density f evolves under the Liouville theorem. Thus,

$$\frac{\mathrm{d}f}{\mathrm{d}t} = 0. \tag{3.16}$$

So, it must be valid

$$f = f_0 = Z_0^{-1} \exp(\beta \mathcal{H}_0) \tag{3.17}$$

In such system, the ensemble average $\langle \exp(-\beta W) \rangle$ may be expresses as

$$\begin{aligned} \langle \exp(-\beta W) \rangle = & \int f \exp[-\beta(\mathcal{H}_1 - \mathcal{H}_0)] \mathrm{d}z = \\ = & \int Z_0^{-1} \exp(\beta \mathcal{H}_0) \exp[-\beta(\mathcal{H}_1 - \mathcal{H}_0)] \mathrm{d}z = \\ = & Z_0^{-1} \int \exp(-\beta \mathcal{H}_1) \mathrm{d}z = \\ = & Z_0^{-1} Z_1 \end{aligned} \tag{3.18}$$

The Helmholtz free energy difference ΔF_H is defined by

$$\Delta F_H = -\beta^{-1} \ln \frac{Z_1}{Z_0} \tag{3.19}$$

or

$$\frac{Z_1}{Z_0} = \exp(-\beta \Delta F_H) \tag{3.20}$$

From this, it is possible to write directly Jarzynski fluctuation theorem (or Jarzynski equality)

$$\langle \exp(-\beta W) \rangle = \exp(-\beta \Delta F_H). \tag{3.21}$$

Jarzynski fluctuation theorem can be simplified to relation (3.14) via Jensen's inequality [114]. It says that for every convex function $y(x)$ (second derivation is positive function) and its mean values (see Figure 3.3) is valid

$$\langle y(x) \rangle \geq y(\langle x \rangle). \tag{3.22}$$

Thus, the backward derivation starts with rewriting Equation (3.21) to an explicit form for ΔF_H

$$\Delta F_H = \beta^{-1} \ln \langle \exp(-\beta W) \rangle. \tag{3.23}$$

On the right side of Equation (3.23), Jensen inequality is applied and the rest are simple

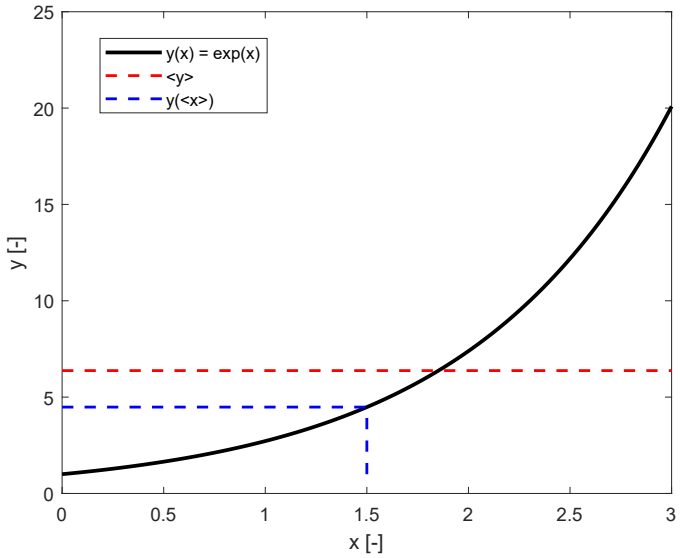

Figure 3.3: Graphical illustration of Jensen's inequality for the exponential function.

algebraic modifications

$$\beta^{-1}\ln\langle\exp(-\beta W)\rangle \geq -\beta^{-1}\ln\exp\langle-\beta W\rangle = -\beta^{-1}(-\beta)\langle W\rangle = \langle W\rangle. \tag{3.24}$$

Thus, the initial relation for mean work is obtained

$$\langle W\rangle \geq \Delta F_H. \tag{3.14}$$

3.4.2 Langevin equation

In the scale of molecular motors is not the Newton second law sufficient. It has to be enhanced by a term that describes the thermal fluctuations (Brownian motion). There is also an influence of the drag force. The Langevin equation fulfils both, and this is why many authors use it for the description of the molecular motion [69, 137].

The Langevin equation takes random thermal forces as an input and generates the variable's stochastic process, such as the Brownian particle position (x), as an output. Although the random thermal force is supposed to contain no memory, i.e., no finite temporal correlations, the Langevin equation transforms this stochastic process into the output, which has a memory of the past [114].

The equation itself is created by a balance among a total force F_T, a drag force F_{drag}, which is caused by the surroundings, and a Brownian force of random motion F_B

$$F_T = F_{drag} + F_B. \tag{3.25}$$

The total force can be expressed according to the Newton second law

$$F_T = m\frac{\mathrm{d}^2x}{\mathrm{d}t^2}. \tag{3.26}$$

The drag force (or viscosity) is defined as

$$F_{drag} = -\gamma_{drag}\frac{\mathrm{d}x}{\mathrm{d}t}, \tag{3.27}$$

where γ_{drag} is a drag coefficient.

The Brownian force describes the stochastic property of the system. It behaves like a Gaussian white noise [114, 137], i.e.

$$\langle F_B \rangle = 0. \tag{3.28}$$

The simplest form of Langevin equation can be written in a form [29]

$$m\frac{\mathrm{d}^2x}{\mathrm{d}t^2} = -\gamma_{drag}\frac{\mathrm{d}x}{\mathrm{d}t} + F_B. \tag{3.29}$$

A more advanced form of the equation can be modified, for example, by a control force created by a potential V [137]. The enhancing requires to make a transition from the ordinary differential equation to a partial one

$$m\frac{\partial^2x}{\partial t^2} = -\gamma_{drag}\frac{\partial x}{\partial t} - \frac{\partial V}{\partial x} + F_B. \tag{3.30}$$

For myosin II molecular motor, the mass m is typically about 10^{-21} kg, the drag coefficient γ_{drag} is about 10^{-7} pNs/nm [29].

3.4.3 Fokker-Planck equation

In my thesis, the Fokker-Planck equation (in some sources called the Smoluchowski equation [29]) is considered only in following version [133]

$$\frac{\partial \rho}{\partial t} = \frac{D}{k_B T}\frac{\partial}{\partial x}\left(\frac{\partial V}{\partial x} - F_{Load}\right)\rho + D\frac{\partial^2 \rho}{\partial x^2}, \tag{3.31}$$

where ρ is the probability density, D diffusion coefficient and F_{Load} is a force of an external load. Other variables have been defined earlier.

The Fokker-Planck equation says that the time evolution of the probability density is given by two parts – by two terms. The first term is controlled transport by an effective potential ϕ [102]

$$\phi = V - x \cdot F_{Load}. \tag{3.32}$$

It is possible to derive many versions of the Fokker-Planck equation from the Langevin equation by even more kinds of derivatives [38, 118, 134, 97]. However, all of them have in common the transition from a phase-space to a state-space.

Properties of the Fokker-Planck equation

The Fokker-Planck equation has several interesting properties [114]:

- *Principle of superposition*
  The Fokker-Planck equation is a linear one. Thus, convolution of the initial condition and Green function create the solution. The same applies to diffusion equation, see Section 5.2.

- *Equation of continuity for probability densities*
  The Fokker-Planck equation can be written as a set of partial differential equations

$$\frac{\partial \rho}{\partial t} = -\frac{\partial J}{\partial x} \tag{3.33}$$

$$J = -\frac{D}{k_B T}\left(\frac{\partial V}{\partial x} - F_{Load}\right)\rho - D\frac{\partial \rho}{\partial x}, \tag{3.34}$$

  where J is probability density flux. The Equation (3.33) corresponds to the Fick law (the continuity equation), which is well-known from diffusion theory [59].

- *Equilibrium state under homogeneous temperature*
  The Fokker-Planck equation's solution closes to the canonical equilibrium distribution, see Section 3.3.2, if the temperature T is a constant. In this case, the flux J vanishes for all x.

- H-*theorem*
  The distance between a Fokker-Planck equation solution in an arbitrary time and the stationary solution can be expressed by the Kullback-Leibler distance. This distance is a kind of entropy – the relative one, which is non-negative and disappears only if the solution in time and the equilibrium are identical. Chapter 9 uses this property. there I show the mathematical definition of the Kullback-Leibler distance. The definition is also in Section 3.4.4.

3.4.4 Information

"Information is physical." Rolf Landauer originally said this famous statement. It is the name of his famous article from 1991 [70].

Information is characterised by the probability of choosing a specific event from a large group of events and by receiving remembering such choice [129]. It brings new view to a convention thermodynamic problem, see Figure 3.4.

The definition of information is according to Ref. [52] as follows

1) "Knowledge obtained from investigation, study, or instruction.
2) Intelligence, news, facts, data.
3) The attribute inherent in and communicated by one of two or more alternative sequences or arrangements of something (such as the nucleotides in DNA and RNA or binary digits in a computer program) that produce a specific effect.
4) A quantitative measure of the uncertainty in the outcome of an experiment to be performed.
5) A formal accusation of a crime made by a prosecuting officer as distinguished from an indictment presented by a grand jury.
6) Anything or any process that is associated with a reduction in uncertainty about something.
7) Information is always associated with making a choice or a selection between at least two alternatives or possibilities."

The Shannon definition of information is analogical to entropy in statistical physics. Shannon entropy H uses probabilities to its description [80]

$$\mathrm{H}(X) = -\int \rho(x)\log\rho(x)\mathrm{d}x, \tag{3.35}$$

where X is a random variable. It says a less probable event produces more information when it occurs. The base of the logarithm is equal to 2 in a case, the entropy is in bits. If it is in nats, the logarithm is natural one – the base is equal to Euler number e [21]. The notation H comes from Boltzmann's H-teorem [120]. This entropy is defined in a different way than entropy shown in Section A.1.

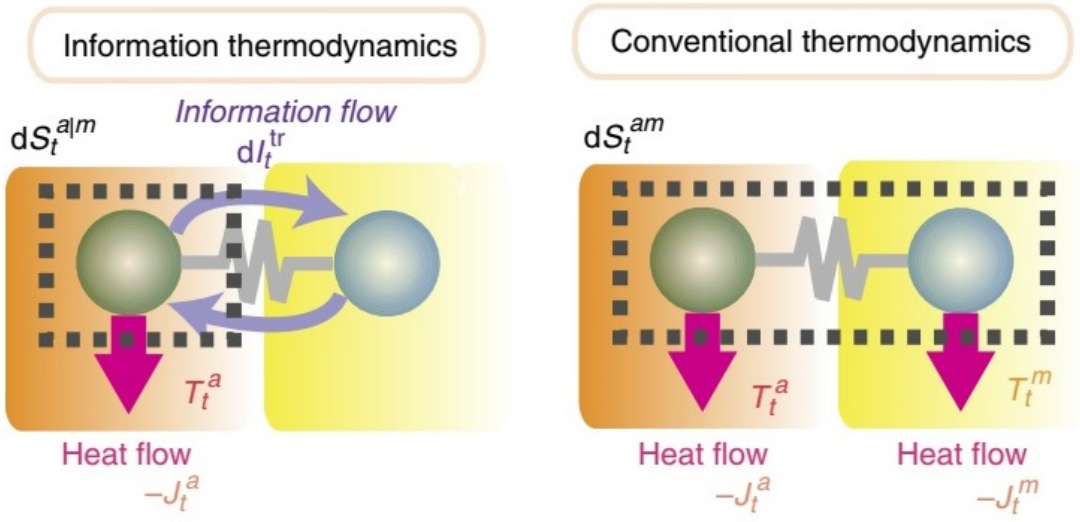

Figure 3.4: The difference between information thermodynamics (on the left) and classical thermodynamics (on the right). The information thermodynamics allows to have an external agent which is not included to the system but it is able to influence the system via information flow dI. Adapted from [46]

Following important parameters in information theory are joint entropy and condition entropy.

The joint entropy is defined as follows

$$\mathrm{H}(X,Y) = -\int\int \rho(x,y)\log\rho(x,y)\mathrm{d}x\mathrm{d}y \tag{3.36}$$

and conditional one

$$\mathrm{H}(Y|X) = -\int\int \rho(x,y)\log\rho(y|x)\mathrm{d}x\mathrm{d}y, \tag{3.37}$$

respectively.

These parameters are very important, no doubt. But the key role in information theory have Kullback-Leibler distance and mutual information [21]. Kullback-Leibler distance has been already mentioned in Section 3.4.3 as a property of the Fokker-Planck equation. It expresses how two distribution ρ_a and ρ_b are similar to each other

$$\mathcal{D}(\rho_a \parallel \rho_b) = \int \rho_a \log\frac{\rho_a}{\rho_b}\mathrm{d}x\,. \tag{3.38}$$

The Kullback-Leibler distance is sometimes noted as information [63].

Mutual information I indicates the correlation between two probability variables [112], it is sometimes called also as transfer entropy [111]. Its definition can be written with using Shannon

entropy [21] as

$$I = \mathrm{H}(X) + \mathrm{H}(Y) - \mathrm{H}(X,Y)\,. \tag{3.39}$$

This relation can rewritten with probability densities [21]

$$I = \iint \rho(x,y) \log \frac{\rho(x,y)}{\rho(x)\rho(y)} \mathrm{d}x\mathrm{d}y \tag{3.40}$$

This equation make easier to show why the mutual entropy is denoted as mean value of Kullback-Leibler distance. To do this, it is important relation [108]

$$\rho(x,y) = \rho(x|y)\rho(y)\,. \tag{3.41}$$

Then, it is clearly

$$I = \iint \rho(x,y) \log \frac{\rho(x,y)}{\rho(x)\rho(y)} \mathrm{d}x\mathrm{d}y = \tag{3.42}$$

$$= \iint \rho(x|y)\rho(y) \log \frac{\rho(x|y)\rho(y)}{\rho(x)\rho(y)} \mathrm{d}x\mathrm{d}y = \tag{3.43}$$

$$\int \rho(y) \int \rho(x|y) \log \frac{\rho(x|y)}{\rho(x)} \mathrm{d}x\mathrm{d}y = \int \rho(y) \mathcal{D}(\rho(x|y) \parallel \rho(x) \mathrm{d}y. \tag{3.44}$$

Generalised second law of thermodynamics

The second law of thermodynamics can be generalised by information term

$$-\Delta U + \sum_{m=1}^{n} \frac{T}{T_m} Q_m \leq -\Delta F + k_B T I, \tag{3.45}$$

where U is a difference of system internal energy system between the begging and the end of the studied interval, Q_m is heat exchanged between the system process with temperature T_m and the heat reservoir with temperature T. The parameter F is free energy difference [113].

The inequality can be simplified for case of an isothermal process of a system with single heat bath with using first thermodynamics law [93, 113] as

$$W_{ext} + \Delta F \leq k_B T I. \tag{3.46}$$

For this form of second law of thermodynamics, it is possible to modify also Jarzynski fluctuation theorem by a term with mutual information dependent on its trajectory γ

$$\langle \exp(-\beta(W - \Delta F) - \gamma) \rangle = 1. \tag{3.47}$$

For the mutual information dependent on its trajectory γ is valid simple connection to classical mutual information I

$$\langle \gamma \rangle = \langle I \rangle. \tag{3.48}$$

The validity of Equation (3.47) was proved in Refs. [62, 93].

Information is connected closely to idea of Maxwell's demon (see Section 3.4.5). It influences the system somehow. To do so, it performs a kind of measurement. The measurement and its

memory reset require to perform a work (W_{meas} and W_{reset}, respectively). An inequality to describe such works establishes as

$$W_{meas} + W_{reset} \leq k_B T I. \tag{3.49}$$

The inequality is called the generalised Landauer principle [93].

3.4.5 Maxwell's demon

In 1871, James Clerk Maxwell introduced a being, which can break the second law [72, 86]. In the beginning, Maxwell supposed to have only "faculties and instruments were so sharpened that we could detect and lay hold of each molecule and trace it through all its course." [86] The time, the idea of faculties and instruments change to a "being" that has these abilities. The principle of acting the being was simple. Consider a vessel with an almost precisely uniform spatial distribution of particles. Some of them are hotter, some colder. Then divide the vessel into two parts with a connection - some door controlled by the being. The being can distinguish the hotter and colder particles, respectively. Thus, its ability to control the door by opening and closing allows releasing the hotter particles to, for example, the right part and the more cold ones into the vessel's left part. The being does not perform any work, but it obtains the hotter right part and colder left part of the vessel. It is in contradiction to the second law.

William Thomson named the being Maxwell's demon. The word demon is used here without any malicious meaning [72, 125]. It is just a hypothetical agent or device of arbitrary small mass [72]. The demon evolved during its existence several times. It received "metabolism" in 1923 from demon:lewis and Randall [72, 74] and "intelligence" in 1924 from demon:nyquist [72, 90]. Also, it obtained "eyes" for watching molecules via light signals in 1951 from Brillouin [72], or in other words, an ability to measure [103], which have been modified to observe even quantum effects, like black body radiations [72, 103]. The demon has, from its definition ability of feedback control. Some of the skills also cause temporal exorcism. The best known was a Brillouin one. Nevertheless, Maxwell's demon has returned among living physical problems [72].

During the Maxwell demon history, not only its skills changed. The change was also in a physical realisation of the demon. Smoluchowski considered the demon as automated trapdoor [103, 72], see Figure 3.5. The trapdoor can be connected with a spring and then serves as a one-way valve which allows for an increase in density on one side while preventing flow in the reverse direction[103]. Szilard invented a single molecule engine, see Figure 3.6. The engine's working substance is a single-molecule gas in a box of a given volume, immersed in a thermal reservoir at temperature T, and manipulated by an external agent (demon). The demon splits the box into two halves and measures on which side the molecule is. Then, the demon carries out a reversible expansion to the original volume to extract work $W_{ext} = k_B T$ [93]. Later, different kind of ratchets embodied the demon [102]. The most famous one is the Feynman ratchet wheel, and pawl [47, 114]. This device's task is simple – to prevent movement in the opposite direction than is required, see Figure 3.7.

Nowadays, Maxwell's demon is no longer just a theoretical construct. However, it is still a kind of metaphor. Several experiments were set-up to prove Maxwell's demon. Recently, an experiment with a single-electron box (SEB) controlled by a gate voltage V_g and monitored by a single-electron transistor (SET). The scheme of the experiment is in Figure 3.8 [93]. Ref. [67] shows a similar experiment. It was done with a colloidal particle and two optical traps,

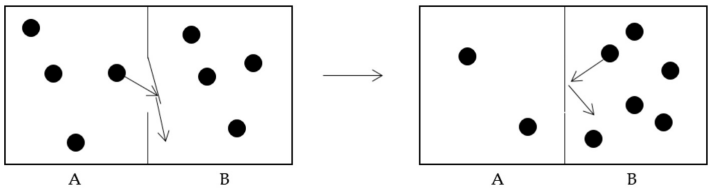

Figure 3.5: Smoluchowski automated trap door. Molecules are kept in one part (B) by a trap mechanism (spring) and molecules from the second part (A) have an allowance to pass through. Adapted from [103].

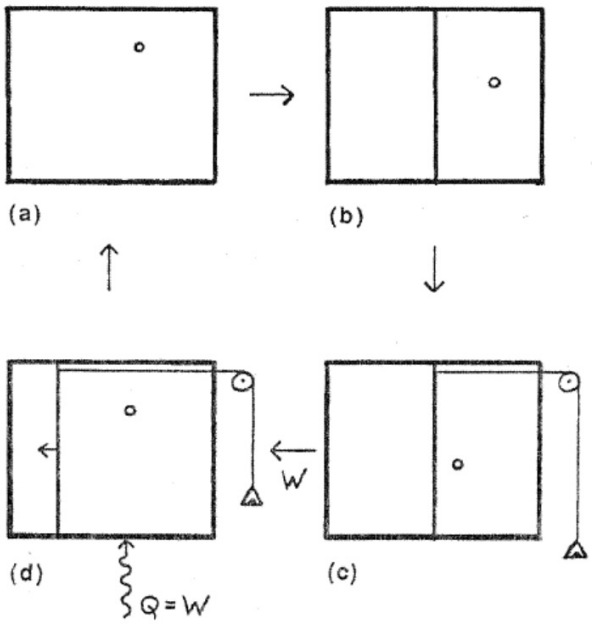

Figure 3.6: Szilard one molecule engine. In an initial state, a free molecule is moving in a box (a). Then the box is divided into two parts by a movable partition (b). A weight connected to the partition (c) is moved due to thermal collisions with the molecule far away from the weight. Thus, the weight goes higher. Taken from [103].

see Figure 3.9 or rotating colloidal particle, see Figure 3.10. The next experiment came back to Maxwell's original mental experiment. The setup uses energy from thermal system measurements and feeds forward, in order to extract work, see Figure 3.11, [8, 127]. Maxwell's demon was discovered on the quantum level in different experiments [8, 20].

Also, biochemical signal transduction [46], and molecular motors fulfil properties of Maxwell's demon [64]. Furthermore, a filament segment's shape was compared to a ratchet due to its sawtooth shape even before [77] – this kind of model of Maxwell's demon description applied on the myosin II motor I use in the thesis.

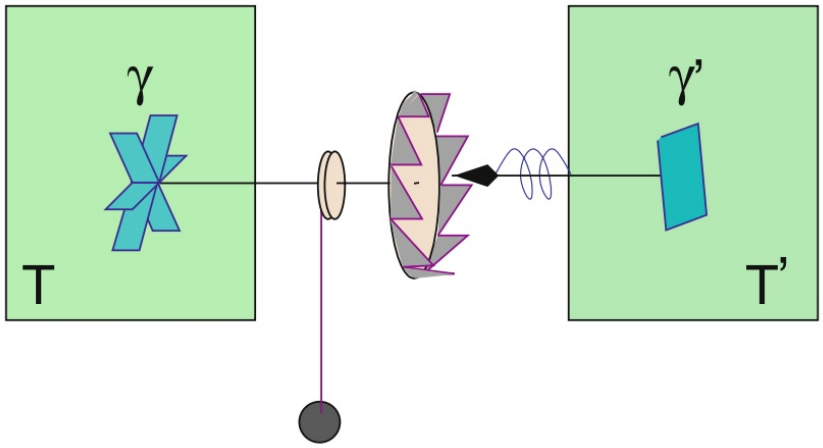

Figure 3.7: Feynman ratchet wheel and pawl. Thermal collisions with a paddle wheel make a turn of a spool with a weight. The spool rotates only in the desired way due to the ratchet wheel, which prevents movement in the opposite direction. For this device's correct work, it is necessary to have two different temperatures baths [47]. Adapted from [114].

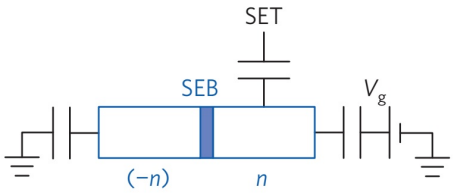

Figure 3.8: Experimental realization with a single-electron box (SEB) controlled by a gate voltage V_g and monitored by a single-electron transistor (SET). The controlling system decides according to the electron number (n=0,1). Adapted from [93]

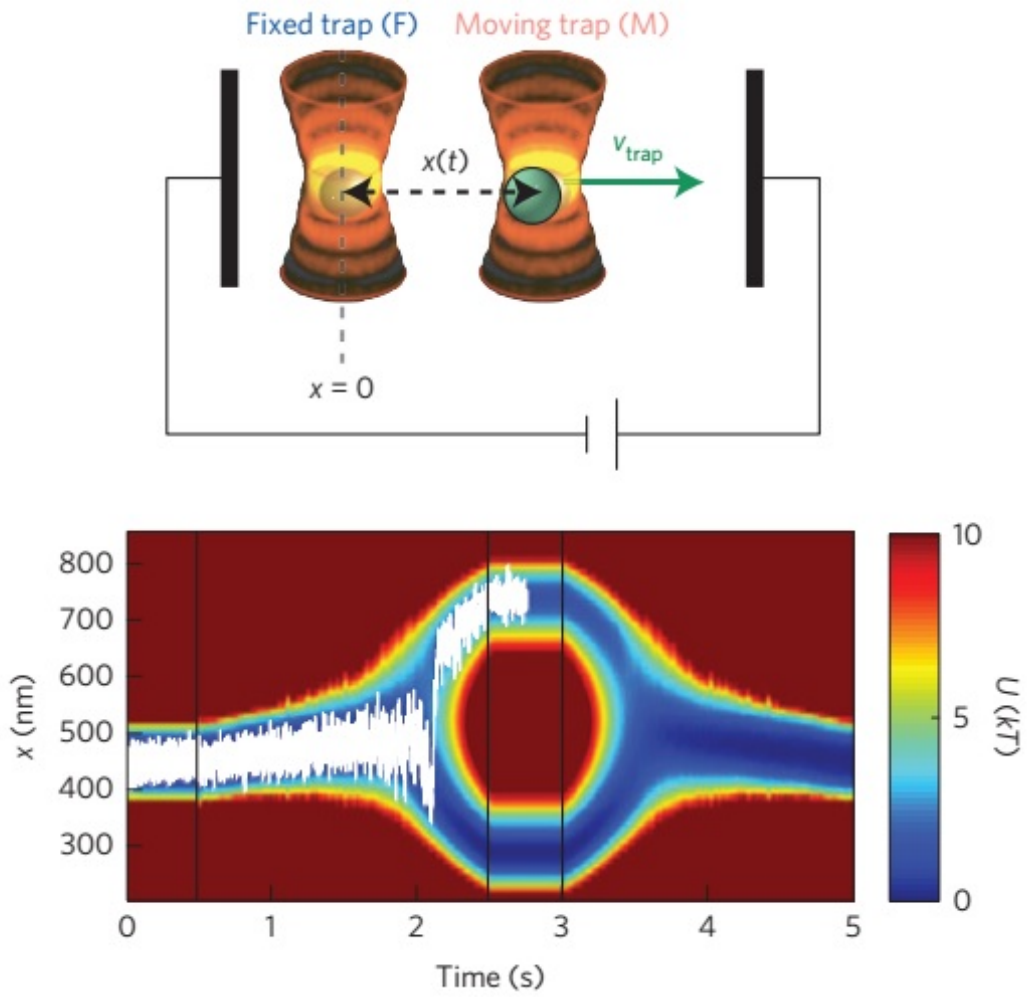

Figure 3.9: Schematic representation of a colloidal particle and two optical traps. The top figure shows the experimental set-up: one trap keeps fixed at position $x = 0$, and the other is shifted horizontally at velocity v_{trap}. A controllable electrostatic field created by two electrodes biases the particle towards one of the traps. The bottom figure shows a contour plot of the potential affecting the particle during a process where the moving trap is shifted and then moved back to its initial position. A realisation of the particle's trajectory is visualised as a fluctuating white line. The Szilárd cycle achieved by measuring the trap. The particle lies in the middle of the process and biasing the trap in the second half. Adapted from [93].

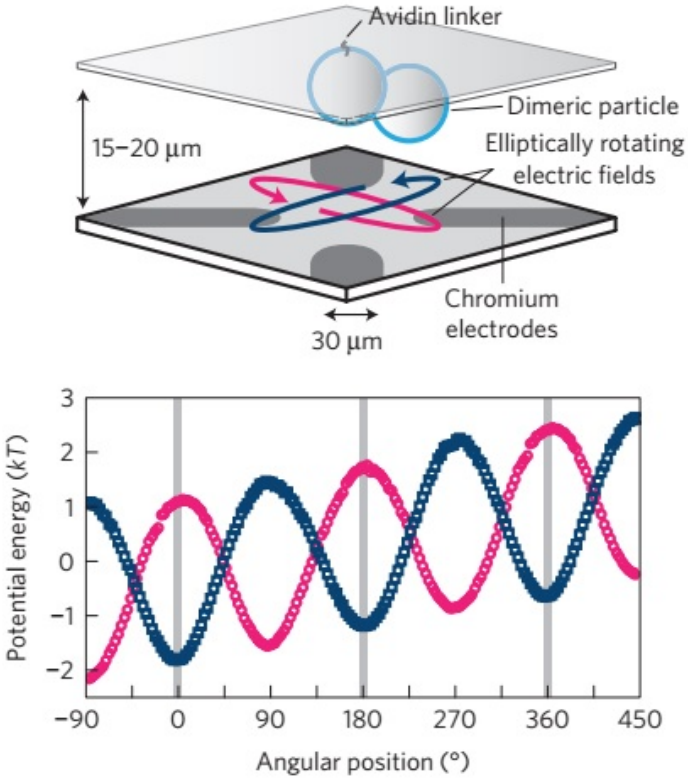

Figure 3.10: Experimental realisation using a rotating colloidal particle. The top figure shows the experimental set-up, where two particles are attached to the cover glass. One of the particles is regarded as a rotating Brownian particle. Four electrodes controllers induce an electric field. The bottom figure shows two shapes of the effective potential. It is a superposition of a sinusoidal potential and a constant torque. The particle's position is measured, and the potential is switched from one shape to the other when the particle crosses the potential minima in the uphill direction. Adapted from [93].

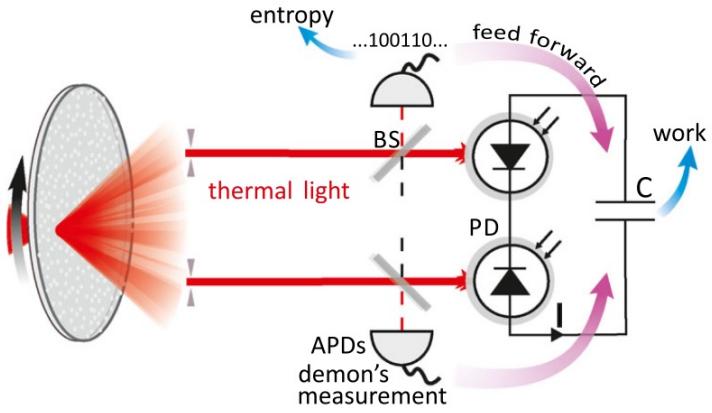

Figure 3.11: Thermal light is produced by collecting laser pulses scattered from a spinning glass diffuser wheel. High transmittance beam splitters (BS) and highly sensitive avalanche photodiodes (APDs) implemented as the demon's measurement. The two final linear photodiodes are the work extraction mechanism, acting as an electromotive source that charges a capacitor (C). A nonzero average voltage across C can be obtained by feed-forward of the demon's measurement, swapping its polarity according to the APD measurement outcomes. Adapted from [127].

3.4.6 Information motors

Information motors are also considered a kind of Maxwell's demon [65]. These motors (sometimes called feedback motors) can convert information to work [42]. Ref. [83] studies the connection between information and Maxwell's demon. There is a simple three-state model, where a demon reads a data strip (bits) and lifts a weight according to the obtained data, see Figure 3.12.

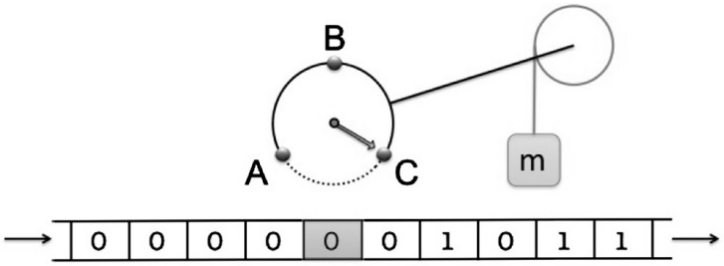

Figure 3.12: Information demon collects information from a data strip (bits) and in every transition $A \rightarrow C$ lifts the weight m by an amount Δh. Adapted from [83].

Part II

Objectives and hypotheses

Chapter 4

Objectives and hypotheses

Topics of molecular motors and Maxwell's demon are vast. The thesis cannot contain everything. Thus, I have chosen to focus on the Fokker-Planck framework applied to the myosin head. The approach is already used by many researchers groups, like Chen's, Wang's, and Yin's [16, 133, 136].

The initial step is to study literature about molecular motors, Maxwell's demon and information motors.

The first necessary objective concerning the modelling is to make own verification of the used algorithms. As was mentioned before, the Fokker-Planck equation is the base equation in the model which describe the system behaviour. It is a partial differential equation of first-order in time and second in space variable, respectively. Its solving can bring some different results in comparison with an analytical solution.

The second task is to find a simplification of the myosin head movement model (how to discretise the movement cycle), which is not commonly used in this framework but is still well applicable to the problem. If the model does not use even some dependence on the ATP molecules concentration, add to it.

Next, the Fokker-Planck framework provides probability densities of the myosin head presence. It can be interesting to watch the normalising condition's necessity to ensure the myosin head is within the domain. I hypothesise that the different boundary conditions influence the total sum of the probability density a lot.

The model requires to have an output comparable with an experiment. For this reason, I study the molecular motor's velocity here.

The last objective is to connect the myosin head description with Maxwell's demon concept. The demon has many different abilities – watching the procedure of the movement or controlling the movement. These "powers" are simulated by numerical means. Here, I focus on watching the myosin head movement only. The next ability (system control) can be attached to the model in future. However, it is complicated to validate these simulations of controlling system procedure.

Part III

Methodology

Chapter 5

Analytic solution of the diffusion equation and the stationary Fokker-Planck equation

This thesis focuses on myosin II head which moves along actin filament and causes a muscle contraction. The surroundings influence the head movement. Thus, it needs a stochastic approach for its simulation.

The Fokker-Planck equation describes stochastic behaviour of the given object's probability density in time t and space x. Therefore, the myosin II head is the object from the Fokker-Planck equation. It is the essential equation in the model.

The equation is as follows

$$\frac{\partial \rho}{\partial t} = \frac{D}{k_B T} \frac{\partial}{\partial x} \left(\frac{\partial V}{\partial x} - F_{Load} \right) \rho + D \frac{\partial^2 \rho}{\partial x^2} \,, \tag{3.31}$$

where $\rho = \rho(x,t)$ is the probability density, D diffusion coefficient and F_{Load} is an external load force. V is internal potential of the actin-myosin complex. Parameter $k_B T$ is a product of the Boltzmann constant k_B and thermodynamic temperature T.

Concerning the model, I solve the equation numerically. However, it is instructive to simplify the equation and solve it analytically to compare these two approaches.

I compare two simplified versions of the equation (the solution of the complete Fokker-Planck equation is not trivial [23] and exceeds the scope of the thesis). The simplified versions are called stationary Fokker-Planck equation and the diffusion equation.

The modification to the stationary Fokker-Planck equation is simple. It is

$$0 = \frac{D}{k_B T} \frac{\partial}{\partial x} \left(\frac{\partial V}{\partial x} - F_{Load} \right) \rho + D \frac{\partial^2 \rho}{\partial x^2} \,. \tag{5.1}$$

To obtain diffusion equation from (3.31), it is necessary to say, there are no internal or external drifting forces. It means

$$\frac{\partial V}{\partial x} - F_{Load} = 0 \,. \tag{5.2}$$

Then the diffusion equation is indeed

$$\frac{\partial \rho}{\partial t} = D \frac{\partial^2 \rho}{\partial x^2} \,. \tag{5.3}$$

I compare analytical and numerical solutions of these simplified equations in Chapter 10. Chapter 6 describes the used numerical algorithm (called the WPE algorithm).

5.1 Analytic solution of the stationary Fokker-Planck equation

The stationary Fokker-Planck equation is as follows

$$0 = \frac{D}{k_B T}\frac{\partial}{\partial x}\left(\frac{\partial V}{\partial x} - F_{Load}\right)\rho + D\frac{\partial^2 \rho}{\partial x^2}\,. \tag{5.1}$$

With using notation

$$\psi = \frac{\partial V}{\partial x} - F_{Load}\,, \tag{5.4}$$

and divided by D, the stationary equation is simply

$$0 = \frac{1}{k_B T}\frac{\partial}{\partial x}\psi\rho + \frac{\partial^2 \rho}{\partial x^2}\,. \tag{5.5}$$

By simple modification, I obtain

$$0 = \frac{\partial}{\partial x}\left[\frac{\psi\rho}{k_B T} + \frac{\partial \rho}{\partial x}\right] = \frac{\partial J}{\partial x}\,. \tag{5.6}$$

It says, the flux J needs to be a constant in stationary state. Moreover, to have finite probability density ρ, the flux has to equal to zero [85], i.e. $J \equiv 0$.

The idea of finite probability density simplifies the solution finding problem of the stationary Fokker-Planck equation, which is of the second order in space variable, find a solution of the first order equation. Therefore

$$\frac{\psi\rho}{k_B T} + \frac{\partial \rho}{\partial x} = 0\,. \tag{5.7}$$

Its solution is straightforward[1]

$$\rho = C\exp\left(-\frac{\tilde{\phi}}{k_B T}\right)\,. \tag{5.8}$$

where $\tilde{\phi}$ is a primitive function to ψ. I identify it to the effective potential directly

$$\tilde{\phi} \equiv \phi = V - x \cdot F_{load}\,. \tag{5.9}$$

The integration constant C has a meaning of the corresponding inverse partition sum Z^{-1}. Thus,

$$C^{-1} = Z = \int \exp\left(-\frac{\tilde{\phi}}{k_B T}\right)\mathrm{d}x\,. \tag{5.10}$$

Hence, the full solution in the original variables is

$$\rho = \frac{\exp\left(-\dfrac{V - x \cdot F_{load}}{k_B T}\right)}{\int \exp\left(-\dfrac{V - x \cdot F_{load}}{k_B T}\right)\mathrm{d}x}\,. \tag{5.11}$$

[1] The procedure is described for example in Ref. [6]

5.2 Analytic solution of the diffusion equation

I choose the diffusion equation to show time dependency difference between analytical and numerical (WPE algorithm) solution. It is a very easy simplification of the Fokker-Planck equation by "turning off" the drifting term. The diffusion equation has a form

$$\frac{\partial \rho}{\partial t} = D \frac{\partial^2 \rho}{\partial x^2}\,. \tag{5.3}$$

The solution to the equation is well-known [24] or [31]. Usually, it depends on the solution's interval – infinite or finite spatial variable [24]. Here, the analytical solution is required to a comparison with the numerical solution. Only the analytical solution on a finite interval with connected Neumann boundary conditions at both sides is used in the thesis.

$$\frac{\partial \rho(t,0)}{\partial x} = 0, \tag{5.12}$$

and

$$\frac{\partial \rho(t,L)}{\partial x} = 0. \tag{5.13}$$

Parameter L; $L = 36\,\mathrm{nm}$ is the finite domain's length. It says, there is zero flux across the borders. Thus, the myosin head cannot leave the domain and it is pushed back. It corresponds to the reflecting boundary, see Section 6.1.

The solution has a form

$$\rho(t,x) = \frac{1}{2}A_0 + \sum_{n=1}^{\infty} A_n \exp\left[-\left(\frac{n\pi}{L}\right)^2 Dt\right] \cos\frac{n\pi x}{L}. \tag{5.14}$$

and the initial condition must obey

$$\rho(0,x) = \frac{1}{2}A_0 + \sum_{n=1}^{\infty} A_n \cos\frac{n\pi x}{L}. \tag{5.15}$$

Chapter 6

Wang-Peskin-Elstone algorithm

In this thesis, I use Wang-Peskin-Elstone algorithm (shortly the WPE algorithm [133]) for numerical integration of the Fokker-Planck equation, see (3.31). The original version of this algorithm was introduced in 2003 [132]. In 2007 an improved version of the algorithm was published [131]. This later version can handle discontinuous version of the Fokker-Planck equation. The discontinuity is in the potential V. The biggest advantage of the WPE algorithm is the preservation of detail balance [132]. It means no additional numerical error in a stationary state[1].

In this chapter, I present the original version of the algorithm. It is entirely sufficient for the thesis's scope. Other authors[16, 136] use this algorithm to deal with numerical simulations of molecular motors as well.

The algorithm can be modified to solve spatially dependent diffusion coefficient, but it is not the thesis's objectives. More information about that problem can be found in Appendix A of Ref. [132].

The spatial variable x is divided into N equidistanted nodes x_n with step Δx, i.e.

$$\Delta x = x_{n+1} - x_n \,. \tag{6.1}$$

The principal algorithm assumes the flux $J_{n+1/2}$ between nodes x_n and x_{n+1} can be rewritten with a help of forward F and backward B fluxes.

$$J_{n+1/2} = F_{n+1/2} p_n - B_{n+1/2} p_{n+1} \tag{6.2}$$

where p_n is a probability of finding the motor at site x_n .

The solution of the WPE algorithm can be interpreted as a spatially discrete Markov chain [132]. The solution has a form of the master equation

$$\frac{\mathrm{d}p_n}{\mathrm{d}t} = -(B_{n-1/2} + F_{n+1/2}) p_n + F_{n-1/2} p_{n-1} + B_{n+1/2} p_{n+1}, \tag{6.3}$$

and satisfies, for a space step Δx, a relationship

$$p_n(t) \approx \int_{x_n - \Delta x/2}^{x_n + \Delta x/2} \rho(x,t) \mathrm{d}x \approx \rho(x_n, t) \Delta x \,. \tag{6.4}$$

Parameters $F_{n+1/2}$ and $B_{n+1/2}$ are between nodes x_n and x_{n+1}, respectively, see Fig. 6.1.

[1] For more details about balance see Appendix B

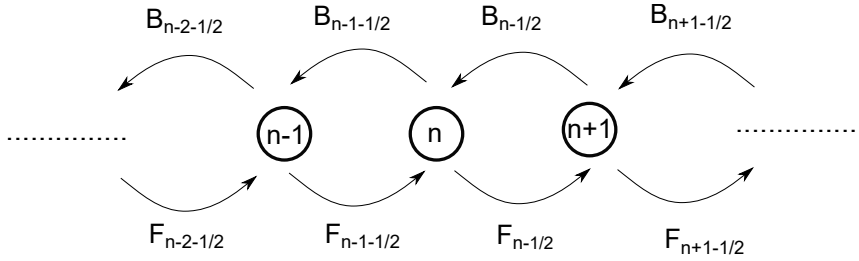

Figure 6.1: Scheme of spatial fluxes in the WPE algorithm.

These parameters are determined by a stationary solution of the originally solved equation. For the Fokker-Planck equation (3.31) can be written as follows[132]

$$F_{n+1/2} = \frac{D}{(\Delta x)^2} \frac{\dfrac{\Delta\phi_{n+1/2}}{k_B T}}{\exp\left(\dfrac{\Delta\phi_{n+1/2}}{k_B T}\right) - 1} \qquad \forall n \in \langle 0; N \rangle \tag{6.5}$$

and

$$B_{n+1/2} = \frac{D}{(\Delta x)^2} \frac{-\dfrac{\Delta\phi_{n+1/2}}{k_B T}}{\exp\left(-\dfrac{\Delta\phi_{n+1/2}}{k_B T}\right) - 1}, \tag{6.6}$$

where $\Delta\phi_{n+1/2}$ is defined to be

$$\Delta\phi_{n+1/2} = \phi(x_{n+1}) - \phi(x_n), \tag{6.7}$$

where $\phi(x) = V(x) - x \cdot F_{Load}$ is called the effective potential [102].

6.1 Boundary conditions

The WPE algorithm work with three kinds of boundary conditions – periodic, absorbing and reflecting.

The first, called the periodic boundary condition, assumes an infinite number of actin-myosin head complexes. They are periodically repeated. Therefore, each system has the same probability densities as its neighbours. The scheme is in Figure 6.2.

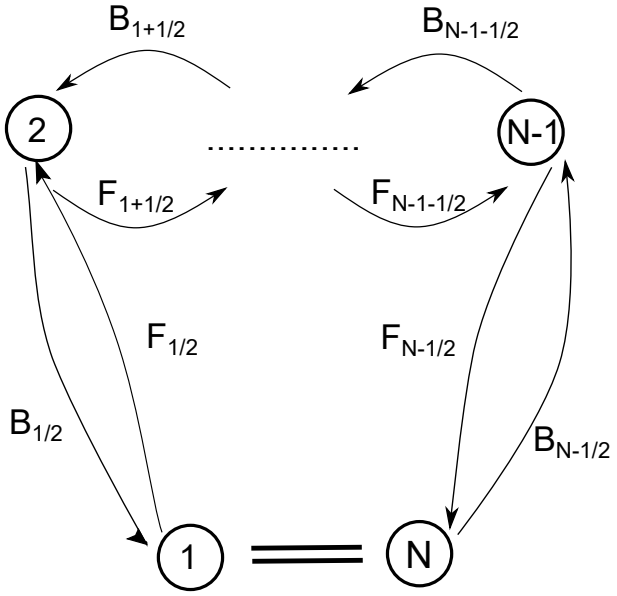

Figure 6.2: Scheme of periodic boundary condition of the WPE algorithm.

The second, called absorbing conditions, assumes that myosin head can go out of the studied domain never return inside. The situation is similar to a rupture on a swing ride. The seat is out of the fairground amusement and never can return there just by itself, it needs a repair.

The usage of this condition for numerical analysis without any normalisation condition is quite tricky. Nobody can tell if the decrease in a probability is given by this boundary condition or by numerical integration method. Its scheme is shown in Figure 6.3.

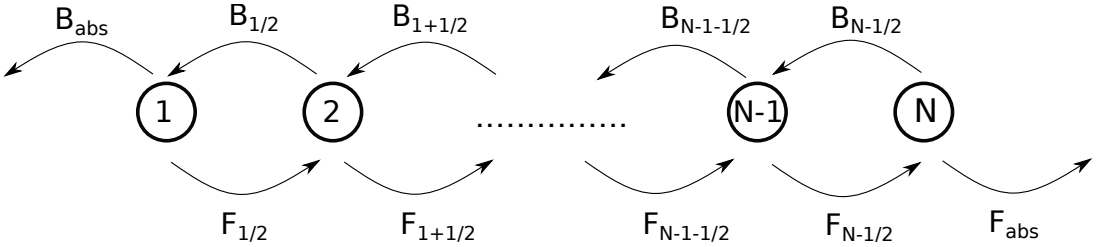

Figure 6.3: Scheme of absorbing boundary condition of the WPE algorithm.

The last possible boundary condition is called reflecting one. It means if the myosin head goes to the boundary, The head returns to the domain of interest. It is like the reflection in a mirror. In other words, it goes back like a yoyo in its lowest position.

This boundary condition can help with determining the total probability decrease source in case of absorbing boundary conditions.

The scheme of reflecting boundary condition is in Figure 6.4.

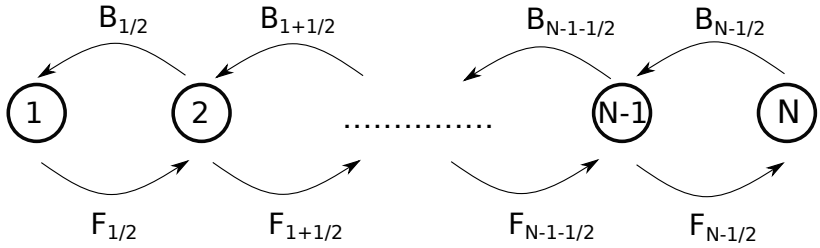

Figure 6.4: Scheme of reflecting boundary condition of the WPE algorithm.

Chapter 7

Three state model of myosin II

In 1999, a three-state model of myosin II was introduced in Ref. [25] and further developed in articles [27, 128]. The last mentioned model is based on an ensemble approach. Authors call these mechanochemical states the unbound (motor is loaded with ADP and P), the weakly-bound (myosin is bent to the actin filament) and the post-power-stroke, see Figures7.1 and 7.2. Ref. [27] uses transition rates based on Ref. [128] as follows: The transitions between the unbound and the weakly-bound is $k_{12} \simeq 40\,\mathrm{s}^{-1}$ and $k_{21} \simeq 2\,\mathrm{s}^{-1}$, respectively. Between the weakly-bound and the post-power-stroke state was determined similarly for both directions $k_{23} \simeq k_{32} \simeq 1 \cdot 10^3\,\mathrm{s}^{-1}$. The last step is irreversible and can be done from the post-power-stroke state to the unbound with the rate

$$k_{31}(x) = 80 \exp\{-k_m(x+d)/F_0\}, \tag{7.1}$$

where $k_m \simeq 2.5 \cdot 1 \cdot 10^{-3}\,\mathrm{Nm}^{-1}$ is the spring constant of myosin neck linkers. These linkers are schematically shown in Figure 7.2. The parameter $d \simeq 8\,\mathrm{nm}$, which corresponds to a length of the myosin power-stroke. The force $F_0 = 12.6\,\mathrm{pN}$ corresponds to the motor inside load.

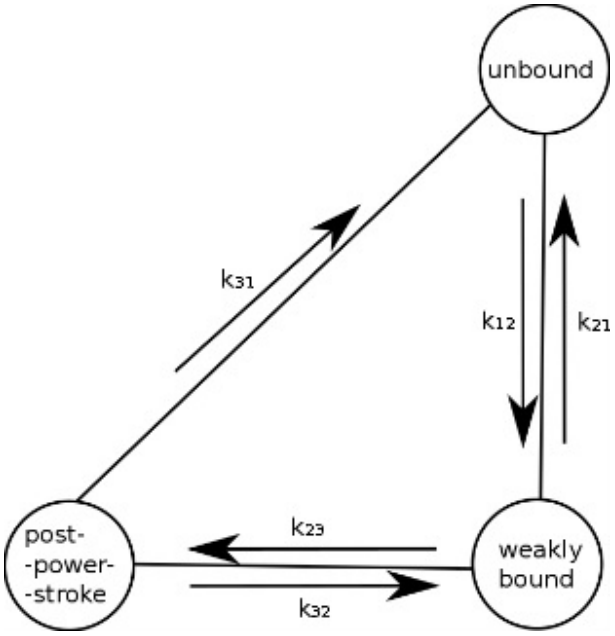

Figure 7.1: Mechanochemical states of myosin II molecular motor used in the three-state model with possible transitions between them. Adapted from [27].

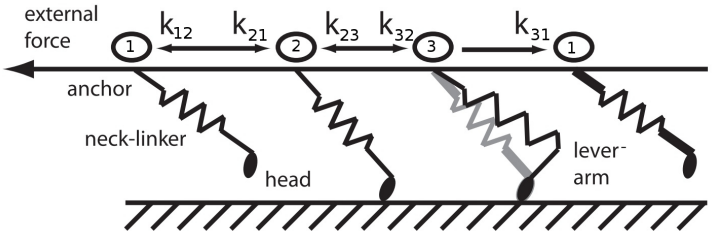

Figure 7.2: Scheme of mechanochemical states of myosin II molecular motor as springs. The unbound state is denoted as 1, the weakly-bound state as 2, and the post-power-stroke as 3. Adapted from [27].

This Erdmann's model [27] serves as an inspiration to this thesis. From this model, only the myosin head movement's discretisation is taken (including the irreversible transition from the post-power stroke state to the unbound one). I base my model on the Fokker-Planck equation (3.31) which is in a set with its two clones (one equation for each state) connected via transition rates k_{ij} and k_{ji} as follows

$$\frac{\partial \rho_i}{\partial t} = \frac{D}{k_B T}\frac{\partial}{\partial x}\left(\frac{\partial V_i}{\partial x} - F_{Load}\right)\rho_i + D\frac{\partial^2 \rho_i}{\partial x^2} + \sum_{j=1}^{3} k_{ji}\rho_j - \sum_{j=1}^{3} k_{ij}\rho_i \,. \tag{7.2}$$

The myosin head movement is controlled by an action potential, $V_i(x)$, and applied load force, F_{Load}, and the amplitude ΔG in $\mathrm{k_B T}$ units representing the energy derived from one ATP hydrolysis [16], in the Fokker-Planck framework. This is adjusted according to the meaning of each state considered in the model. The unbound state is represented by a constant potential, which equals zero in the model. The other potentials are given by the Fourier series FS,

$$V_2^{FS}(\Delta G, x) = \quad \Delta G\left(\sin\frac{2\pi x}{L} - 0.5\sin\frac{4\pi x}{L} + 0.3\sin\frac{6\pi x}{L}\right), \tag{7.3}$$

The Fourier series is often used for ratchet models in the Fokker-Planck framework [16, 133]. There are only two states models (constant and pure Fourier series). For this reason, I add the third potential. Its definition comes from an idea of the myosin head moving with actin filament, which changes the actin-binding site position. This assumption allows me to define the post-power stroke potential in two way.

The easiest way is only to reverse the potential for the weakly-bound state, i.e.

$$V_3^{FS}(-\Delta G, x) = -\Delta G\left(\sin\frac{2\pi x}{L} - 0.5\sin\frac{4\pi x}{L} + 0.3\sin\frac{6\pi x}{L}\right) \tag{7.4}$$

This set of potentials is in Figure 7.4.

The second version of the post-power stroke potential in this thesis as well. It uses the stroke-distance d

$$V_3^{FS}(\Delta G, x+d) = \quad \Delta G\left(\sin\frac{2\pi(x+d)}{L} - 0.5\sin\frac{4\pi(x+d)}{L} + 0.3\sin\frac{6\pi(x+d)}{L}\right). \tag{7.5}$$

This set is shown in Figure 7.5

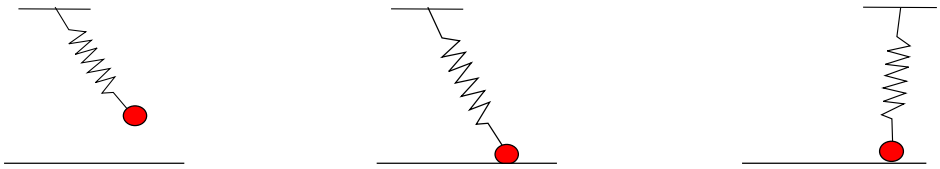

(a) The unbound state *(b) The weakly-bound state* *(c) The post-power stroke state*

Figure 7.3: A schematic representation of three-state model of the myosin head (red ellipse) in relation to the actin filament (long black line). In unbound state, Figure 7.3a, the myosin head is detached from the actin filament, and the myosin neck (spring) is relaxed. In the weakly-bound state, Figure 7.3b, the myosin head is touching actin filament. The myosin neck is stretched. In the post-power state, Figure 7.3c, the myosin moved together with the actin filament.

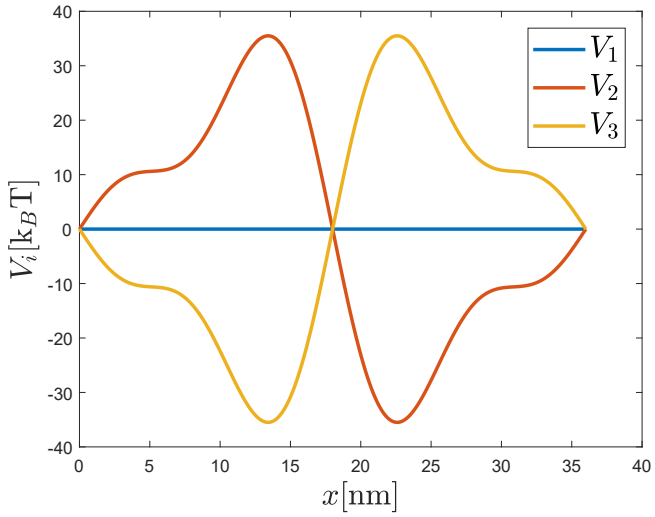

Figure 7.4: The potentials for the unbound state (V_1), the weakly-bound state (V_2) and the post-power stroke (V_3), respectively.

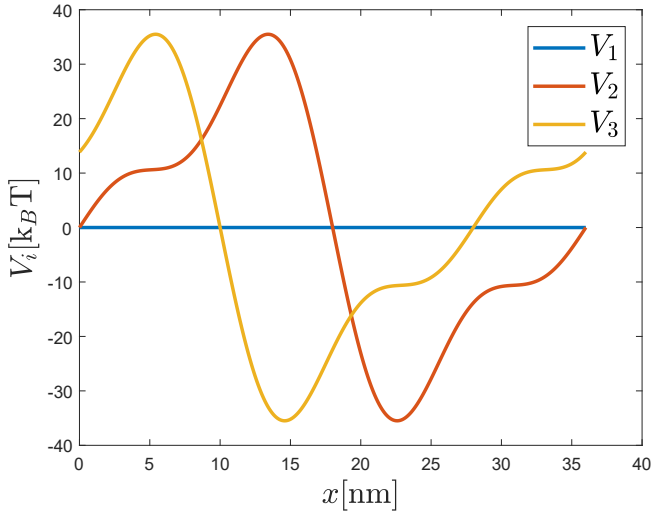

Figure 7.5: The potentials for the unbound state (V_1), the weakly-bound state (V_2) and the post-power stroke (V_3), respectively. The potential V_3 has its alternative form according to Equation (7.5).

Chapter 8

Condensation of states

In Section 2.3, I describe some possibilities of how to myosin continuous cycle divide into several chemo-mechanical states. It makes comparable results with different models harder. It also makes putting experimentally obtained data as an input to the model more difficult.

The solution of putting experimental data to the model is by condensation of model states. Ref. [136] introduced condensation of five states into two. I innovate the procedure for obtaining the three-state model of myosin head movement. Thus, it can be considered as the method modification.

The most elementary procedure's assumption is to have more states for the experimental data than for the numerical model.

Let's assume to have myosin cycle, see Figure 8.1, as follows [136]. As the first step is considered myosin bounded to actin filament in the presence of adenosine diphosphate and free phosphorus (AMDP). In the next phase, the phosphorus is released (AMD). The third step is bounding adenosine triphosphate molecule (AMT), which causes releasing from actin filament (MT). The molecule of ATP hydrolyses to adenosine diphosphate (ADP) and free phosphorus (P) and the state is AMDP again. It means the cycle is over.

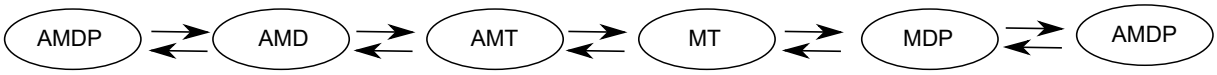

Figure 8.1: Myosin chemo-mechanical cycle according to [136]. A stands for actin, M for myosin, D for adenosine diphosphate and T for triphosphate, respectively. P denotes free phosphorus. Arrows are representing transitions rates between states. The notation is inspired by [44].

I chose the three states model as the myosin head cycle in my thesis, see Chapter 7. The states are the unbound, the weakly-bound and the post-power stroke. Figure 8.2 shows the connection between these two models.

The procedure's key point is to determine helpful ending points in the original cycle to condensed one. In this case, they are the states denote in Figures 8.1 and 8.2 as MDP ($2'$) and AMD ($5'$). In the mathematical description, they are coded only by numbers. Transition rates k have its index according to the lower number of the state. In anticlockwise cases, there is in upper index sign minus moreover.

These approximations give the transition rates between the unbound state and weakly-bound state, k_{12} and k_{21}

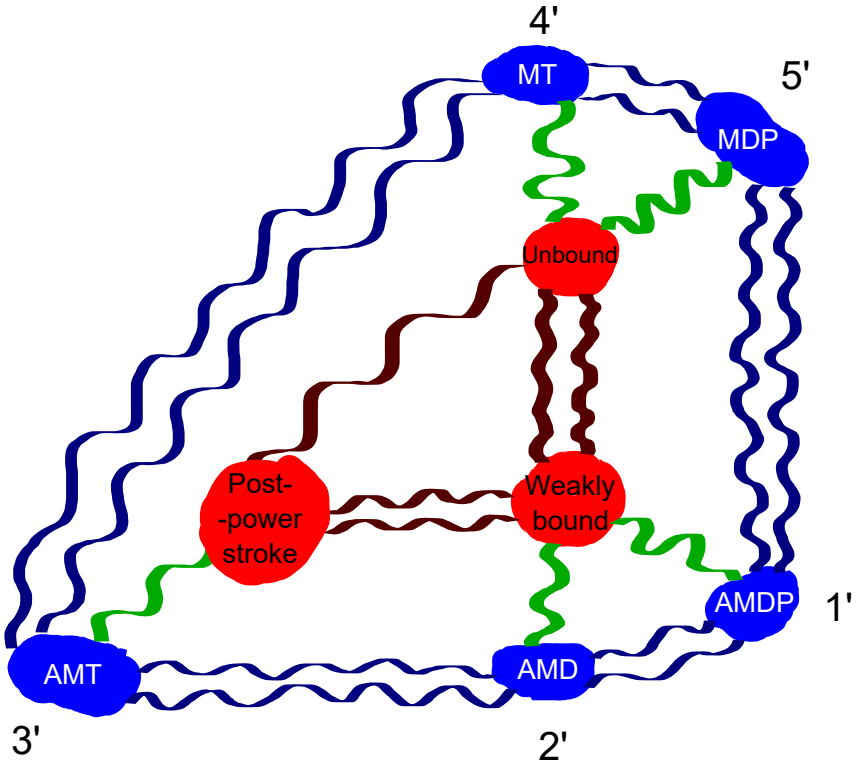

Figure 8.2: The connection between the original five states model from [136], see Figure 8.1 and the three states model, see Figure 7.1 is denoted by green ribbons. Dark red ribbons stands for transitions rates in the three states model and dark blue in the five states model, respectively.

$$\frac{1}{k_{12}} \approx \frac{1}{k_{5'}} + \frac{1}{k_{1'}} \tag{8.1}$$

$$\frac{1}{k_{21}} \approx \frac{1}{k_{5'}^{-}} + \frac{1}{k_{1'}^{-}}. \tag{8.2}$$

Similar relations is possible to obtain for transitions between the post-power stroke and unbound state, but there is a small catch. The transition rate k_{13} is forbidden. To solve this issue, the transition k_{31} is defined by a difference of these condensed rates

$$\frac{1}{k_{31}} \approx \left(\frac{1}{k_{3'}} + \frac{1}{k_{4'}}\right) - \left(\frac{1}{k_{3'}^{-}} + \frac{1}{k_{4'}^{-}}\right) \tag{8.3}$$

This difference is not shown in the article [136] and thus this is an innovation.

Due to the identification AMT state as the post-power stroke state the rates between AMD and AMT states are kept as they are.

$$k_{23} = k_{2'}, \tag{8.4}$$

$$k_{32} = k_{2'}^{-}. \tag{8.5}$$

This condensation process allows including dependences of different ion concentrations from the literature to the model. These relations were not found in the available sources for the three-state model.

Chapter 9

Position determination

The Fokker-Planck equation predicts chemo-mechanical state and position via probability density $\rho(x,t)$. Imagine, that a control mechanism, which is in the muscle cell [73] (the demon), needs to locate "precise" position (and state of the myosin head) in time $t = t_m$. Here, I present a simple numerical prediction of the localisation of the head. However, this prediction influences the next evolution of the system, and it is connected with mutual information production and generation of relative entropy as well.

I presume in this localization model, the prediction is influenced by an error in Gaussian form

$$\rho_e(x|\tilde{x}) \propto \exp\left[-\frac{(x-\tilde{x})^2}{\sigma^2}\right], \tag{9.1}$$

where $\tilde{x}$ is mean value of the distribution and σ is called standard deviation[1]. The Gaussian form is normalised to 1, i.e.

$$\int \rho_e(x|\tilde{x})\mathrm{d}x = 1\,. \tag{9.2}$$

Random number generator provides the mean value of the error (if not said otherwise). The used generator is in MATLAB software. The precise algorithm of the determination is as follows. The generator provides a number in interval <0;1> with a uniform distribution. This interval comes from the definition of probability [141]. This generated number corresponds with the cumulative probability distribution value, see Figure 9.1. Then, there is a crucial step to assign the position along axis x (actin filament). The inversion of the cumulative probability function does it. The generator's single number determines the mean value of the error distribution and the actual chemo-mechanical state precisely due to the normalisation condition for all three chemo-mechanical states.

The prediction allows to continue in the evolution according the Fokker-Planck equation with a new initial condition. I determine the new initial condition ρ_{ini} proportional to intersection of the output of the Fokker-Planck equation in time t_m, i.e. $\rho(x,t_m)$, and the prediction error $\rho_e(x|\tilde{x})$, see Figure 9.2. Thus,

$$\rho_{ini}(x) \propto \rho(x,t_m) \cap \rho_e(x|\tilde{x})\,. \tag{9.3}$$

The sign of proportionality is here because of the assumption of certainty of the presence of the

[1] Many forms how to express Gaussian distribution exists. Some of them have in denominator inside the exponential function "$2\sigma^2$".

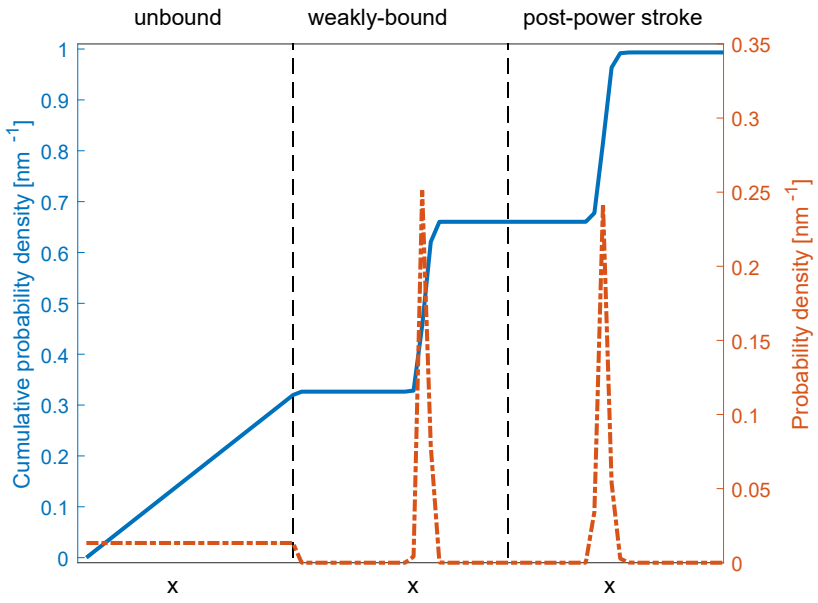

Figure 9.1: Illustrative total cumulative probabilities density distribution function (blue line). The dashed black line denotes border between two chemo-mechanical states. The red lines stands for the probability density.

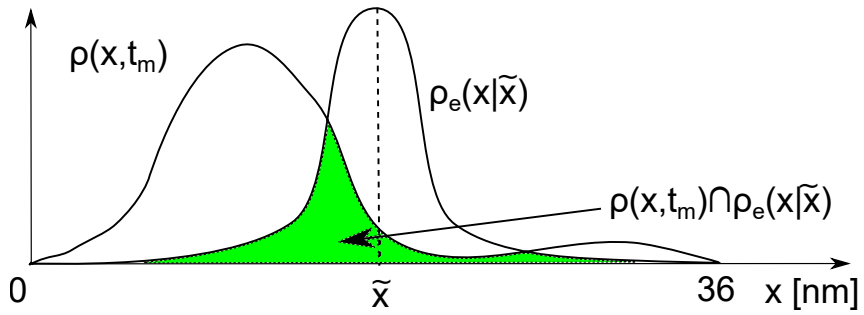

Figure 9.2: The intersection of prediction $\rho(x, t_m)$ and "measured" probability density $\rho(x|\tilde{x})$, respectively. Their intersection serves as a shape to next initial condition of a new simulation of measurement. To have initial condition itself, it is necessary to multiply it by its partition function due to keeping the total probability equal to 1.

myosin head in the interval. It requires normalization condition

$$\int \rho_{ini}(x)\mathrm{d}x = 1\,. \tag{9.4}$$

Hence, it is necessary to multiply it by its partition function.

This approach corresponds with the Bayes theorem where ρ_{ini} and $\rho_e(x|\tilde{x})$ serves as conditional probabilities and partition function can be called marginal probability in statistical terminology. Moreover, in Bayesian theory $\rho(x, t_m)$ is called prior [17].

This change from $\rho(x, t_m)$ to $\rho_{ini}(x)$ provides a opportunity to calculate relative entropy (Kullback-Leiber distance) and mutual information.

Relative entropy between two distributions is generally defined as follows [21].

$$\mathcal{D}(q_1||q_2) = \int q_1 \ln \frac{q_1}{q_2}\mathrm{d}x. \tag{9.5}$$

To this definition belongs conditions:

$$0 \ln \frac{0}{q_2} = 0 \quad \forall q_2 \tag{9.6}$$

$$q_1 \ln \frac{q_1}{0} = \infty\,. \tag{9.7}$$

It quantifies inefficiency of assumption q_2 if the true distribution is q_1. Relative entropy is always positive [111], non-symmetrical function. It means $\mathcal{D}(q_1||q_2) \neq \mathcal{D}(q_2||q_1)$, in general case. If $\mathcal{D}(q_1||q_2) = \mathcal{D}(q_2||q_1)$, it indicates relative entropies are equal to zero and $q_1 = q_2$ [21]. Relative entropy of $\rho(x, t_m)$ and $\rho_{ini}(x)$ is

$$\mathcal{D}(\rho_{ini}(x)||\rho(x, t_m)) = \int \rho_{ini}(x) \ln \frac{\rho_{ini}(x)}{\rho(x, t_m)}\mathrm{d}x. \tag{9.8}$$

Mutual information I, on the other hand, is symmetrical function. It definition is as follows

$$I = \iint \rho(x, y) \log \frac{\rho(x, y)}{\rho(x)\rho(y)}\mathrm{d}x\mathrm{d}y \tag{3.40}$$

With assumption of independence of variables $\rho(x, t_m)$ and ρ_{ini}, the definition equation become

$$I = \iint (\rho(x, t_m) \cap \rho_{ini}(y)) \ln \frac{\rho(x, t_m) \cap \rho_{ini}(y)}{\rho(x, t_m)\rho_{ini}(y)}\mathrm{d}x\mathrm{d}y\,. \tag{9.9}$$

This defined mutual information describes relation between the distribution given by final time step of evolution according the Fokker-Planck equation $\rho(x, t_m)$ and new initial condition given by $\rho_{ini}(y)$. This definition can be modified to characterise relation between other probability densities as well.

Part IV

Results

Chapter 10

Comparison of the analytical and the numerical solution of the Fokker-Planck equation and diffusion equation

The comparison between analytical and numerical solution helps with verification process. When the data are close to each other it is possible to say, the model working in the desired way. Because an analytical solution of the Fokker-Planck equation is not trivial [23], two simplified forms of the equation

$$\frac{\partial \rho}{\partial t} = \frac{D}{k_B T}\frac{\partial}{\partial x}\left(\frac{\partial V}{\partial x} - F_{Load}\right)\rho + D\frac{\partial^2 \rho}{\partial x^2} \tag{3.31}$$

were chosen.

The first one is the stationary version

$$0 = \frac{D}{k_B T}\frac{\partial}{\partial x}\frac{\partial \phi}{\partial x}\rho + D\frac{\partial^2 \rho}{\partial x^2}. \tag{5.5}$$

The second version of the Fokker-Planck equation is with "turn off" effective potential ϕ. This case is called the diffusion equation

$$\frac{\partial \rho}{\partial t} = D\frac{\partial^2 \rho}{\partial x^2}. \tag{5.3}$$

Their analytical solution is in Chapter 5.

The difference between analytical $\rho_{ana}(x)$ and numerical $\rho_{num}(x)$ solution is shown by parameters e_a for absolute error

$$e_a = |\rho_{ana}(x) - \rho_{num}(x)| \tag{10.1}$$

and e_r for relative error. It is determined as

$$e_r = \max \frac{e_a}{\rho_{ana}} \cdot 100\,. \tag{10.2}$$

The numerical solution of the Fokker-Planck equation is made by the WPE algorithm (see Chapter 6) and MATLAB solver `ode15s` (time evolution) or the method of the Lagrange multipliers (stationary solution).

Lagrange multipliers extends the equation produces by the WPE algorithm $M \cdot p^s = 0$ by condition to sum of stationary probability p^s to equal 1 and by a Lagrange multiplier λ [106] to set of equations

$$\begin{pmatrix} M & \mathbf{1} \\ \mathbf{1}^{\mathcal{T}} & 0 \end{pmatrix} = 0 \tag{10.3}$$

where $\mathbf{1}$ is a matrix of ones with size of p^s and $\mathcal{T}$ denotes transposition of matrix.

For all simulations results shown in this chapter, it is necessary to determine parameters D and k_BT. The diffusion coefficient is set $D = 5.47 \cdot 10^7\,\mathrm{nm}^2/\mathrm{s}$. The value is set according to Refs [16, 136], which studies myosin II molecular motor. The parameter k_BT is taken from Ref. [136], too. Thus, it is $k_BT = 4.1\,\mathrm{pN/nm}$. Parameter L corresponds to characteristic length between two actin bounding places, which is $L = 36\,\mathrm{nm}$.

10.1 Stationary Fokker-Planck equation

The analytical solution of stationary Fokker-Planck equation is according to Section 5.1

$$\rho_{ana} = \frac{\exp\left(-\frac{V - x \cdot F_{load}}{k_B T}\right)}{\int \exp\left(-\frac{V - x \cdot F_{load}}{k_B T}\right) \mathrm{d}x} \,. \tag{5.11}$$

Here, I use periodic boundary condition for analytical and numerical approach. I work with two different load forces $F_{Load} = 0$ and $10\,\mathrm{pN}$ to show behaviour of the system.

The chemical potential V is the same for both cases. The Fourier series determine the used chemical potential as follows

$$V = \quad \Delta G \left(\sin \frac{2\pi x}{L} - 0.5 \sin \frac{4\pi x}{L} + 0.3 \sin \frac{6\pi x}{L} \right). \tag{7.3}$$

The resulting effective potentials $\phi = V - x \cdot F_{Load}$ for $F_{Load} = 10\,\mathrm{pN}$ as well as $F_{Load} = 0\,\mathrm{pN}$ are shown in Figure 10.1.

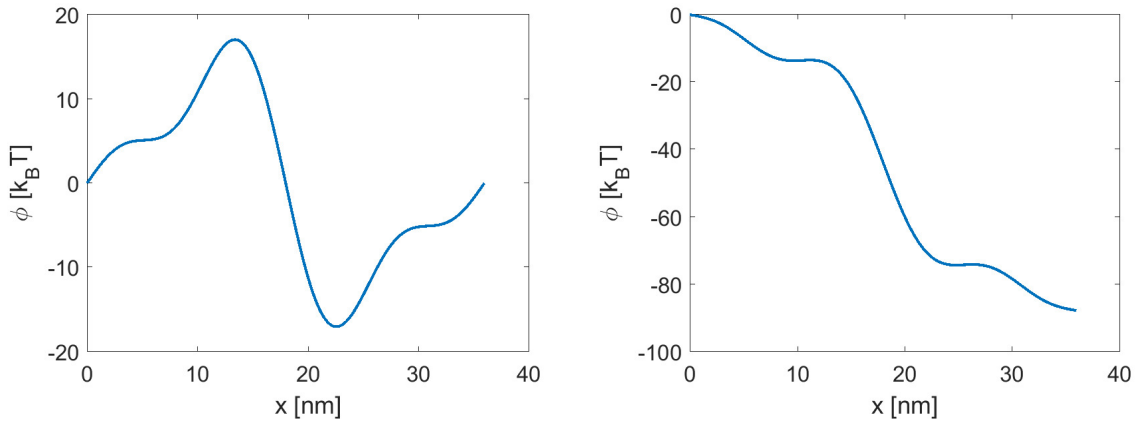

Figure 10.1: Effective potential ϕ with $F_{Load} = 0\,\mathrm{pN}$ (left) and $F_{Load} = 10\,\mathrm{pN}$ (right), respectively.

For both cases, numerical solution are almost identical to the analytical one, see Table 10.1 and Figure 10.2. The differences are numerical errors, which is a good result.

Table 10.1: Maximum absolute (max e_a) and maximum relative errors (e_r) between analytical and numerical solution of stationary Fokker-Planck equation for loads $F_{Load} = 0\,\mathrm{pN}$ and $10\,\mathrm{pN}$.

	0 pN	10 pN
max e_a [nm^{-1}]	$1.37{\cdot}10^{-14}$	$1.73{\cdot}10^{-14}$
e_r [%]	$2.74{\cdot}10^{-12}$	$2.22{\cdot}10^{-12}$

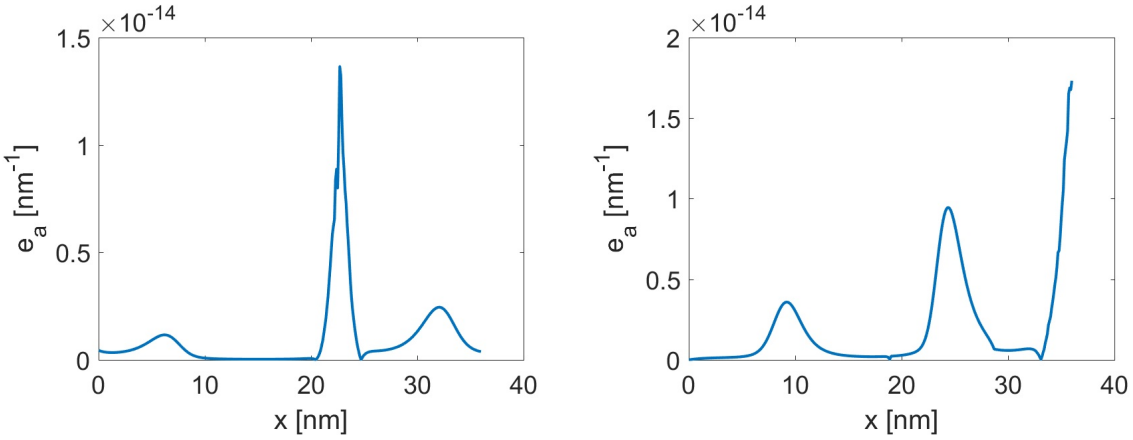

Figure 10.2: The difference between the stationary analytic solution and numerical solution e_a with $F_{Load} = 0\,\mathrm{pN}$ (left), and $F_{Load} = 10\,\mathrm{pN}$ (right), respectively. The maximum difference in in order of $1 \cdot 10^{-14}\,\mathrm{nm}^{-1}$. The agreement is very good.

10.2 Diffusion equation

The diffusion equation is here as a time-dependent simplification of the Fokker-Planck equation (without the term of the effective potential) to verify the model ability to describe the Fokker-Planck equation correctly.

Here, I use the diffusion equation with zero Neumann boundary conditions

$$\left.\begin{aligned}\frac{\partial \rho(0,t)}{\partial x} &= 0\\ \frac{\partial \rho(L,t)}{\partial x} &= 0\end{aligned}\right\} \forall t\,. \tag{10.4}$$

I compare this analytical solution with the diffusion equation numerical solution given by reflecting boundary conditions described in Chapter 6.1. Both kinds of boundary conditions do not allow any transition from the domain.

The initial condition in the comparison is given by

$$\rho(0,x) = \left(1 - \cos\frac{2\pi x}{L}\right)/L\,. \tag{10.5}$$

It produces solution as follows

$$\rho(t,x) = 1/L - \left\{\exp\left[-\left(\frac{2\pi}{L}\right)^2 Dt\right]\cos\frac{\pi x}{L}\right\}/L\,. \tag{10.6}$$

The result of the analytical solution is in Figure 10.3. Due to low errors between the numerical and analytical solution, the numerical solution is not shown. These errors are visible in Figures 10.4 and 10.5. Figure 10.4 shows the maximum error in each time step. The maximum of the absolute error e_a in all computed times is slightly higher than $1.2 \cdot 10^{-4}\,\mathrm{nm}^{-1}$. The maximum of relative error in all time is slightly lower than 2.5%. Figure 10.5 shows whole evolution of the relative error. It helps to find where these methods produce different results. The biggest difference is in the first time step of the evolution close to the boundaries.

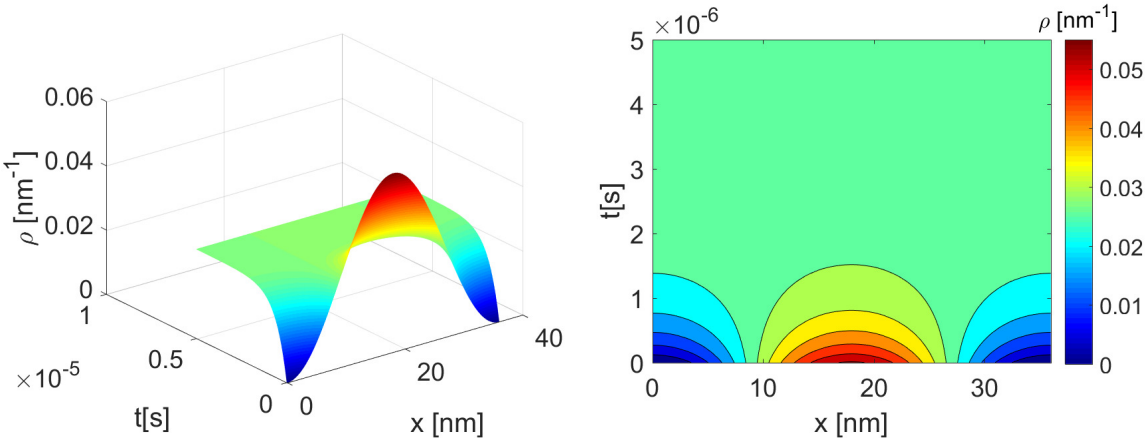

Figure 10.3: Analytical solution of diffusion equation with reflecting boundaries.

All found errors are small enough to say the numerical method provides sufficiently good results.

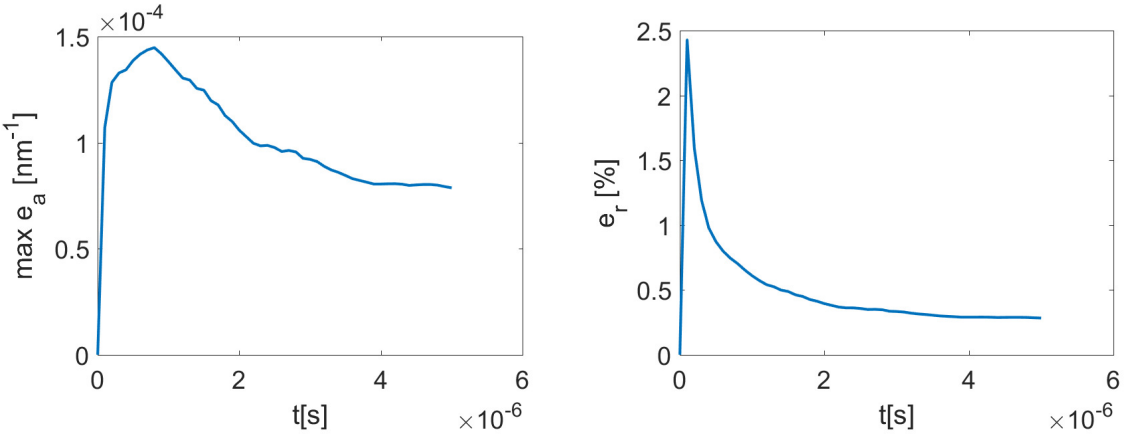

Figure 10.4: The maximum absolute $\max e_a$ *and the relative error* e_r *between analytical and numerical solution of diffusion equation with reflecting boundaries, respectively.*

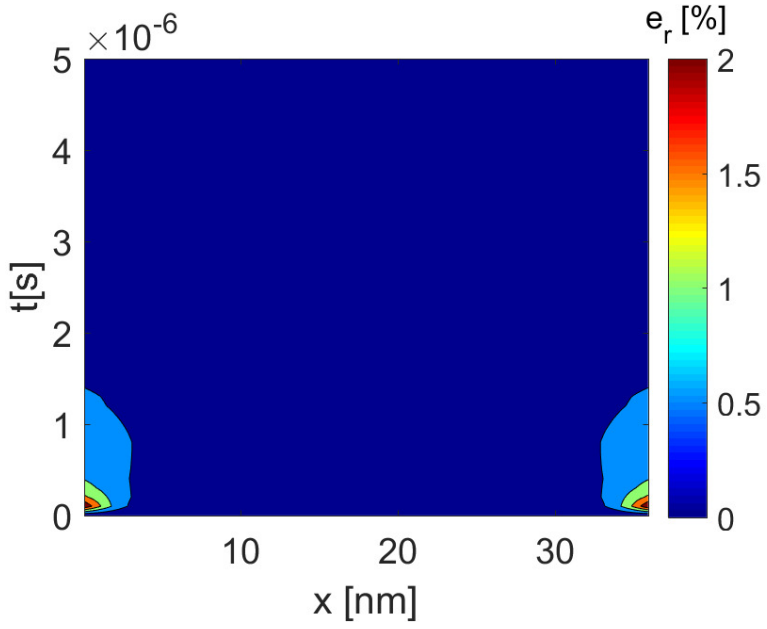

Figure 10.5: The time and spatial evolution of relative error e_r *between analytical and numerical solution of diffusion equation with reflecting boundaries.*

Chapter 11

Influence of boundary conditions and barriers

The absorbing boundary condition's influence is studied in [13] and of barriers in [9], respectively. The first Ref. focuses on the transition path time statistics, and the second on finding exact solutions of distribution of several different properties with symmetric barriers and wells. For example, one of the properties is the first-time passage. These recent articles prove this is one of the current science problems in the nanoscale world.

In this chapter, I study the influence of different boundary conditions (reflecting, absorbing) on the total probability in different times to the classical three states model described in Chapter 7 by solving the WPE algorithm, see Chapter 6, and MATLAB solver `ode15s`. Thus, it is necessary to omit the normalising condition to the Fokker-Planck framework's simulation results. Moreover, the effect of the energy barrier is studied, as well. The energy barrier has a meaning of the spring energy in the myosin neck. The energy prevents the myosin head to go out of the domain. The definition of the energy E_m is defined as follows

$$E_m = \frac{1}{2} k_m (\delta x)^2 \,. \tag{11.1}$$

where k_m is the spring stiffness. Its value is $2.5 \cdot 10^{-3}\,\mathrm{Nm}^{-1}$ [27]. The parameter δx is

$$\delta x = x - L/2 \tag{11.2}$$

where x is spatial variable and must obey $x \in [0; L]$. Thus, this is a standard definition of the energy in a spring [140].

I test several variants of potential described in details in Chapter 7. All potentials can be written as a sum of Fourier series FS and myosin neck energy E_m.

$$FS(\Delta G, x) = \Delta G \left(\sin \frac{2\pi x}{L} - 0.5 \sin \frac{4\pi x}{L} + 0.3 \sin \frac{6\pi x}{L} \right) , \tag{11.3}$$

The Fourier series FS has two main parameters: $x \in [0; L]\,\mathrm{nm}$, where $L = 36\,\mathrm{nm}$ [44]. The spatial variable x can be shift by constant d which is the stroke distance. According to [44], it is $d = 8\,\mathrm{nm}$. The second parameter, $\Delta G = 12\,\mathrm{k_B T}$, is produced energy by ATP hydrolysis. Its value is set based on article [16]. There it is set $\Delta G_{Chen} = 25\,\mathrm{k_B T}$. However, this article is not concerning experimental articles [57, 58], where is said one ATP molecule provides energy

enough to several myosin steps. Every used options of potentials are written in Table 11.1. Their visualisation is shown in Appendix C.

Table 11.1: Different cases of potentials. The Fourier series FS is written in Equation (11.3). *E_m is myosin neck energy defined in Equation* (11.1). *Parameter d is the stroke distance. Energy produced by ATP hydrolysis is denoted as ΔG.*

	V_1	V_2	V_3
case 1	0	$FS(\Delta G, x)$	$FS(-\Delta G, x)$
case 2	E_m	$FS(\Delta G, x) + E_m$	$FS(-\Delta G, x) + E_m$
case 3	0	$FS(\Delta G, x) + E_m$	$FS(-\Delta G, x) + E_m$
case 4	0	$FS(\Delta G, x)$	$FS(\Delta G, x + d)$
case 5	E_m	$FS(\Delta G, x) + E_m$	$FS(\Delta G, x + d) + E_m$
case 6	0	$FS(\Delta G, x) + E_m$	$FS(\Delta G, x + d) + E_m$

The model has three states. Thus, there are some transition rates between these states. They are well-described in Chapter 7. For a better overview, I summarise them in Table 11.2.

Canonical distribution (see Section 3.3.2) is used as a base of initial condition for the computation. For purposes of the Fokker-Planck equation framework, it is necessary to make a transition from one given particle r to one given state i. Moreover, the probability of the given particle p_r is in equation

$$p_r = Z^{-1} \exp(-\beta E_r) \tag{3.7}$$

replaced by probability density function ρ_i, where the index i stands for state of myosin molecular motor according to Chapter 7. The state energy E_i is given by potential V_i, which is determined as

$$V_i = V_i^{FS} + E_m, \tag{11.4}$$

where the myosin neck energy is applied. Otherwise, $E_m = 0\,\mathrm{k_B T}$. Thus,

$$V_i = V_i^{FS}\,. \tag{11.5}$$

The initial condition has a form of if $\mathrm{k_B T}$ units are applied for the potentials

$$\rho_i(0, x) = Z^{-1} \exp(-\beta V_i)\,. \tag{11.6}$$

Table 11.2: Transition rates of the three-state model. States written in rows are starting ones i. The ending states j are written in columns. State 1 stands for the unbound state, state 2 for the weakly bound state and state 3 for the post-power stroke state, respectively. The values of transition rates k_{ij} are in s^{-1} units. Values are based on article [27]. N/A means "Not Available".

i \ j	state 1	state 2	state 3
state 1	N/A	40	*forbidden*
state 2	2	N/A	1000
state 3	$3.32 \cdot 10^{-16}$	1000	N/A

The partition function is set to fulfil the total probability equals to 1, i.e.

$$\int (\rho_1(0,x) + \rho_2(0,x) + \rho_3(0,x))\,\mathrm{d}x = 1\,. \tag{11.7}$$

Some other parameters are used as well. They are diffusion coefficient $D = 5.47 \cdot 10^7\,\mathrm{nm}^2/\mathrm{s}$ [16, 136] and product of thermodynamic temperature and Boltzmann constant $k_B T = 4.1\mathrm{pN/nm}$ [136]. There is also possibility of an external load F_{Load}. However, all shown results in this chapter have the load fixed to zero pico-Newtons.

11.1 Reflecting boundary condition

The reflecting boundary conditions should keep the total probability density equal to 1 by its definition. However, the results show (see Table 11.3) that the decrease can happen, and an additional condition is good to keep the value of total probability density normalised to one. It seems the only adding energy barriers to the edge for attached states (weakly-bound and post power stroke) is sufficient for keeping the simulation stable even longer than shown results – more than 10^{-2} s. Adding barriers to the unbound state does not affect the total probability of the simulations' maximum time. However, the change in potentials for the post-power stroke state can influence the decrease of the probability.

Table 11.3: The obtained total probability in different time steps with reflecting boundary conditions and with different potentials V_i. The description of single potentials for each case is shown in Table 11.1.

	Total probability obtained by numerical simulation in different times [10^{-4} s]					
Case of potential	5	15	30	50	75	100
Case 1	1.000	0.984	0.982	0.981	0.981	0.980
Case 2	1.000	1.000	1.000	1.000	1.000	1.000
Case 3	1.000	1.000	1.000	1.000	1.000	1.000
Case 4	1.000	0.996	0.994	0.992	0.992	0.992
Case 5	1.000	1.000	1.000	1.000	1.000	1.000
Case 6	1.000	1.000	1.000	1.000	1.000	1.000

11.2 Absorbing boundary condition

Absorbing boundary conditions cannot hold the total probability equal to 1 by its very nature. They allow myosin head to go out of the domain. However, the barriers added to the domain ends can prevent leaking out of the domain. Results are shown in Table 11.4.

Case 1 and Case 4, having no barriers, serve as a limit situation for absorbing boundaries. The post-power states' potential for these two cases are plot in Figure 11.1. This state is the only difference between these cases. Moreover, the change is sufficient to slow down the decrease. The biggest influence has adding barriers to the unbound state. In this variant, the probability keeps stable, and further research suggests these cases are very good at keeping non-zero total probability density for times longer than shown in Table 11.4. The effect continues longer than 10^{-2} s. Without these barriers for the unbound state (Cases 3 and 6), the sum of probability densities decreases equally.

Table 11.4: The obtained total probability in different time steps with absorbing boundary conditions and with different potentials V_i. The description of single potentials for each case is shown in Table 11.1.

	Total probability obtained by numerical simulation in different times [10^{-4} s]					
Case of potential	5	15	30	50	75	100
Case 1	1.000	0.314	0.148	0.054	0.015	0.004
Case 2	1.000	1.000	1.000	1.000	1.000	1.000
Case 3	1.000	0.666	0.665	0.664	0.662	0.661
Case 4	1.000	0.606	0.550	0.483	0.411	0.350
Case 5	1.000	1.000	1.000	1.000	1.000	1.000
Case 6	1.000	0.666	0.665	0.664	0.662	0.661

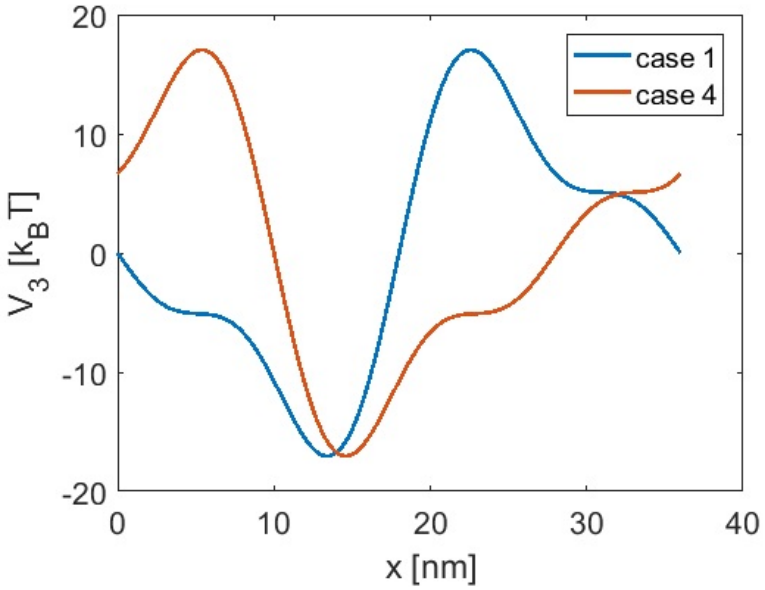

Figure 11.1: Potential V_3 for post-power stroke state in cases 1 and 4.

Reflecting boundary conditions provides a more stable sum of the total probability than absorbing ones. Thus, absorbing boundary conditions are not used to much in this thesis.

Chapter 12

Transition rates according to Arrhenius type equation and concentration of ATP

In this chapter, I modify the three-state model to accept ATP molecules' concentration with the Arrhenius equation's help. Other muscle contraction models often use the concentration of ATP [16, 84, 107]. However, this kind of three-state model of myosin head with irreversible transition is rare and with a lack of data concerning transition rates dependent on ATP concentration. Thus, I modify a procedure shown in [136], where a five-state model is simplified to a two-state model, and I produce the three-state model as shown in Chapter 8.

The Arrhenius equation describes how to evaluate transition rates in different temperatures or with different potential barriers. It is given by [44]

$$k = k_0 \exp\left(-\frac{\Delta G_{ab}}{k_B T}\right) \tag{12.1}$$

where k_0 is pre-exponential factor, and ΔG_{ab} is

$$\Delta G_{ab} = G_{activated\ state} - G_{base\ state}. \tag{12.2}$$

The energy $G_{base\ state}$ is in the initial state, and $G_{activated\ state}$ is the peak of the final state's energy barrier. Thus, ΔG_{ab} is Gibbs energy between the initial and final states.

This equation provides a standard means of how to deal with transition rates. Here, it allows to include the influence of the ATP concentration into the model. The concentration is vital for the muscle contraction [44].

An alternative version of the evaluation exists. It is by the external load F_{Load} which is applied to the myosin [136]. The equation is as follows

$$k = k_0 \exp\left(-\frac{dF_{Load}}{k_B T}\right), \tag{12.3}$$

where d is the power-stroke distance. This equation is used for states AMDP (the myosin head is connected to actin filament in presence of ADP and free phosphorus; in Chapter 8 denotes as 1') and AMD (the myosin head is connected to actin filament in presence of ADP only; in Chapter

8 denotes as 2') in the five-state model. The transition rate for the state AMT (myosin head is connected to the actin filament in presence of ATP; in Chapter 8 denotes as 3') is set according to Equation [136]

$$k_3' = k_{30}[ATP]\,. \tag{12.4}$$

It means this transition rate depends on $[ATP]$, i.e. the ATP concentration. I determine the backward transitions according to detail balance condition[1] [136]. The equation is as follows [133]

$$\frac{k_{ij}}{k_{ji}} = \exp\left(\frac{G_i(x) - G_j(x)}{k_B T}\right)\,. \tag{12.5}$$

Barriers G_i were set according to article [69], see Figure 12.1. However, these values are for a much more complicated model, which takes into account even some less probable states. There are eight states. Thus, I recommend experimental checking of the barrier values considering only three states of myosin head – unbound, weakly bound and post-power states.

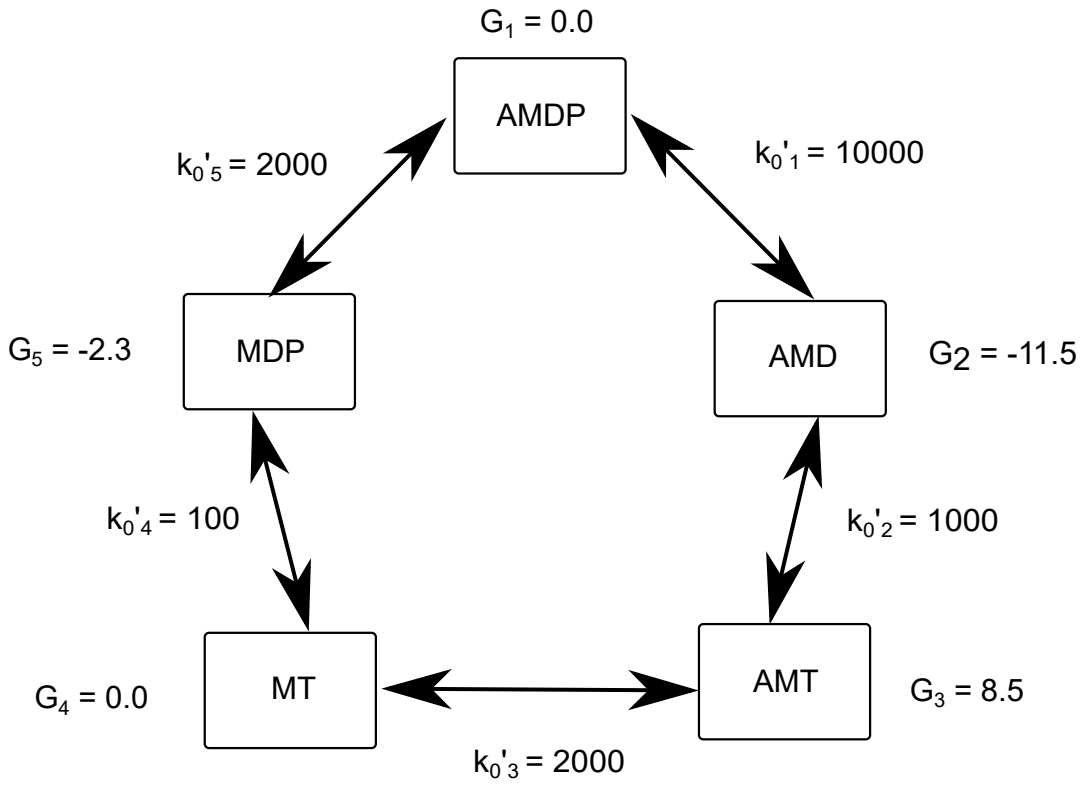

Figure 12.1: Transition rates between states of the five-state model of myosin and energy barriers these state. Values are taken from [136] and [69].

This modification of the five-state model produces transition rates values in the three-state model, depending on the ATP concentration parameter. Its value is $[ATP] \sim 0.1\,\mathrm{mMol}$. Values of transition rates are written in Table 12.1. These values vary from the three-state model's original values; see Table 11.2. The biggest difference is in the transition rate from the post-power stroke state (3) to the unbound state (1). The original model has this value in order of $1 \cdot 10^{-16}\,\mathrm{s}^{-1}$. However, my model increases this value to $71.44\,\mathrm{s}^{-1}$. This value variates for

[1] The difference between detail balance and classical balance is described in Appendix's Chapter B.

different $[ATP]$. It is increasing with a higher ATP concentration. This transition rate contains the ability to break the force that keeps the myosin head connected to the actin filament [78]. The dependence of the transition rate k_{31} on ATP concentration is shown in Figure 12.2. The increasing is very rapid for lower values of $[ATP]$, and it slows down for higher values of $[ATP]$. The growth reminds the saturation curve. It is logical that the next ATP concentration increase does not influence the rate and has to exist.

Table 12.1: Transition rates of the from five-state model modified to the three-state model without any external load. States written in the first rows are starting one i. The ending states j is written in columns. State 1 stands for the unbound state, state 2 for the weakly bound state and state 3 for the post-power stroke state, respectively. The concentration of ATP $[ATP] = 0.1\,mMol$. *The values of transition rates* k_{ij} *are in* s^{-1} *units. The transition rates are also dependent on the the amplitude of amplitude of the the potential barriers* ΔG *and* F_{load}*, respectively. Here, it is set be equal to* $\Delta G = 12\,k_BT$ *and* $F_{load} = 0\,pN$.

i \ j	state 1	state 2	state 3
state 1	N/A	1666.67	*forbidden*
state 2	200.52	N/A	1000.00
state 3	71.44	0.34	N/A

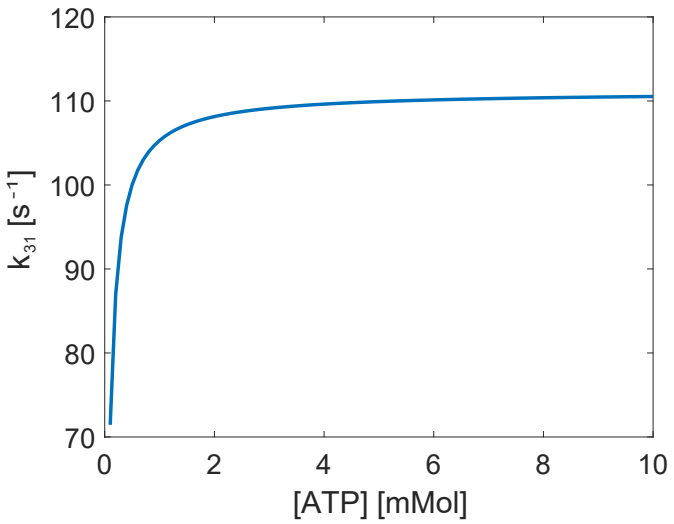

Figure 12.2: The dependence of transition rate from the post-power stroke state to the unbound one on ATP concentration.

The time evolution of the probability densities in all three states and its sum is shown in Figure 12.3. For these results, periodic boundary conditions are set with potentials denoted as 5 in Table 11.1, i.e. E_m for unbound state, $FS(\Delta G, x) + E_m$ for the weakly-bound state and $FS(\Delta G, x+d) + E_m$ for the post-power stroke state, $F_{Load} = 0\,\mathrm{pN}$. The initial condition is given by these potentials as

$$\rho_i(x, 0) = Z^{-1} \exp\left(-V_i + x \cdot F_{Load}\right) \tag{12.6}$$

where Z^{-1} is the normalisation factor to fulfil normalizing condition

$$\int \sum_i \rho_i(x,0)\mathrm{d}x = 1\,. \tag{12.7}$$

The transition rates decrease in the unbound state and the weakly-bound state. They increase in the post-power stroke state. However, the probability density for the unbound state is rising with higher ATP concentration. The rising is well visible in Figure 12.4a. The weakly-bound state is rising as well, see Figure 12.4b. A decrease is only in the post-power stroke state, which is visible in Figure 12.4c. This fact corresponds with the increasing transition rate k_{31} with rising $[ATP]$. These figures have different scales on vertical axes for better visibility of probability densities distributions.

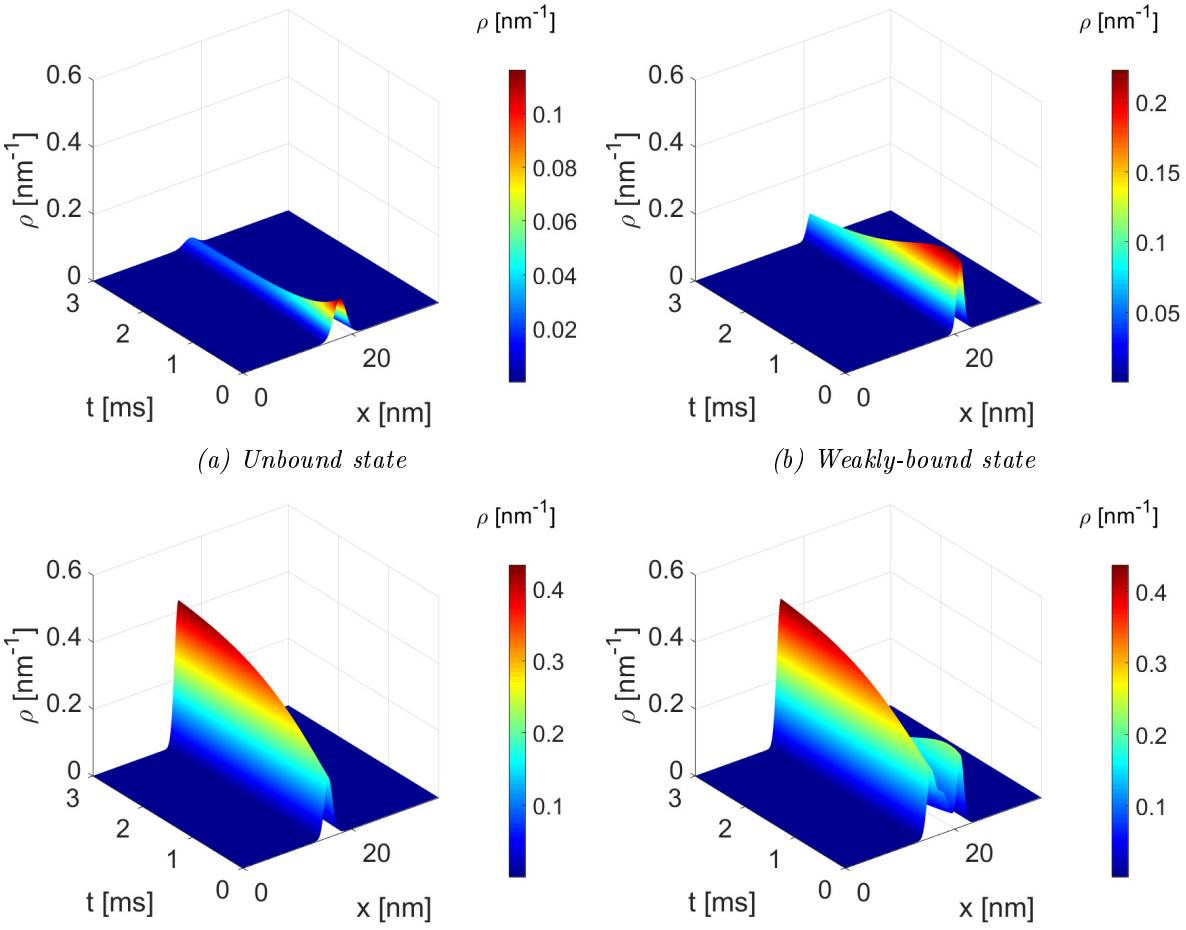

(a) Unbound state

(b) Weakly-bound state

(c) Post-power stroke state

(d) Total probability density (the unbound state, the weakly-bound state and the post-power stroke state summed together)

Figure 12.3: Probability densities distribution for the unbound state (a), the weakly-bound state (b),the post-power stroke state (c) and the total probability density (d) (normalized in every time step) for ATP concentration $[ATP] \sim 0.1\,mMol$. The shape is mainly influenced by potential for given state. The potential is given by E_m for unbound state, $FS(\Delta G, x) + E_m$ for the weakly-bound state and $FS(\Delta G, x + d) + E_m$ for post-power stroke state. The function FS stands for Fourier series given by the Equation (11.3).

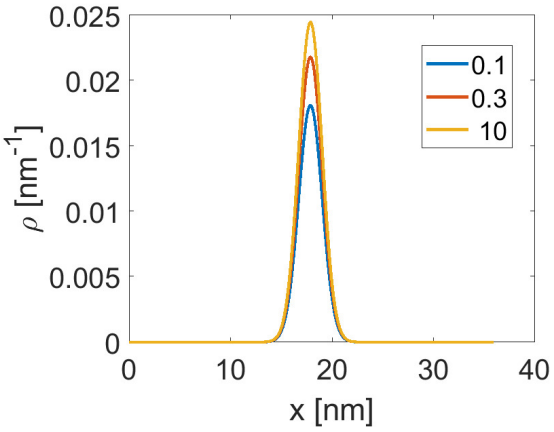

(a) Unbound state

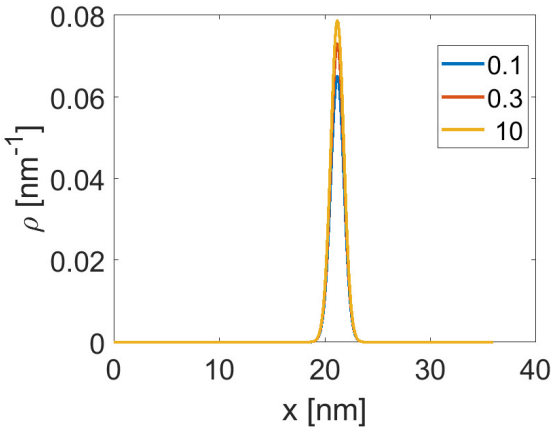

(b) Weakly-bound state

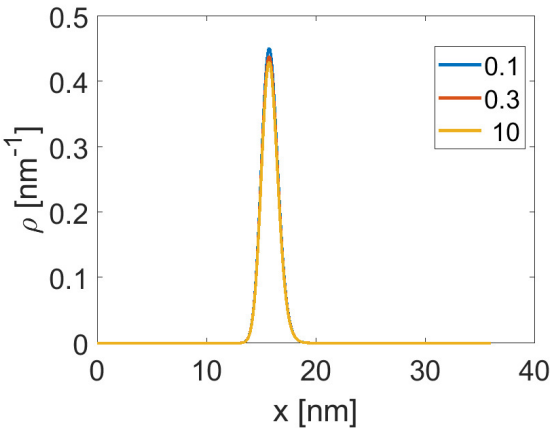

(c) Post-power stroke state

Figure 12.4: The probability density for the three-state model with different ATP concentrations (in mMol*) in time* $t = 3\,\text{ms}$.

12.1 Dependence on an external load

The probability density distribution is depended on an external load as well. As was mention before, some transition rates are determined with help of Equation

$$k = k_0 \exp\left(-\frac{dF_{Load}}{k_B T}\right) . \tag{12.3}$$

This is included to transition rates k_{12}, k_{21}, k_{23} and k_{32}. These dependences are shown in Figure 12.5. Minimum difference for small loads is observable in case of k_{21} (weakly-bound state to unbound state). This is caused by barriers which prevents entering to the considered state G_i given by balance condition, see Equation (12.5).

The time evolution is in Figures 12.6 and 12.7, where the F_{Load} is set to 0 and 5 pN, respectively. The different external load causes big changes in the shape and evolution of probability densities.

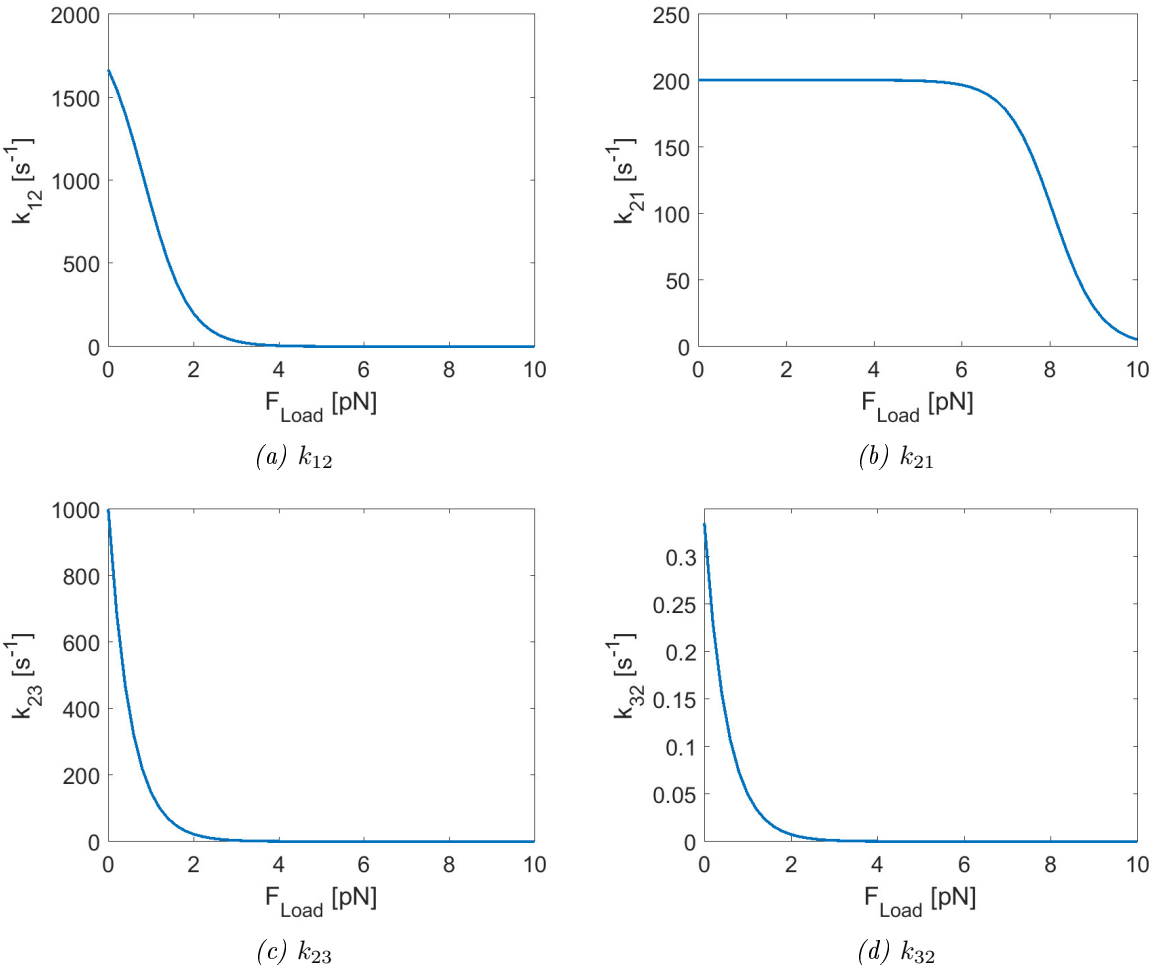

(a) k_{12} *(b)* k_{21} *(c)* k_{23} *(d)* k_{32}

Figure 12.5: Dependence of different transition rates given by the Arrhenius equation: (a)unbound to weakly-bound, b) weakly-bound to unbound, c) weakly-bound to post-power stroke and d) post-power stroke to weakly-bound) on the external load force F_{Load} *with* $[ATP] \sim 1\,mMol$ *[44] and* $\Delta G = 12\,\mathrm{k_B T}$.

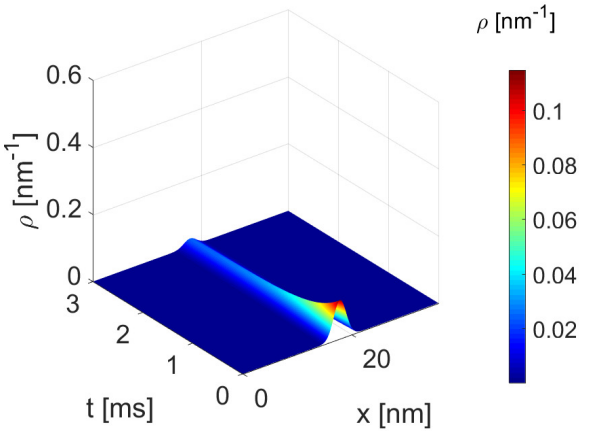

(a) Unbound state

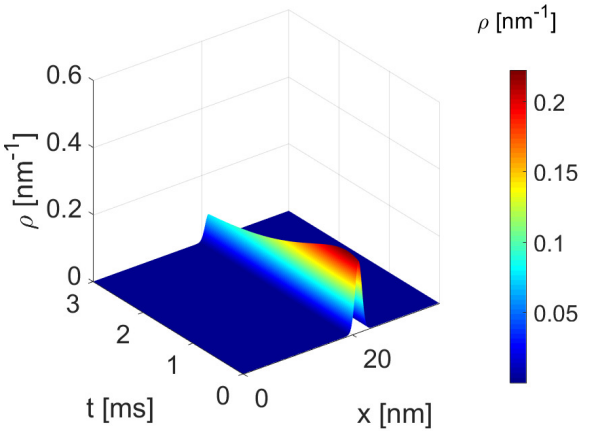

(b) Weakly-bound state

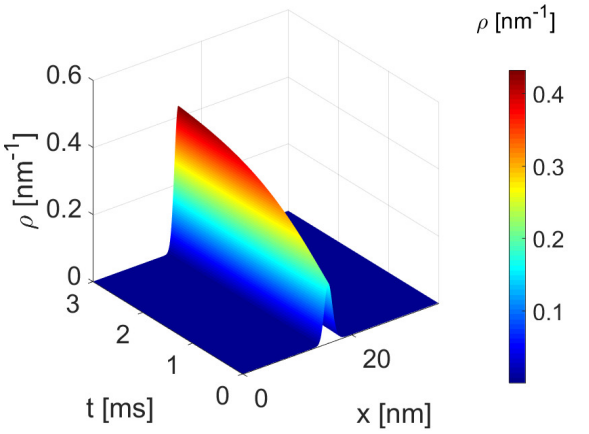

(c) Post-power stroke state

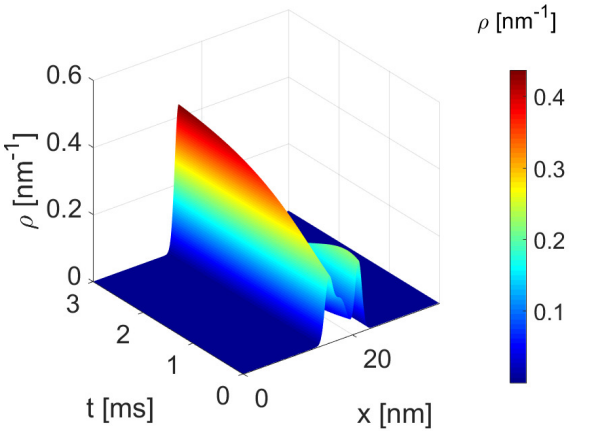

(d) Total probability density (the unbound state, the weakly-bound state and the post-power stroke state summed together)

Figure 12.6: Probability densities with different transition rates defined by the external load force F_{Load}. Probability densities distribution for the unbound state (a), the weakly-bound state (b), the post-power stroke state (c) and the total probability density (d) (normalized in every time step) with respect of ATP, ADP and P concentrations. These parameters are set as follows: $[ATP] \sim 1\,mMol$, $\Delta G = 12\,\mathrm{k_B T}$ and with external load force $F_{Load} = 0\,pN$. The potential is given by E_m for unbound state, $FS(\Delta G, x) + E_m$ for the weakly-bound state and $FS(\Delta G, x + d) + E_m$ for post-power stroke state. The function FS stands for Fourier series given by Equation (11.3)

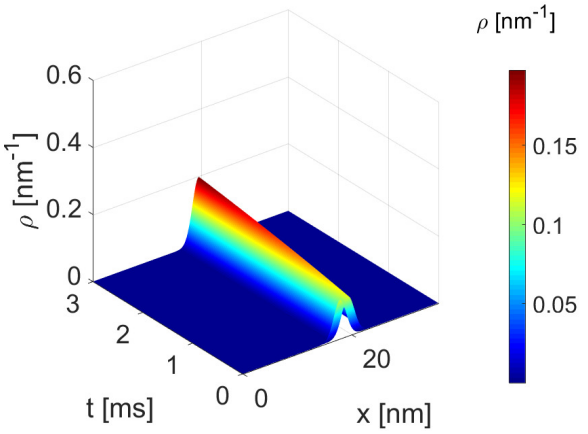

(a) Unbound state

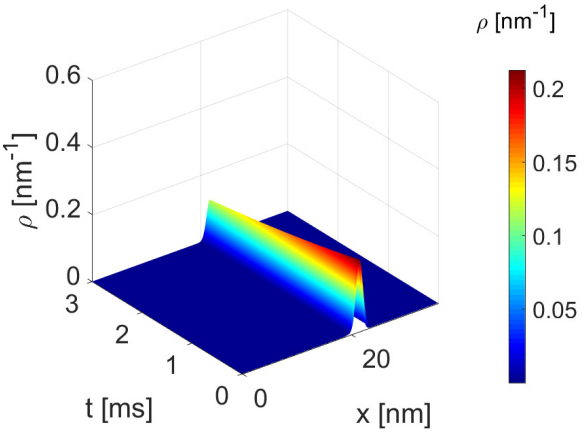

(b) Weakly-bound state

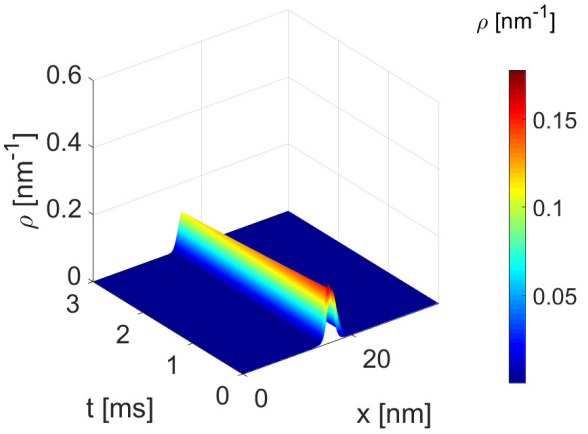

(c) Post-power stroke state

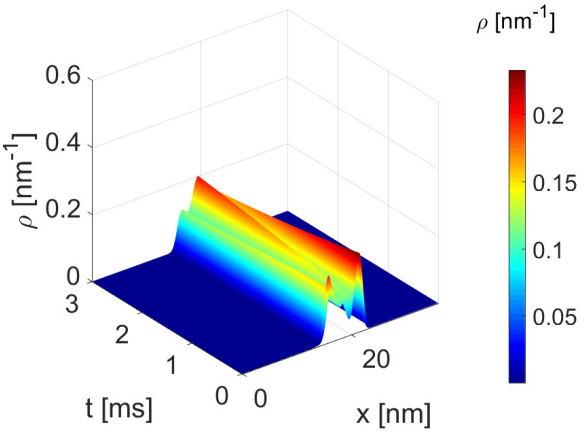

(d) Total probability density (the unbound state, the weakly-bound state and the post-power stroke state summed together)

Figure 12.7: Probability densities with different transition rates defined by the external load force F_{Load}. Probability densities distribution for the unbound state (a), the weakly-bound state (b), the post-power stroke state (c) and the total probability density (d) (normalized in every time step) with respect of ATP, ADP and P concentrations. These parameters are set as follows: $[ATP] \sim 1\,mMol$, $\Delta G = 12\,\mathrm{k_B T}$ and with external load force $F_{Load} = 5\,pN$. The potential is given by E_m for unbound state, $FS(\Delta G, x) + E_m$ for the weakly-bound state and $FS(\Delta G, x + d) + E_m$ for post-power stroke state. The function FS stands for Fourier series given by Equation (11.3)

12.2 Amplitude of state potential as a function of ATP concentration

Transition rates are not the only things that depend on ATP concentration. The potential of the given state depends as well. More precisely, the amplitude of the Fourier series is relying on the concentration according to Equation [44]

$$\Delta G' = -\Delta G_0 - k_B T \ln \frac{[ATP]}{[ADP][P]}, \tag{12.8}$$

where $\Delta G_0 = 54 \cdot 10^{-21}$ J [44]. However, the previous simulations have $\Delta G > 0$, which is in correspondence with papers [16, 136]. This leads to the decision to keep this convention for better results comparison. So, the amplitude is computed as

$$\Delta G = \Delta G_0 + k_B T \ln \frac{[ATP]}{[ADP][P]}. \tag{12.9}$$

Parameters $[ADP]$ and $[P]$ are the concentration of ADP and P, respectively. The dependence of ΔG in $k_B T$ units is visible in Figure 12.8.

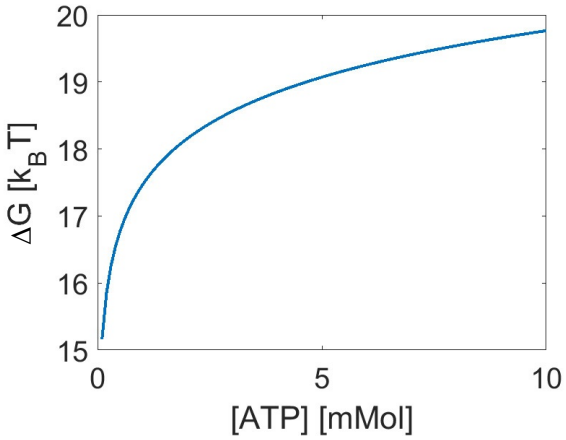

Figure 12.8: Increasing dependence of ΔG on concentration of ATP.

Results of probability density distribution are in Figures 12.9 and 12.10. The biggest visible differences due to increasing of [ATP] value are between 12.9b and 12.10b, and 12.9c and 12.10c, respectively. The weakly bound state is increased with a higher concentration of ATP and the post-power stroke state is decreasing.

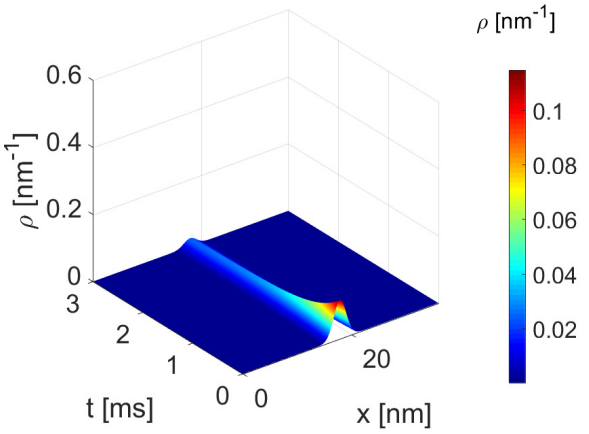

(a) Unbound state

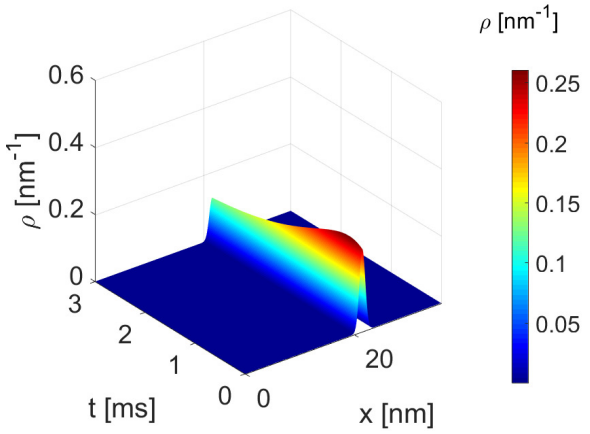

(b) Weakly-bound state

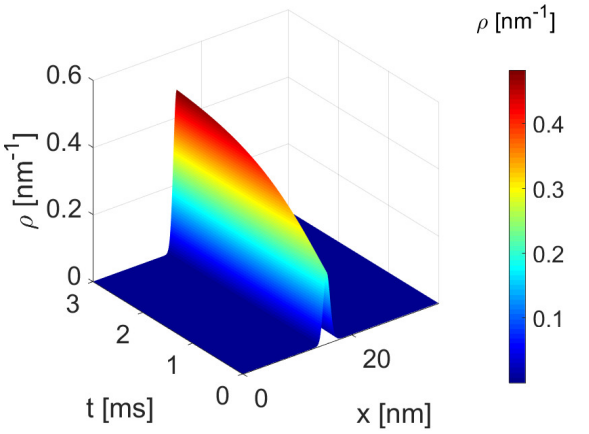

(c) Post-power stroke state

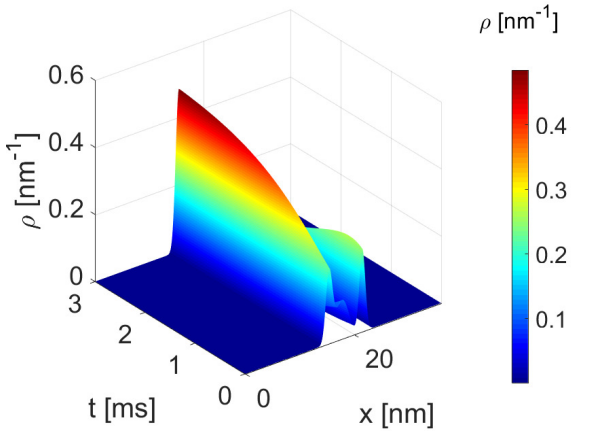

(d) Total probability density (the unbound state, the weakly-bound state and the post-power stroke state summed together)

Figure 12.9: Probability densities in the three state model with $\Delta G = \Delta G([ATP])$*, i.e.* $\Delta G = 17.46\,\mathrm{k_B T}$ *for the unbound state (a), the weakly-bound state (b), the post-power stroke state (c) and the total probability density (d) (normalized in every time step) with respect of ATP, ADP and P concentrations. These parameters are set as follows:* $[ATP] \sim 1\,mMol$*,* $[ADP] \sim 10{\cdot}10^{-3}\,mMol$ *and* $[P] \sim 1\,mMol$ *with external load force* $F_{Load} = 0\,pN$*. The potential is given by* E_m *for unbound state,* $FS(\Delta G, x) + E_m$ *for the weakly-bound state and* $FS(\Delta G, x+d) + E_m$ *for post-power stroke state. The function FS stands for Fourier series given by Equation* (11.3)

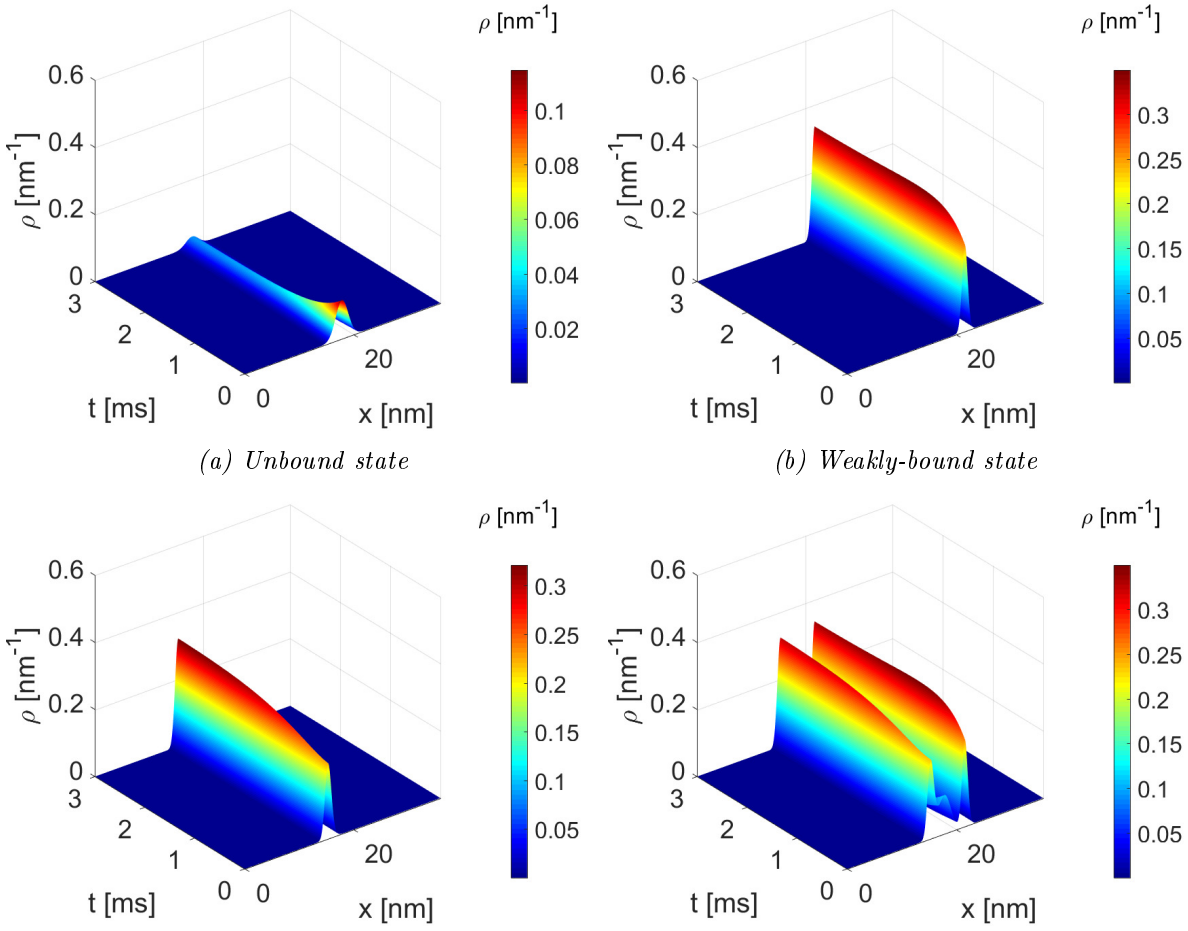

(a) Unbound state

(b) Weakly-bound state

(c) Post-power stroke state

(d) Total probability density (the unbound state, the weakly-bound state and the post-power stroke state summed together)

Figure 12.10: Probability densities in the three state model with $\Delta G = \Delta G([ATP])$*, i.e.* $\Delta G = 19.76\,\mathrm{k_B T}$ *for the unbound state (a), the weakly-bound state (b), the post-power stroke state (c) and the total probability density (d) (normalized in every time step) with respect of ATP, ADP and P concentrations. These parameters are set as follows:* $[ATP] \sim 10\,mMol$*,* $[ADP] \sim 10 \cdot 10^{-3}\,mMol$ *and* $[P] \sim 1\,mMol$ *with external load force* $F_{Load} = 0\,pN$*. The potential is given by* E_m *for unbound state,* $FS(\Delta G, x) + E_m$ *for the weakly-bound state and* $FS(\Delta G, x + d) + E_m$ *for post-power stroke state. The function FS stands for Fourier series given by Equation* (11.3)

Chapter 13

Velocity of the myosin head

Mechanical properties serve as a validation of the model. Here, I focus on the molecular motor's velocity, which is studied in many Refs. [4, 16, 26, 27, 91, 92, 116, 117, 133, 136]. Refs. [16, 27, 133, 136] focus on theoretical studying of the molecular motor's velocity, and Refs. [26, 91, 92, 116, 117] are devoted to experimental studying. Refs. [4, 91] review this topic.

However, a large scattering of values and characteristics are in these papers. In Refs. [26, 92, 116, 117], the difference is given by different kinds of myosin (rabbits' vs algas' vs frogs'), see Figures 13.1a and 13.1b and different experimental settings. Moreover, some experiments suggest that velocity dependence is not only linear, but it can be deformed to double-hyperbolic for small loads[4].

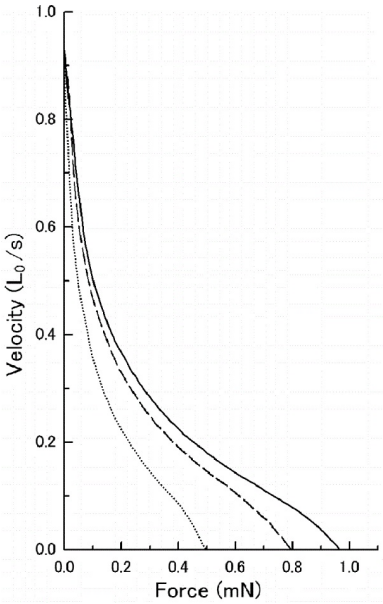

(a) Rabbit muscle fibers. Adapted from [116]

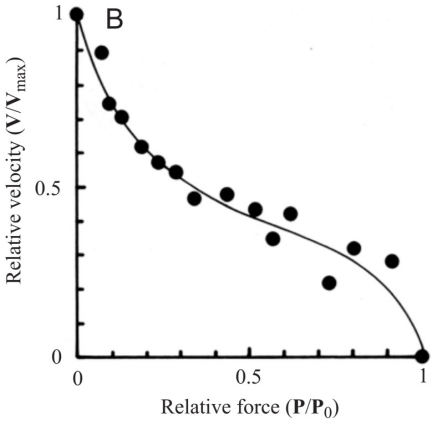

(b) Algae myosin II. Adapted from [92].

Figure 13.1: Experimental measurements of myosin II force-velocity dependence.

Refs. [16, 133, 136] define velocity of a molecular motor as an average velocity ν in each state

$$\nu(x) = \frac{1}{\mathcal{N}} \sum_{i=1}^{\mathcal{N}} L J_i(x)\,, \tag{13.1}$$

where $\mathcal{N}$ is number of states (i.e. $\mathcal{N} = 3$), L is characteristic length – it is for myosin 36 nm, and flux J in i-th state.

The flux is obtained from the Fokker-Planck equation's properties

$$J_i = -\frac{D}{k_B T}\left(\frac{\partial V_i}{\partial x} - F_{Load}\right)\rho_i - D\frac{\partial \rho_i}{\partial x}\,. \tag{3.34}$$

According to Ref. [16], the velocity is evaluated in a stationary state. Thus, the Fokker-Planck equation is reduced to

$$0 = \frac{D}{k_B T}\frac{\partial}{\partial x}\frac{\partial \phi}{\partial x}\rho + D\frac{\partial^2 \rho}{\partial x^2} \tag{5.5}$$

where ϕ is the effective potential $\phi = V - x \cdot F_{Load}$. In terms of flux, Equation (5.5) can be reformulated for one state to

$$0 = \frac{\partial J}{\partial x}\,. \tag{13.2}$$

However, the model is created by three mechanochemical states which allows transitions between them (with exception of direct transition between unbound to post-power stroke, see Chapter 7). It requires additional terms which describe these transitions

$$0 = -\frac{\partial J_i}{\partial x} - \sum_i k_{ji}\rho_i + \sum_j k_{ij}\rho_j \quad \forall \text{ acceptable combinations of } i,\ j \tag{13.3}$$

Nevertheless, the transition rates k_{ij} are set in the model to provide balance, see Chapter 7 and Appendix B. Thus, there cannot be any non-zero total flux among all three states. It means the average velocity is zero. However, the molecular motor is still moving in one direction of chemo-mechanical states. In this direction the velocity can be obtain as

$$\frac{\partial J_i^+}{\partial x} = \sum_j k_{ji}\rho_j,\,. \tag{13.4}$$

The index + means that flux J_i is given only by transition probability densities between states coming to state i.

Equation (13.4) can integrated to

$$J_i^+ = \int \sum_j k_{ji}\rho_j \mathrm{d}x \tag{13.5}$$

The right side of the equation can be modified by the Levi theorem [54] ($k_{ij}\rho_j$ is non-negative integrable function).

$$J_i^+ = \sum_j \int k_{ji}\rho_j \mathrm{d}x\,. \tag{13.6}$$

Taking into account that transition rates k_{ij} are constant with respect to x, it changes into

$$J_i^+ = \sum_j k_{ji} \int \rho_j \mathrm{d}x\,. \tag{13.7}$$

The integral can be evaluated by definition of probability

$$p = \int \rho \mathrm{d}x \,. \tag{13.8}$$

Thus,

$$J_i^+ = \sum_j k_{ji} p_j \,. \tag{13.9}$$

The relation expands to possible variations

$$J_1^+ = k_{31} p_3 + k_{21} p_2 \,, \tag{13.10}$$
$$J_2^+ = k_{12} p_1 + k_{32} p_2 \,, \tag{13.11}$$
$$J_3^+ = k_{23} p_2 \,. \tag{13.12}$$

The average velocity along x is expressed as follows

$$\nu(x) = \frac{1}{\mathcal{N}} \sum_{i=1}^{\mathcal{N}} \nu_i(x) = \frac{1}{\mathcal{N}} \sum_{i=1}^{\mathcal{N}} L \sum_j k_{ji} p_j(x) \,. \tag{13.13}$$

It means, the velocity is still dependent on the position along the x axis (actin filament). Thus (based on derivation in Ref. [16]), the total velocity is its sum, i.e.

$$v = \sum_x \nu(x) \,. \tag{13.14}$$

This summation does not require any normalisation condition, because all variables except p_j are constant and p_j is already normalised by its definition $\sum_j \sum_x p_j = 1$.

The flux J_i^+ is function of the probability p_j. To obtain p_j, the WPE algorithm (see Chapter 6) is applied to Equation (13.3). It provides simple matrix equation

$$0 = Mp \tag{13.15}$$

where M is matrix given by fluxes F and B along x axis (actin filament). For inner nodes, the matrix M is given as follows

$$M(n,n) = -(B_{n-1/2} + F_{n+1/2}) \tag{13.16}$$
$$M(n-1,n) = F_{n-1/2} \tag{13.17}$$
$$M(n+1,n) = B_{n+1/2} \tag{13.18}$$

where n is a node position in the computation grid length N. Thus, $(n-1,n)$ is bellow M diagonal and $(n+1,n)$ is above the diagonal. The precise form of M is dependent on added boundary conditions.

Equation (13.15) provides a very important information based on singularity or regularity of matrix M [89]. If the matrix is singular, the only solution is the trivial one, i.e. vector of zeros. If the matrix is singular, a non-trivial solution exists.

The Lagrange multipliers method provides the same results for singular matrices as the Singular Value Decomposition method, which is in `MATLAB` software.

Various boundary conditions provide different singularity or regularity of the matrix M. In the case of absorbing boundary condition, the matrix is regular, and thus, the only solution of Equation (13.15) is the trivial one. On the other hand, reflecting and periodic boundary conditions provide singular matrix M. Hence, these two boundary conditions are proper to obtain non-zero myosin head velocity.

As the above procedure of calculating the myosin head velocity shows, this motor velocity is not identical with muscle contraction velocity.

13.1 Velocity dependence on the load

The velocity dependence on the load is not linear for my three-state model. It is closer to double hyperbolic trend, see Figure 13.2. This dependence is identical for periodic and reflecting boundary conditions and even for all six variants of potentials.

However, in closer look along x-axis (actin filament), the fluxes and thus velocity $\nu(x)$ changes with different potentials and boundary conditions, respectively. These velocities $\nu(x)$ for periodic boundary condition and $F_{Load} = 0\,\mathrm{pN}$ are in Figures 13.3, 13.4, and 13.5.

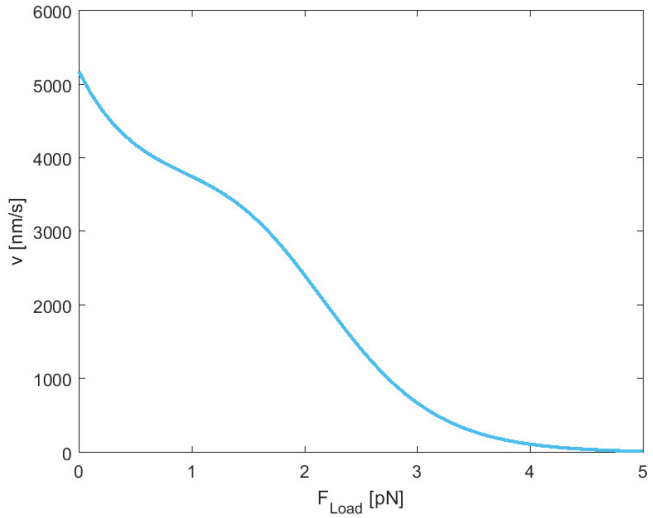

Figure 13.2: Velocity dependent on the load. The result is identical for all 6 cases of potential.

Figure 13.3 contains velocities $\nu(x)$ in the unbound state. Some potential cases redraw the other one. In the first (left) peak, potential denoted as 3 redraws potential 2, and potential 6 goes over potential 5. For the second (right) peak, potential 4 is identical to potential 1; potential 6 hides others.

In Figure 13.4, it is possible to find all six fluxes. Only two potentials produce zero fluxes at the boundary region. There denoted as cases 2 and 5. These two potentials are special due to energy E_m in the unbound state. This defined unbound state produces zeros probabilities in boundary regions. Otherwise, it is bigger than zero and multiplying by high transition rates causes a clear difference in these regions.

In Figure 13.5, only two peaks are visible. The first one covers potentials 2, 3, 5 and 6. he second one is created by identical potentials 1 and 4.

The obtained results are similar to velocity published in Ref [136], see Figure 13.6. The absolute values are not fitting. The different number of used states causes the change, three in my model in comparison with two in Yin's model[136]. However, there is a good agreement in the velocity order between these two models. In Yin's model, velocity also closes to zero for higher load force.

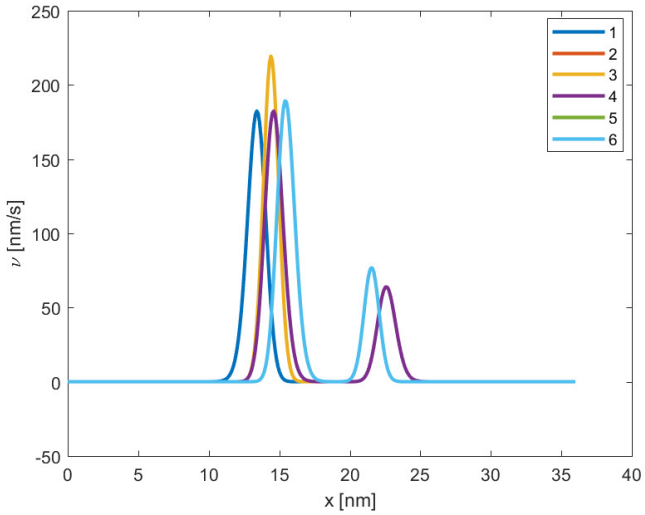

Figure 13.3: Velocity $\nu(x)$ in the unbound state along actin filament.

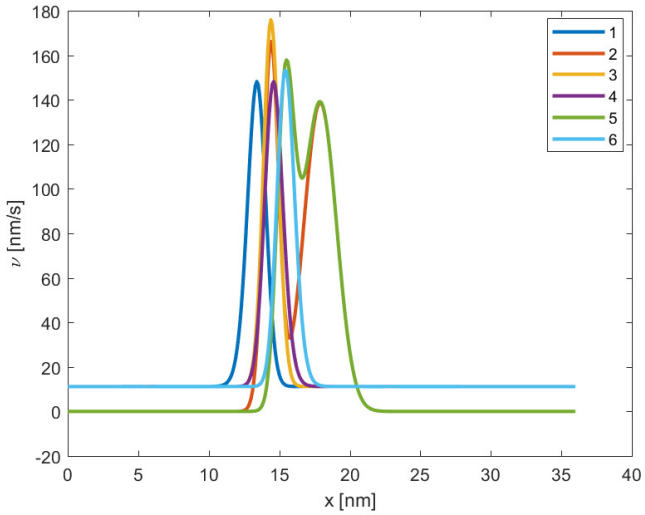

Figure 13.4: Velocity $\nu(x)$ in the weakly-bound state along actin filament.

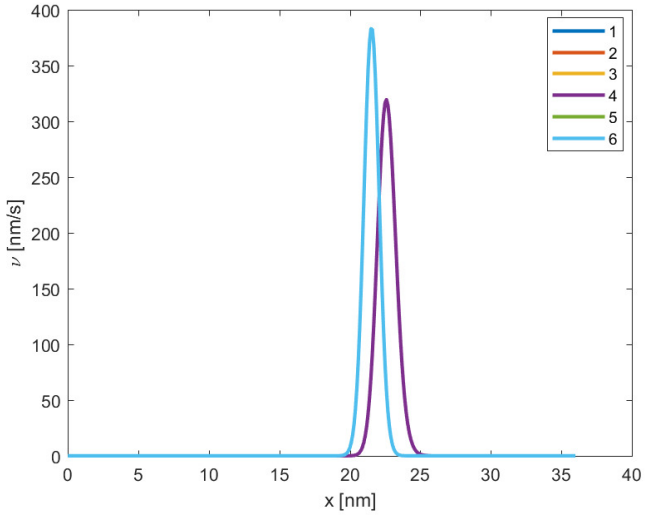

Figure 13.5: Velocity $\nu(x)$ in the post-power stroke state along the actin filament. There is some overlapping of plotted lines. The left peak covers fluxes for cases 2,3,5 and 6. The right peak covers cases 1 and 4.

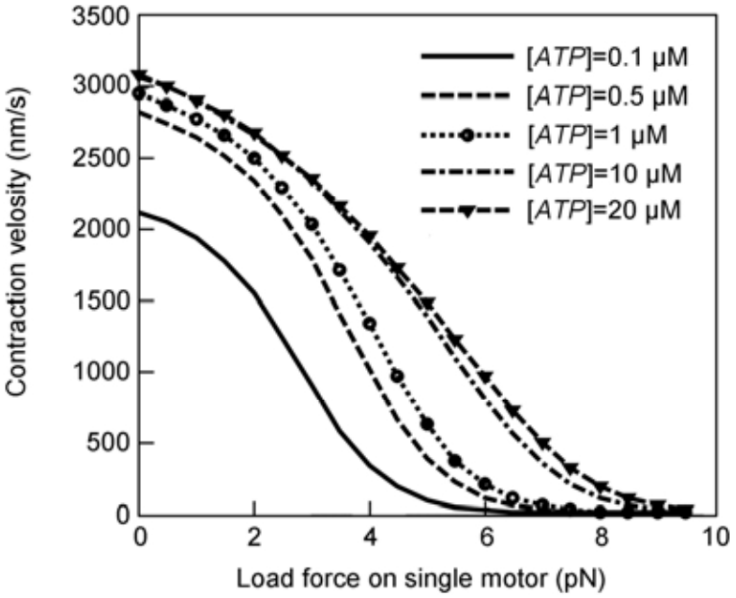

Figure 13.6: Velocity dependent on external load force with several ATP concentrations. Adapted from [136].

13.2 Velocity dependence on the ATP concentration

The molecular motor's velocity is dependent on the available amount of fuel (ATP) in the surroundings. In Figure 13.7 is shown several lines, which corresponds to different loads (0 pN, 1 pN, 2 pN, 3 pN, 4 pN). All these lines are rising. The load damps the growth. This correlates with a presumption about the motor.

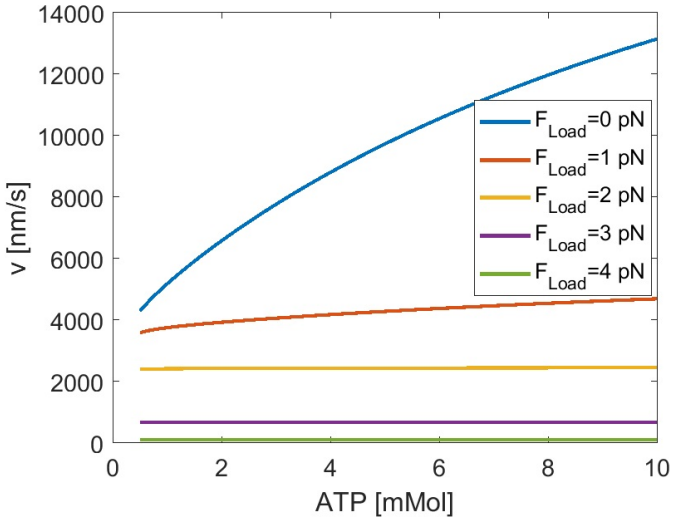

Figure 13.7: Velocity v dependence on ATP concentration for different external load force F_{Load}.

The velocity goes to zero for $F_{Load} > 4\,\mathrm{pN}$. The potential and relatively big external load have the influence. Even rough estimation shows that a limit value, where the velocity closes to zero, must exists. The crucial equation for the estimation is a simple definition of external work

$$W_{ext} = F_{Load} L\,. \tag{13.19}$$

Mechanical work W is created by potentials. Its mean value, which is around $40\mathrm{k_B T}$. It approximately corresponds to $1.6 \cdot 10^{-19}\,\mathrm{J}$. L is as usual $36 \cdot 10^{-9}\,\mathrm{m}$. From Figure 13.8 is clear, the velocity closes to zero between 4 pN and 5pN. It is $4(\text{or } 5)\cdot 10^{-12}\,\mathrm{N}$. So, for these two values the estimation is as follows:

- $F_{Load} = 4\,\mathrm{pN}$
  $W_{ext} = 4 \cdot 10^{-12}\,\mathrm{N} \cdot 36 \cdot 10^{-9}\,\mathrm{m} = 1.4 \cdot 10^{-19}\,\mathrm{J}$
  Thus, the $W > W_{ext}$ and the system should produce enough energy to have non-zero velocity.

- $F_{Load} = 5\,\mathrm{pN}$
  $W_{ext} = 5 \cdot 10^{-12}\,\mathrm{N} \cdot 36 \cdot 10^{-9}\,\mathrm{m} = 1.8 \cdot 10^{-19}\,\mathrm{J}$
  It implies, the $W < W_{ext}$ and the system produces not enough energy to have non-zero velocity.

To find a precise value of F_{Load}, where the motor has zero speed is possible by this simple equation. However, the model produces a non-zero velocity (tiny one) at higher external loads. For this reason, the load which stops the motor is not determined by analytical means (it is an estimation only).

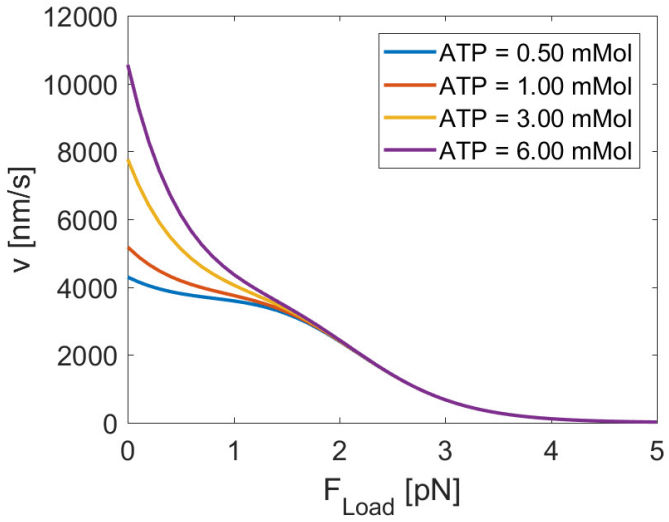

Figure 13.8: Velocity dependence on ATP concentration for different loads and different concentration of ATP. The higher concentration increases the myosin head velocity to a certain limit. The effect vanishes with higher loads.

Figure 13.9 contains comparison with experimental data. As was mentioned earlier in this chapter, a large scattering of experimentally obtained data exists in the literature. The comparison is in Figure 13.10. There are experimental results of velocity dependence on a force measured on sarcomere. The difference between sarcomere and single myosin head causes some differences in values. Thus, I compare the shape only. The next difference is in used units ($\mathrm{N/mm^2}$) for experimental data.

Both data show a kind of double hyperbolic behaviour. In my model, the change to the second hyperbole happens around 0.3 of relative load ($F_{Load}/\max F_{Load}$). In the experimental data, the second hyperbole starts later, around 0.2 ($\mathrm{N/mm^2}$). The length of the first hyperbole ratio is increasing for higher ATP concentration in my model. It is easy to presume the next increasing ATP concentration (to a certain limit) will cause more similar simulated data to the measured in Ref. [26].

Some similarities are also visible in comparison between 13.9 and 13.1b. The algae experiment does not show so clear double-hyperbolic behaviour like the frog one, but seeing a beginning of the second hyperbole around 0.8 relative force is possible. For very low relative loads (<0.5), the shape is very similar.

Both experimental data start the second hyperbole later than my model.

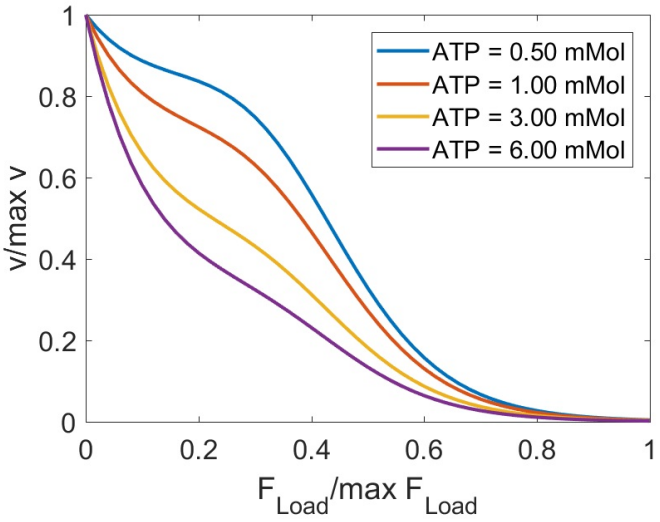

Figure 13.9: Normalised velocity dependence on ATP concentration for different loads and different concentration of ATP. Each increase of ATP concentration causes a shift in doublehyperbolic shape.

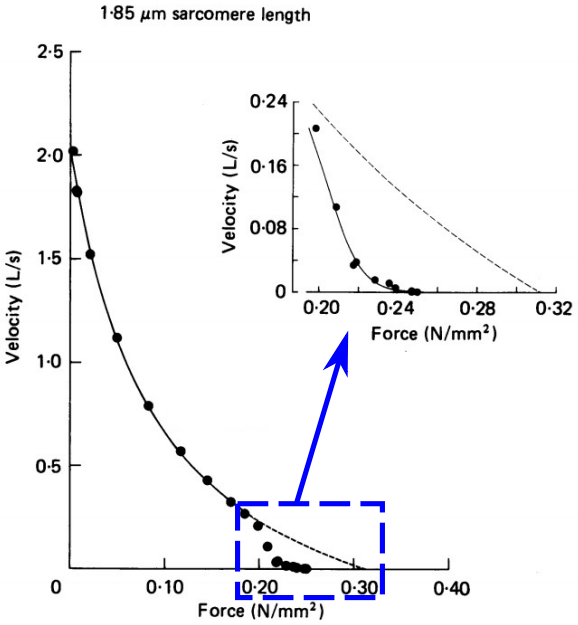

Figure 13.10: Double-hyperbolic experimental data of velocity dependence on external load from frog muscle fibres (a sarcomere). Continues line is a double-hyperbolic fit, and the dashed line is a single-hyperbolic fit. The force is normalized on $1\,\mathrm{mm}^2$*. Adapted from [26]*

Chapter 14

Numerical prediction of the myosin II head position

This chapter is devoted to describing the observing mechanism's behaviour in the living system, which is akin to Maxwell's demon. It focuses on how much relative entropy and mutual information are obtained with different parameters values – standard deviation, position, load – and how a random prediction of position and state changes the distribution. The prediction follows Chapter 9 in Methodology part (Part III).

Shown results are with potential denoted as case 6, i.e. $V_1 = 0\,k_BT$, $V_2 = FS(\Delta G, x) + E_m$, $V_3 = FS(\Delta G, x + d) + E_m$, where FS is Fourier series and E_m is energy of the myosin neck. ATP concentration is set as 1mMol, $ADP = 1\,\mu$Mol, $P = 1$mMol [44].

The non-symmetry of relative entropy complicates results description. It is crucial to focus on which probability density is compared to another.

On the contrary, mutual information is a symmetric variable, which makes things easier.

14.1 Value of standard deviation

For this simulations, I fix the $\tilde{x}$ position to 18 nm, and the myosin head is in the unbound state.

The prediction assumes the error as a Gaussian one. It means information is strongly dependent on standard deviation value σ, which has a meaning of the prediction precision. If the precision is low, the standard deviation is big, which produces a small amount of relative entropy. If the precision is high, the reasoning is similar. A small standard deviation brings a significant amount of relative entropy. I obtain it by my model too, see Figure 14.1.

The situation for mutual information is more complicated than for relative entropy. It says that the most similar probability density distribution given by the evolution of the Fokker-Planck equation and the new initial condition obtained by the Bayes theorem is for $\sigma = 5\,\text{nm}$. For this value of σ, mutual information has its maximum value. Even at this point, the mutual information is still low, i.e. $I = 1.7 \cdot 10^{-3}$ bit.

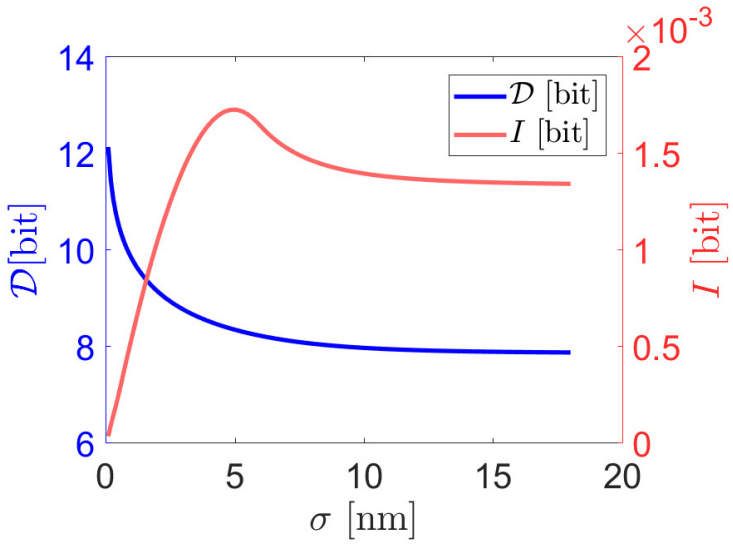

Figure 14.1: Relative entropy and mutual information in the dependence on value of standard deviation.

In other states, relative entropy and mutual information are very qualitatively similar. However, they are quantified differently.

14.2 Different position of myosin head on actin filament

In this section, standard deviation σ is set to 5 nm (where is the maximum of mutual information for the unbound state, see Section 14.1) and localized position $\tilde{x}$ is varying. It produces results shown in Figure 14.2. Here, the state is not playing any role.

Maximum mutual information is for $\tilde{x} = 18.3\,\text{nm}$. The area between peaks corresponds to the most probable value given by the distribution after the Fokker-Planck equation solution. At the same point, there is the minimal value of relative entropy ($\tilde{x} = 15.5\,\text{nm}$).

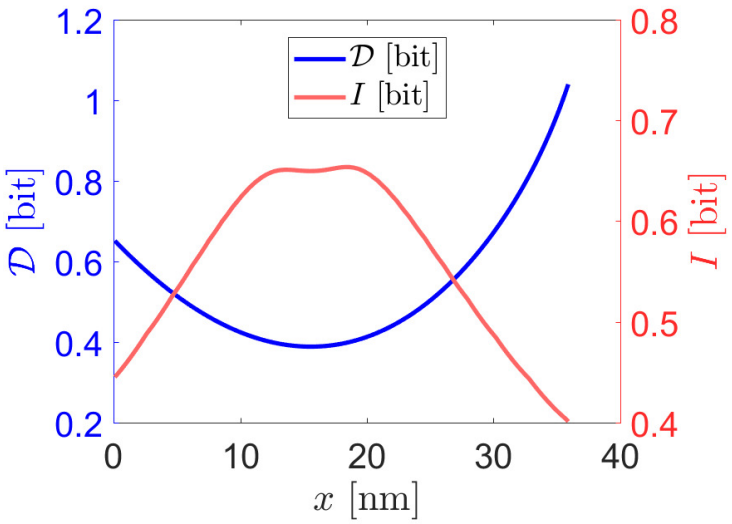

Figure 14.2: Relative entropy and mutual information in dependence on position $\tilde{x}$ along action filament.

14.3 Load influence on obtained information

In this section, I assume the prediction has standard deviation $\sigma = 5\,\text{nm}$ and the myosin head is located with the highest probability on $\tilde{x} = 18\,\text{nm}$. It corresponds to half of the studied interval.

Here, the predicted state do not have influence again.

The effect of increasing load is in Figure 14.3. The limitation of movement by the load force causes increasing in relative entropy. The situation with mutual information is more difficult to describe. The minimum and thus, the biggest difference between distribution is for $F_{Load} = 1.9\,\text{pN}$. If any other value of $\tilde{x}$ is set, the minimum moves to a different position.

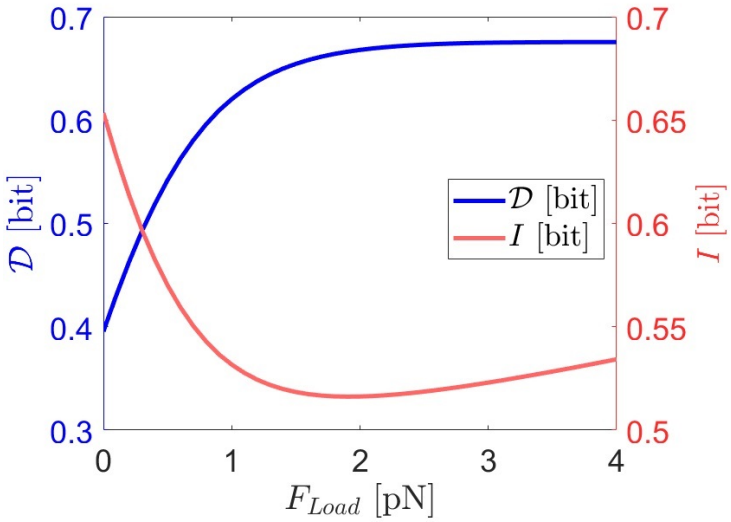

Figure 14.3: Information and mutual information in dependence on value of standard deviation.

14.4 Repeated prediction

Repeated prediction is a designation for simulation running from the initial condition evolving according to the Fokker-Planck equation. The state where the simulation ends, I call before measurement. Then, the prediction procedure is performed, which takes 0.001 ms. It brings a new initial condition (localisation outcome) which develops in the Fokker-Planck framework. The interval of solving is the same as in the first part (0.5 ms). The repeated prediction procedure ends before the second prediction process. However, it is possible to extend it to more iterations.

The position and state predictions are random. Standard deviation is set to $\sigma = 5\,\mathrm{nm}$.

All importing probability densities are in Figure 14.4. Moreover, there is visible the second evolution middle step $\rho_{tot}(t = 0.751\,\mathrm{ms})$. It is there due to visualisation of the second evolution from the predicted probability density.

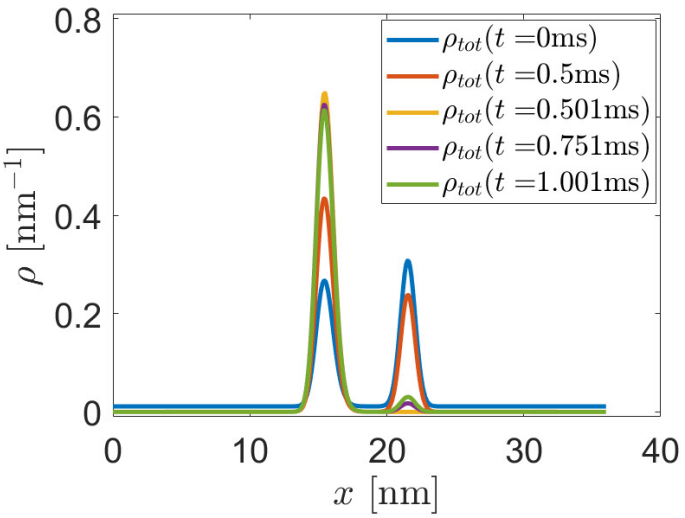

Figure 14.4: Information and mutual information in dependence on value of standard deviation.

Table 14.1 shows relative entropy for four probability density distributions (initial condition, before measurement, measurement outcome and the end of the second evolution) and all possible variants. The results are in a matrix, which has on its diagonal zeroes only. It is caused by evaluating identical probability densities. The comparison of measurement outcome with others produces infinite relative entropy. It is caused by the state of the myosin head determined without any mistake (zero probability densities in undetermined states), and the denominator of the logarithms equals zero in this area. According to the relative entropy definition, the matrix is non-symmetrical.

On the other hand, mutual information has its maximum on the diagonal; see Table 14.2. Due to the intersection of two different probability densities, it is smaller than if they are identical; hence, mutual information is lower. Furthermore, the matrix is symmetric.

Thus, the results are in agreement with theoretical assumptions.

Table 14.1: Relative entropy in bits for different probability densities – initial condition, evaluation of the Fokker-Planck equation in the first interval (before localization), localization outcome, evaluation of the Fokker-Planck equation in the end of second interval

	initial condition	before localization	localization outcome	end of the second evaluation
initial condition	0.00	0.28	0.92	0.74
before measurement	0.34	0.00	0.39	0.25
measurement outcome	∞	∞	0.00	∞
end of the second evolution	1.05	0.43	0.04	0.00

Table 14.2: Mutual information for different probability densities – initial condition, evaluation of the Fokker-Planck equation in the first interval (before localization), localization outcome, evaluation of the Fokker-Planck equation in the second interval

	initial condition	before localization	localization outcome	end of the second evaluation
initial condition	2.34	1.09	0.38	0.47
before measurement	1.09	1.54	0.65	0.76
measurement outcome	0.38	0.65	0.94	0.91
end of the second evolution	0.47	0.76	0.91	1.13

Part V

Conclusion

Chapter 15

Conclusion and Summary of the thesis

This thesis focuses on an essential biology topic: interaction of myosin and actin in muscle filaments. It is a crucial mechanism of muscle working process in all eukaryote organisms. The topic is exciting for biologist, physiologist, and even medical doctors for many reasons. It is fascinating for the newly developing field of artificial nanorobots as well.

The interaction between myosin head and actin filament occurs at petite length, time scales and small forces – lengths in tens of nanometers, time in milliseconds, and forces in picoNewtons. Thus, the typical energy exchange is in k_BT units (1 Joule corresponds to $4.11 \cdot 10^{-21}\, k_BT$ in standard temperature conditions). It means that interactions, described here, cannot be characterised by mechanical models (Hill's, Huxley's, respectively [107]) only. There is a need to consider that interaction happens in a thermal environment; in other words, the energy is indeed in k_BT units. It means that models cannot neglect the thermal environment influence. Hence, its deterministic description is very complicated or even impossible.

Therefore, I choose a stochastic description, where the probability density function, $\rho(x,t)$, characterised the position of the myosin head on actin filament at given time t.

In the current statistical physics, the concept of information, i.e. what we know about the information, have a significant role. Hence, a short description of modern statistical physics approaches, including information, is in the thesis. These approaches are examined in the context of Maxwell's demon, significantly. This imagined "being" serves as a system model that controls the whole structure via a feedback control which uses the information gain. This point of view allows analysing a lot of dynamic problems in living organisms.

The interaction between myosin head and actin filament is a complex process, which I simplify to three states. The first one is called the unbound state. In this state, there is no physical connection between the head and the actin filament. The second one is the weakly-bound state, in which the myosin head weakly attaches to the actin. The last state is called the post-power stroke one. It happens after the contraction of the muscle.

Probability densities ρ_i; $i = 1, 2, 3$, in one of the above-defined state denotes particular probability density in a given state, where i stands for the given state. Transition rates between two allowed states k_{ij}(reversibly from unbound to weakly bound, from weakly bound to post-power stroke and irreversibly from post-power stroke state to unbound) are obtained by the method of condensation of state from a more detailed description. Their precise values obey detail balance condition and the Arrhenius equation.

The Fokker-Planck equation describes the stochastic system, including deterministic interac-

tions (realised by internal and external potential forced), diffusion decay and chemical reactions.

$$\frac{\partial \rho_i}{\partial t} = \frac{D}{k_B T}\frac{\partial}{\partial x}\left(\frac{\partial V_i}{\partial x} - F_{Load}\right)\rho_i + D\frac{\partial^2 \rho_i}{\partial x^2} + \sum_{j=1}^{3} k_{ji}\rho_j - \sum_{j=1}^{3} k_{ij}\rho_i\,, \tag{7.2}$$

where D is the diffusion coefficient, V_i internal potential in the given state including actin filament configuration. Other parameters are mentioned above.

I solve this equation by so-called WPE algorithm [132] in several simulation cases:

- in full generality as express in Equation (7.2),
- when describing one state alone without transition rates k and transportation term $\frac{D}{k_B T}\frac{\partial}{\partial x}\left(\frac{\partial V_i}{\partial x} - F_{Load}\right)\rho_i$,
- the stationary form of the equation without transition rates.

The model uses three kinds of boundary conditions. Periodic, absorbing (myosin head may leave the studied 36 nm wide domain), and reflexing, where boundary conditions reflect (mirror) myosin head back to the domain.

In this thesis, I calculate the whole process during its 3 ms evolution in which the myosin head is attached and detached to the actin filament. Results are in the form of the probability density distribution of myosin head in each state and each time. I study the influence of ATP (adenosine triphosphate) and external load on this process.

Moreover, I simulate transition rates dependency on the external load. The results show that external load higher than 2 pN significantly complicates transition between states.

Next, I study how the amplitude of the potentials depends on ATP concentration. In these results, it is possible to see that a given transition happens with a certain probability, confirming the whole process's stochastic character.

An essential parameter for validation with an experiment is myosin head velocity dependent on the external load. Chapter 13 describes it. There is an extensive scattering of velocity values found in the literature. The results show that myosin head velocity is 5000 nm/s (i.e. 5 nm/ms, which corresponds with timescale in Figures 12.3, 12.4, 12.6, 12.9 and 12.10). Velocity decreases with increasing load rapidly. The explanation is related to that higher load limit transition rates, and the head movement is more restricted.

From a modern statistic perspective, it is fascinating to see the whole process as an information interchange. Due to this reason, I study this simple model where I describe space localisation of myosin head as an information process, in which the information obtained by measurement with an inevitable error. Probability methods are demonstrated, and relative entropy with mutual information is defined in this illustrative example. I show different influences of various system parameters on information flux. Repeated measurement procedure provides an interesting comparison of how the relative entropy and mutual information change with reverse order of arguments and how in single steps of measurement.

By completing all these results, it is possible to say I fulfilled all objectives.

The topic of the thesis is very interdisciplinary. Except for the necessary knowledge of biologic phenomena, there is a need to combine mechanics, statistical physics and information theory. This thesis is unique by using many various science fields. Results may inspire anatomists, biologists and experimenters, who work with these structures. Designers who develop working

mechanisms and smart systems working on feedback control in nanoscale may use these results, too. I believe the thesis is valuable even from a pedagogic point of view. It provides a primary picture of new, rapidly evolving topics, and it is possible to continue on this by many applications.

Resume [Czech language]

Předkládaná práce je věnována mikromechanice na molekulární úrovni. V dnešní době jde o velice aktuální téma. Během posledních pěti let (v r. 2016 a v r. 2017) byly uděleny 2 Nobelovy ceny na toto téma. Jedná se o velmi širokou vědeckou oblast, proto jsem se zaměřila především na molekulární motor myosinu II.

Tento molekulární motor (krátce jen myosin) je zodpovědný za svalovou kontrakci. Myosinová hlavička musí být připojena na aktinové vlákno, aby způsobila kontrakci. Hlavička je tak malá, že podléhá Brownovo pohybu. V tomto případě není možné tento vliv zandedbat (pokud se neřeší jen čistě mechanický model typu Hilla, nebo Huxleyho a podobně). Pro dosažení statistických predikcí polohy myosinové hlavičky je použit Fokker-Plankův popis.

Pohyb myosinu je řízen mnoha mechanismy. Lze jej zjednodušit jako „bytost“, která ovliňuje pohyb jen jako prostředník. Na první pohled je tedy tato „bytost“ pouze pozorovatelem a dá se připodobnit k Maxwellovu démonu.

Numerické řešení Fokker-Planckovy rovnice poskytuje algoritmus WPE (Wang, Peskin, Elstone) a funkce v MATLABu ode15s. Zjednodušené verze Fokker-Planckovy rovnice (stacionární Fokker-Planckova rovnice a difúzní rovnice) byly porovnány s jejich analytickým řešením. To poskytlo lepší náhled do problematiky.

Dále byla provedena studie vlivu okrajových podmínek a potenciálových bariér. K tomu bylo použito 6 různých druhů bariér, které mění chování hlavičky myosinu. Studie ukazuje ztrátu jistoty přítomnosti myosinové hlavičky ve sledované oblasti. Hlavní výhodou této studie je ukázka důležitosti normalizačních podmínek v simulaci (součet všech pravděpodobností v daném čase je roven 1).

Poté byl model modifikován přidáním vlivu koncentrace adenosintrifosfátu (krátce ATP) a rychlostí přechodu mezi stavy definovaných pomocí Arrheniovy rovnice. ATP slouží jako palivo pro molekulární motory. Arrheniova rovnice je jednou ze základních rovnic fyzikální chemie. Zde slouží k zajištění toho, aby model splňoval podmínku detailní rovnováhy, což je důležité pro algoritmus WPE.

Mechanické vlastnosti jsou důležité pro zpětnou vazbu o realistickém výstupu modelu. Jako zástupce byla zvolena rychlost, kterou je možné měřit v reálném experimentu. Model produkuje dvojitě hyperbolické rozložení rychlosti na vnějším zatížení, což odpovídá závěrům z literatury.

Nakonec byl do simulace přidán „pozorovatel“, který zjistí, kolik relativní entropie a vzájemné informace je produkováno numerickou predikcí polohy hlavičky myosinu. Predikce ovšem není přesná. Je ovlivněna chybou měření, která je dána Gaussovo rozdělením. Právě tato chyba umožňuje stanovit relativní entropii a vzájemnou informaci.

Resume [English language]

The presented thesis is devoted to micromechanics on a molecular level. This topic is an actual one. It is proven by 2 Nobel Prizes granted in the last five years (2016 and 2017) which are touching the molecular level. This thesis focuses on myosin II molecular motor.

Myosin II molecular motor (myosin shortly) is responsible for muscle contraction. The myosin head needs to attach actin filament to cause the contraction. The myosin head is so small that it obeys Brownian motion. In such a case, the influence cannot be omitted (if the objective is not a purely mechanical model, like Hill's or Huxley's). Statistical predictions of myosin head are obtained by using the Fokker-Planck framework.

The movement of myosin is controlled by many mechanisms. They can be simplified as "being", who is not interfering to the motion itself, but serves only as a mediator. So,it is only an observer at first look. This "being" has close to the Maxwell demon hypothesis.

The numerical solution of the Fokker-Planck equation is provided by WPE algorithm and MATLAB function ode15s. The simplified version of the Fokker-Planck version (stationary Fokker-Planck equation and diffusion equation) were compared with their analytical solution to have better insight.

Next, a study of the influence of boundary conditions and potential barriers were performed. There are 6 different cases of a barrier which change the behaviour of the myosin head. The study shows loss of certainty of the myosin head presence in the watched interval. Its main benefit is showing the importance of normalisation condition in the simulation (sum of all probabilities in a given time is equal to 1).

Then, I changed the model by adding the influence of adenosine triphosphate (ATP shortly) concentration and transition rates defined via the Arrhenius equation. ATP serves as a fuel for molecular motors. The Arrhenius equation is one of the base equation of physical-chemistry. Here, it ensures the model fulfils the detail balance condition, which is important for the WPE algorithm.

Mechanical properties are important to have feedback about the realistic output of the model. As a representative, I chose the velocity because it is possible to measure in a physical experiment. The model produces double hyperbolic velocity distribution on an external load, which agrees with some literature findings.

At last, the "observer" was added to the simulation to find out how much relative entropy and information is produced by numerical prediction of the myosin head. The prediction is not a precise one. It is influenced by a measurement error (gaussian distribution). The error brings an influence to the myosin head movement which is also studied.

Resummen [German language]

Die vorliegende Arbeit widmet sich der Mikromechanik auf molekularer Ebene. In den letzten fünf Jahren (2016 und 2017) gab es zwei Nobelpreise, die die molekulare Ebene berühren. Das Thema ist weit gefasst, im folgenden konzentrieren wir uns auf den molekularen Motor von Myosin II. Der molekulare Motor von Myosin II (kurz Myosin) ist für die Muskelkontraktion verantwortlich. Myosinkopf muss ein anderes Filament (Actin) anbringen, um eine Kontraktion zu verursachen. Der Myosinkopf ist so klein, dass er der Brownschen Bewegung folgt. Da diese Bewegung nicht weggelassen werden kann (um ein rein mechanisches Modell zu erhalten), muss eine statistische Beschreibung verwendet werden. Hier ist es das Fokker-PlanckFramework. Die Bewegung von Myosin wird durch viele Mechanismen gesteuert. Sie können als "Sein" vereinfacht werden, das die Bewegung selbst nicht stört, sondern nur durch einen Mediator. Auf den ersten Blick ist das "Sein" also nur ein Beobachter. Dieses "Wesen" kommt der MaxwellDamonenhypothese nahe. Die numerische Lösung der Fokker-Planck-Gleichung wird durch den WPE-Algorithmus und die MATLAB-Funktion ode15s bereitgestellt. Die vereinfachte Version der Fokker-Planck-Version (stationäre Fokker-Planck-Gleichung und Diusionsgleichung) wurde mit ihrer analytischen Lösung verglichen, um bessere Einblicke zu erhalten. Als nächstes wurde eine Untersuchung des Einflusses von Randbedingungen und möglichen Barrieren durchgefuhrt. Es gibt 6 verschiedene Fälle einer Barriere, die das Verhalten des Myosinkopfes verändern. Die Studie zeigt einen Verlust der Sicherheit der Myosinkopfpräsenz im beobachteten Intervall. Sein Hauptvorteil besteht darin, die Bedeutung der Normalisierungsbedingung in der Simulation aufzuzeigen (die Summe aller Wahrscheinlichkeiten in einer bestimmten Zeit ist gleich 1). Dann wurde das Modell geändert, indem der Einfluss der Adenosintriphosphat (kurz ATP) -Konzentration und der Übergangsraten hinzugefügt wurde, die über die Arrhenius-Gleichung bestimmt wurden. ATP dient als Kraftstoff für molekulare Motoren. Die Arrhenius-Gleichung ist eine der Grundgleichungen der physikalischen Chemie. Hier dient es dazu sicherzustellen, dass das Modell die Detailausgleichsbedingung erfüllt, die für den WPE-Algorithmus wichtig ist. Mechanische Eigenschaften sind wichtig, um Feedback zur realistischen Ausgabe des Modells zu erhalten. Als Vertreter wurde die Geschwindigkeit gewählt, die in einem realen Experiment gemessen werden kann. Das Modell erzeugt eine doppelte hyperbolische Geschwindigkeitsverteilung auf einer externen Last, was mit einigen Literaturergebnissen übereinstimmt. Zuletzt wurde der "Beobachter" zur Simulation hinzugefügt, um herauszufinden, wie viel relative Entropie und Information durch numerische Vorhersage des Myosinkopfes erzeugt wird. Die Vorhersage ist nicht präzise. Es wird durch einen Messfehler (Gaußsche Verteilung) beeinflusst. Der Fehler beeinflusst ebenfalls die untersuchte Myosinkopfbewegung.

Published papers

1. ROSENBERG, J., KREJČOVÁ, M., NALOS, L., JARKOVSKÁ, D., ŠTENGL, M. Application of the entropy based criteria on the ECG analysis. In PROCEEDINGS OF COMPUTATIONAL MECHANICS 2019. Plzeň: University of West Bohemia, 2019. s. 168-171. ISBN: 978-80-261-0889-4

2. KREJČOVÁ, M., ROSENBERG, J. Charakteristické vlastnosti cytoplazmatického dyneinu v jeho jednoduchém deterministickém modelu. In Studentská vědecká konference 2019 – magisterské a doktorské studijní programy, sborník rozšířených abstraktů. Plzeň: Západočeská univerzita v Plzni, 2019. s. 15-16. ISBN: 978-80-261-0867-2

3. KREJČOVÁ, M., SVĚTLÍK, P. Feedback control of myosin head. In PROCEEDINGS OF COMPUTATIONAL MECHANICS 2019. Plzeň: University of West Bohemia, 2019. s. 101-104. ISBN: 978-80-261-0889-4

4. KREJČOVÁ, M., HOLEČEK, M. Influence of Boundary Conditions on Stochastic Movement of Biological Molecular Motor. Amsterdam, Nizozemsko, 2019.

5. KREJČOVÁ, M., HOLEČEK, M., ROSENBERG, J. MYOSIN, POTENTIAL AND MOTOR?S VELOCITY. In Book of Abstracts of the 25th Congress of the European Society of Biomechanics (ESB 2019). TUVerlag, 2019. s. 593. ISBN: 978-3-903024-96-0

6. LOBOVSKÝ, L.., SALÁŠEK, M.., KREJČOVÁ, M.., MAREŠOVÁ, M.., HARTLOVÁ, J.., TUPÝ, R.., PAVELKA, T.., KŘEN, J.. Minimally invasive internal fixation techniques for management of sacral bone injuries. In 36th Danubia-Adria Symposium on Advances in Experimental Mechanics EXTENDED ABSTRACTS. 2019. s. 95-96. ISBN: 978-80-261-0876-4

7. KREJČOVÁ, M., ROSENBERG, J. Validation of the Simple Model of Cytoplasmic Dynein. In Applied Mechanics 2019 - Conference Proceedings. Ostrava: Vysoká škola báňská - Technická univerzita Ostrava, 2019. s. 103-108. ISBN: 978-80-248-4287-5

8. LOBOVSKÝ, L., HARTLOVÁ, J., SALÁŠEK, M., KREJČOVÁ, M., TUPÝ, R., PAVELKA, T., KŘEN, J. Bimechanics of pelvic ring fixation techniques. In Computational mechanics - BOOK OF EXTENDED ABSTRACTS. Plzeň: Západočeská univerzita v Plzni, Univerzitní 8, 301 00 Plzeň, 2018. s. 55-56. ISBN: 978-80-261-0819-1

9. KREJČOVÁ, M., HOLEČEK, M. Influence of boundary conditions on stochastic movement of biological molecular motors. Applied and Computational Mechanics, 2018, roč. 12, č. 2, s. 147-158. ISSN: 1802-680X

10. KREJČOVÁ, M., HOLEČEK, M. Myosin, Numerical Position Determination and Mechanical Properties. In Computational mechanics - BOOK OF EXTENDED ABSTRACTS. Plzeň: Západočeská univerzita v Plzni, 2018. s. 43-44. ISBN: 978-80-261-0819-1

11. KREJČOVÁ, M. Přechody mezi stavy myosinového molekulárního motoru. In Studentská vědecká konference 2018 - magisterské a doktorské studijní programy, sborník rozšířených abstraktů. Plzeň: Západočeská univerzita, 2018. s. 19-20. ISBN: 978-80-261-0790-3

12. ROSENBERG, J., KREJČOVÁ, M. Simple qualitative deterministic model of dynein. In Engineering Mechanics 2018, Book of Full Texts. Prague: Institute of Theoretical and Applied Mechanics AS CR, 2018. s. 717-720. ISBN: 978-80-86246-91-8 , ISSN: 1805-8248

13. KREJČOVÁ, M., HOLEČEK, M., CHEŁMINIAK, P. THE MEASUREMENT OF SINGLE MYOSIN HEAD IN FOKKER-PLANCK FRAMEWORK AND INFORMATION GAIN. In 20th International Conference Applied Mechanics 2018 Conference Proceedings. Plzeň: Západočeská univerzita, 2018. s. 63-68. ISBN: 978-80-261-0766-8

14. HOLEČEK, M., KREJČOVÁ, M. Maxwell demon, Landauer principle and stochastic processes focused on molecular motors. Adam Mickiewicz University, Poznaň, Polsko, 2017.

15. KREJČOVÁ, M., HOLEČEK, M. Myosin Motor Movement Controlled by a Potential Barrier. In Computational mechanics - EXTENDED ABSTRACTS. Plzeň: Západočeská univerzita, 2017. s. 63-64. ISBN: 978-80-261-0748-4

16. KREJČOVÁ, M., HOLEČEK, M. The Comparison of the Three State Model of Myosin II Motor in the Ensemble Theory and in the Focker-Planck Equation Framework. In Applied Mechanics 2017 Conference Proceedings. Brno: Ústav fyziky materiálů AV ČR, v.v.i., 2017. s. 53-56. ISBN: 978-80-87434-08-6

17. KREJČOVÁ, M. WPE algoritmus aplikovaný na rovnici difuze. In SVK FAV 2017 - magisterské a doktorské studijní programy, sborník rozšířených abstraktů. Plzeň: Západočeská univerzita, 2017. s. 25-26. ISBN: 978-80-261-0706-4

18. KREJČOVÁ, M. Molekulární motory: Smoluchowského rovnice a ?blikající potenciál". In SVK FAV 2016 - magisterské a doktorské studijní programy, sborník rozšířených abstraktů. Plzeň: Západočeská univerzita v Plzni, 2016. s. 37-38. ISBN: 978-80-261-0621-0

List of Symbols

$[X]$	Concentration of X, if X is a variable
α	Effective potential divided by $k_{\mathrm{B}}T$
β	Thermodynamic beta; coldness; $\beta = (k_B T)^{-1}$
$\Delta\varphi$	Difference $\varphi(x_{n+1}) - \varphi(x_n)$
ΔG	Amplitude of Fourier series
ΔG_{ab}	Gibbs energy between the initial and final states
Δx	Space step
γ	Path
γ_{drag}	Drag coefficient
$\mathcal{A}$	Starting point
$\mathcal{B}$	Ending point
$\mathcal{H}$	Hamiltonian of the system
$\mathcal{N}$	Total number of states
$\mathcal{T}$	Transposition of matrix
$\mathcal{V}$	Volume
$\mathfrak{p}$	Momentum
Ω	actual number of all possible microstates
ϕ	Effective potential
ψ	Effective force; $\dfrac{\partial V}{\partial x} - F_{Load}$
ρ	Probability density
ρ_1	Random (arbitrary) distribution
ρ_2	Random (arbitrary) distribution
ρ_e	"Measurement" error

ρ_{ana} Analytical solution of ρ

ρ_{num} Numerical solution of ρ

φ Effective potential ϕ in a given node x_n, i.e. $\varphi = \phi(x_n)$

A Arbitrary parameter

abs Absorbing

B Backward flux

C Integration constant

c_1 Integration constant

c_2 Integration constant

D Diffusion coefficient

E Energy

e_a Absolute error

E_m Myosin neck (spring) energy

E_r Energy of particles in state r

e_r Relative error

F Forward flux

f Distribution function

F_B Brownian force

F_H Helmholtz free energy

F_T Total force

F_{drag} Drag force

F_{Load} External load force

F_{spring} Force in a spring

G Free enthalpy

g Weight function

H Boltzmann H-function, Shannon entropy

H In Appendix enthalpy

J Flux

k_0 Pre-exponential factor in Arrhenius equation

k_B	Boltzmann constant
k_m	Myosin neck (spring) stiffness
L	Distance between two actin bounding sites, i.e. 36 nm
M	Matrix produced by the WPE algorithm
m	Mass
N	Total number of nodes
n	Index number of a node
n_r	Number of particles in state r
p	Probability
p^s	Stationary probability
p_m	Probability in microcanonical ensemble
Q	Heat in the system
r	Index of given particle
$refl$	Reflexing
S	Entropy
s	Given degenerated state
T	Thermodynamic temperature
t	Time variable
T_m	Temperature of m-th process of the system
U	Internal (mean) energy
V	Potential influencing movement of molecular motor
W	Work
x	Independent variable, space variable
x_e	Location of the maximal absolute error on x axis
y	Dependent variable
Z	Partition function
AAA	protein ATPases Associated with diverse cellular Activities
ADP	Adenosine diphosphate

AMD State of the actin-myosin complex – myosin in presence adenosine diphosphate is attached to the actin

AMDP State of the actin-myosin complex – myosin in presence adenosine diphosphate and free phosphorus is attached to the actin

AMT State of the actin-myosin complex – myosin in presence adenosine triphosphate is attached to the actin

APD Avalanche photodiode

ATP Adenosine triphosphate

BS Beam splitters

C Capacitor

D Dimension

Da Dalton; 1 Dalton $\equiv$ 1 Atomic mass unit

DNA Deoxyribonucleic acid

MDP State of the actin-myosin complex – myosin in presence adenosine diphosphate and free phosphorus is not attached to the actin

MT State of the actin-myosin complex – myosin in presence adenosine triphosphate is not attached to the actin

PID Proportional Integral Derivative controller

WPE Wang-Peskin-Elstone

Bibliography

[1] Abraham, Z. et al., Kinesin and dynein Mechanics: Measurement Methods and Research Applications. Journal of Biomechanical Engineering (2018), Volume 140, pp 02805-1 – 02805-11.

[2] Alamo, L. et al., Three-Dimensional Reconstruction of Tarantula Myosin Filaments How Phosphorylation Mya Regulate Myosin Activity. Journal Molecular Biology (2008), Volume 384, pp 780 – 797.

[3] Alberts, B. et al, Essential cell biology, 3rd Edition. New York, Garland Science, 2010.

[4] Alcazar J. et al., On the Shape of the Force-Velocity Relationship in Skeletal Muscles: The Linear, the Hyperbolic, and the Double-Hyperbolic. Frontiers in Physiology (2019), Volume 10, Article number 769, pp 1 – 21.

[5] Allemand, J. F, Desbiolles, P., Physics and Biology: From Molecules to Life. World Scientifc Publishing Co. Pte. Ltd., Singapore, 2015.

[6] Bartsch, H-J. Matematické vzorce. Fourth Edition, Praha: Academia, 2006. [in Czech]

[7] Belaza, A. M. et al. Statistical physics of balance theory. PLOS ONE (2017), Volume 12, Issue 8, Article number e0183696, pp 1 – 19.

[8] Bengtsson, J. et al., Supremacy of the quantum many-body Szilard engine with attractive bosons. arXiv 701.08138v1 (January 2017), pp 1 – 8.

[9] Berezhkovskii, A. M., Dagdug, L., Bezrukov, S. M. Exact Solutions for Distributions of First-Passage, Direct-Transit, and Looping Times in Symmetric Cusp Potential Barriers and Wells. The Journal of Physical chemistry B. (2019), Volume 123, Issue 17, pp 3786 – 3796.

[10] Boksenbojm, E. et al., Nonequilibrium thermodynamics at the microscale: Work relations and the second law. Physica A (2010), Volume 389, pp 4406 — 4417.

[11] Boltzmann, L., Weitere Studien über das Wärmegleichgewicht unter Gasmolekülen, Sitzungdberichte der Kaiserlichen akademie der Wissenschaften (1827), LXVI. Band, erste Abtheilung, pp 275 – 370. [in German]

[12] Braun, S. et al., Negative Absolute Temperature for Motional Degrees of Freedom. Science (2013), Volume 339, Issue 6115, pp 52 – 55.

[13] Caraglio, M. et al. The influence of absorbing boundary conditions on the transition path times statistics. Physical Chemistry Chemical Physics (2018), Volume 20, pp 25676 – 25682.

[14] Carter, A. P. et al., How dynein and dynactin transport cargos: a structural perspective. Current Opinion in Structural Biology (2016), Volume 37, pp 62 – 70.

[15] Chandler, D., Introduction to modern statistical mechanics. Oxford University Press, Oxford, 1987.

[16] Chen, J. et al., Multiscale Modeling of Skeletal Muscle Active Contraction in Relation to Mechanochemical Coupling of Molecular Motors. Micromachines (2015), Volume 6, pp 902 – 914.

[17] Chowdhury, D., Stochastic mechano-chemical kinetics of molecular motors: A multidisciplinary enterprise from a physicist's perspective. Physics Reports (2013), Volume 529, pp 1 -– 197.

[18] Coluccio, L. M., Myosins: A Superfamily of Molecular Motors. Springer, Dordrecht, 2008.

[19] Compendium of Chemical Terminology: Gold Book, Version 2.3.3, 2014-02-24, available on http:goldbook.iuoac.org/pdf/goldbook.pdf.

[20] Cottet, N. et al., Observing a quantum Maxwell demon at work. Proceedings of the National Academy of Sciences of the United States of America - PNAS (2017), Volume 114, Number 29, pp 7561 — 7564.

[21] Cover, T. M., Thomas, J. A. Elements of Information Theory, 2nd Edition. John Wiley & Sons, Inc., Hoboken, New Jersey, 2006.

[22] Debold, E. P., Patlak, J. B., Warshaw, D. M., Slip sliding away: load-dependence of velocity generated by skeletal muscle myosin molecules in the laser trap. Biophysical journal (2005), Volume 89, Issue 5, pp L34 — L36.

[23] Denisov, S.I.,Horsthemke, W., Hänggi, P., Generalized Fokker-Planck equation: Derivation and exact solutions. European Physical Journal B (2009), Volume 68, Issue 4, pp 567 – 575.

[24] Drábek, P., Holubová, G. Parciální diferenciální rovnice: úvod do klasické teorie. 1st Edition. Plzeň: Západočeská univerzita, 2001. [in Czech]

[25] Duke, T. A. J., Molecular model of muscle contraction. Proceedings of the National Academy of Sciences of the United States of America (1999), Volume 96, Issue 6, pp 2770 – 2775.

[26] Edman, K. A. Double-hyperbolic force-velocity relation in frog muscle fibres. The Journal of Physiology (1988), Volume 404, pp 301 – 321.

[27] Erdmann, T., Schwarz, U. S., Stochastic Force Generation by Small Ensembles of Myosin II Motors. Physical Review Letters (2012), Volume 108, Article number 188101, pp 188101-1 – 188101-5.

[28] Evans, D. J., Cohen, E. G. D., Morriss, G. P., Probability of second law violations in shearing steady states. Physical Review Letters (1993), Volume 71, Issue 15, pp 2401 – 2404.

[29] Fall, Ch. P., Computational cell biology. Springer-Verlag, New York, 2002.

[30] Finer, J. T., Simmons, R. M., Spudic, J. A. Single Myosin Molecule Mechanics – Piconewton Forces and Nanometer Steps. Nature (1994), Volume 368, pp 113 – 119.

[31] Frank, H., Fiala, J., Kraus, I. , Elektronová struktura a reaktivita povrchů a rozhraní. Praha, České vysoké učení v Praze, 2013. [in Czech]

[32] Frenkel, D., Smit, B., Understanding Molecular Simulation – From Algorithms to Applications. Academic Press, 2012.

[33] Gallavotti, G., Cohen E. G. D., Dynamical ensembles in Nonequilibrium Statistical Mechanics. Physical Review Letters (1995), Volume 74, Issue 14, pp 2694 – 2697.

[34] Gennerich, A., Vale, R. D., Walking the walk: how kinesin and dynein coordinate their steps. Current Opinion in Cell Biology (2009), Volume 21, pp 59 – 67.

[35] Guo, P. et al., Biological Nanomotors with a Revolution, Linear, or Rotation Motion Mechanism. American Society for Microbiology, Microbiology and Molecular Biology Reviews (2016), Volume 80, Number 1, pp 161 – 186.

[36] Harris, R. J., Schütz, G. M., Fluctuation theorems for stochastic dynamics. Journal of Statistical Mechanics: Theory and Experiment (2007), Volume P07020, pp 1 – 45.

[37] Heissler, S. M., Sellers, J. R., Various Themes of Myosin Regulation. Journal Molecular Biology (2016), Volume 428, pp 1927 – 1946.

[38] Hesam, S., Nazemi, A. R., Haghbin, A., Analytical solution for the Fokker-Planck equation by differential transform method. Scientia Iranica B (2012), Volume 19, Issue 4, pp 1140 – 1145.

[39] Hill, T. L., Theoretical Formalism for the Sliding Filament Model of contraction of Striated Muscle. Part I. Progress in Biophysics and Molecular Biology (1974), Volume 28, pp 267 – 340.

[40] Hill, T. L., Theoretical Formalism for the Sliding Filament Model of contraction of Striated Muscle. Part II. Progress in Biophysics and Molecular Biology (1975), Volume 29, pp 105 – 159.

[41] Hoffmann, P. M., How Molecular Motors Extract Order from Chaos (a key issue review). Reports on Progress in Physics (2016), Volume 79, Article number 032601, pp 1 – 15.

[42] Horowitz, J. M., Sagawa, T., Parrondo, J. M. R, Imitating Chemical Motors with Optimal Information Motors. Physical Review Letters (2013), Volume 111, Article number 010602, pp 010602-1 – 010602-5.

[43] Horowitz, J., Jarzynski, C., Comparison of work fluctuation relations. Journal of Statistical Mechanics: Theory and Experiment (2007), Issue P11002, pp 1 – 14.

[44] Howard, J., Mechanics of Motor Protein and the Cytoskeleton. Sinauer Associates, Inc., Sunderland, Massachusetts, 2018.

[45] Huxley, A. F., Muscle Structure and Theories of contraction. Progress in Biophysics and Biophysical Chemistry (1957), Volume 7, pp 255 – 318.

[46] Ito, S., Sagawa, T. Maxwell's demon in biochemical signal transduction with feedback loop. Nature Communications (2015), Volume 6, Article number 7498, pp 1 – 6.

[47] Ivanitskii, G. R., 21st century: what is life from the perspective of physics?. Physics – Uspekhi (2010), Volume 53, Number 4, pp 327 — 356.

[48] Jarzynski, C., A nonequilibrium equality for free energy differences. Physical Review Letters (1997), Volume 78, Issue 14, pp 2690 – 2693.

[49] Jarzynski, C., Equalities and Inequalities: Irreversibility and the Second Law of Thermodynamics at the Nanoscale. Annual Review Condensed Matter Physics (2011), Volume 2, pp 329 -– 351.

[50] Jarzynski, C., Equilibrium free energy differences from nonequilibrium measurements: a master equation approach. Physical Review E (1997), Volume 56, Issue 5, pp 5018 – 5035.

[51] Jarzynski, C., Nonequilibrium work relations: foundations and applications. European Physical Journal B (2008), Volume 64, pp 331 -– 340.

[52] Ji, S. Molecular Theory of the Living Cell: Concepts, Molecular Mechanism, and Biomedical Applications. Springer-Verlag, New York, 2012.

[53] Johnson, C. M., Investigating the Slow Axonal Transport of Neurofilaments: A Precursor for Optimal Neuronal Signaling, PhD. thesis. Ohio University, 2016.

[54] Jost, J. Postmodern Analysis. 3rd Edition. Springer-Verlag Berlin Heidelberg, 2005.

[55] King, S., M., Dyneins: Structure, Biology and Disease. Academic Press, 2012.

[56] Kinoshita, Y. et al., Step Size and Rate Constants of Single-headed Cytoplasmic Dynein Measured with Optical Tweezers. Scientific Reports (2018), Volume 8, pp 16333-1 – 16333-14.

[57] Kitamura, K. et al., A Single Myosin Head Moves Along an Actin Filament with Regular Steps of 5.3 Nanometers. Nature (19977), Volume 397, pp 129 – 134.

[58] Kitamura, K. et al., Mechanism of Muscle contraction based on stochastic Properties of Single Actomyosin Motors Observed in Vitro. Biophysics (2005), Volume 1, pp 1 – 19.

[59] Kittel, C., Kroemer, H., Thermal Physics (2nd edition). W. H. Freeman and Company, United State of America, 1980.

[60] Kolomeisky, A. B., Motor proteins and molecular motors: how to operate machines at the nanoscale. Journal of Physics: Condensed Matter (2013), Volume 25, Article number 463101, pp 1 – 13.

[61] Kondepudi, D., Introduction to modern thermodynamics. Wiley, Chichester, 2008.

[62] Koski, J. V. et al., Experimental Observation of the Role of Mutual Information in the Nonequilibrium Dynamics of a Maxwell Demon. Physical Review Letters (2014), Volume 113, Article number 030601, pp 1 – 5.

[63] Kullback, S. Information Theory and Statistics. Dover Publication, Inc., United States of America, 1978.

[64] Kurzynski, M., Chelminiak, P., Do biological molecular machines act as Maxwell's demons?. Preprint submitted to Elsevier, version 7 (February 6, 2017).

[65] Kurzynski, M., Chelminiak, P., Information processing in biological molecularmachines. arXiv:1707.07496v2 [physics.bio-ph], cit: 14th January 2020.

[66] Kurzynski, M., Torchala, M., Chelminiak, P. "Output-Input Ratio in Thermally Fluctuating Biomolecular Machines." Physical Review E (2014), Volume 89, Article number 012722, pp 1 – 12.

[67] Kutvonen, A. et al., Thermodynamics and efficiency of an autonomous on-chip Maxwell's demon. Scientific Reports (2016), Volume 6, Article number 21126, pp 1 – 7.

[68] Kyle, B. G., ENTROPY: Reflections of a Classical Thermodynamicist. Kansas State University [cit. 31th July 2019]. Available on https:www.che.ksu.edupeopleemerituskyle

[69] Lan, G., Sun, S. X, Dynamics of Myosin-Driven Skeletal Muscle Contraction: I. Steady-State Force Generation. Biophysical Journal (2005), Volume 88, pp 4107 – 4117.

[70] Landauer, R. Information is Physical, Physics Today (1991), Volume 44, Issue 5, pp 23 – 29.

[71] Lee, C. S., Gonzalez, V. R., Fuzzy logic versus a PID controller for position control of a muscle-like actuated arm. Journal of Mechanical Science and Technology (2008), Volume 22, pp 1475 – 1482.

[72] Leff, H. S., Rex, A. F., Maxwell's demon 2: Entropy, Classical and Quantum Information. Computing, Institute of Physics Publishing Bristol and Philadelphia, 2003.

[73] Lestas, I., Vinnicombe, G., Paulsson, J. Fundamental limits on the suppression of molecular fluctuations. Nature (2010), Volume 467, pp 174 -– 178.

[74] Lewis, G. N., Randall, M., Thermodynamics and The Free Energy of Chemical Substances. McGraw-Hill Book Company, Inc., New York and London, 1923.

[75] Li, L., Alper, J., Alexov, E., Cytoplasmic dynein binding, run length, and velocity are guided by long-range electrostatic interactions. Scientific reports (2016), Volume 6, pp 31523-1 – 31523-12.

[76] Lin, J. et al., Structural mechanism of the dynein powerstroke. Nature Cell Biology (2014), Volume 16, pp 479 – 485.

[77] Lipowsky, R., Klumpp, S., 'Life is motion': multiscale motility of molecular motors. Physica A (2005), Volume 352, pp 53 – 112.

[78] Lodish, H. et al., Molecular cell biology, Eight edition. W. H. Freeman, Macmmillan Learning, New York, 2016.

[79] Lu, W., Gelfand, V. I., Moonlighting Motors: Kinesine, Dynein, and Cell Polarity. Trends in Cell Biology (2017), Volume 27, Number 7, pp 505 – 514.

[80] Lutz, E., Ciliberto, S. Information: From Maxwell's demon to Landauer's eraser. Physics Today (2015), Volume 68, Issue 9, pp 30 – 35.

[81] Maggio, C.D. et al. A Modified Hai–Murphy Model of Uterine Smooth Muscle Contraction. Bulletin of Mathematical Biology 74 (2012), pp 143–158.

[82] Magnasco, M. O., Forced thermal ratchets. Physical Review Letters (1993), Volume 71, pp 1477 – 1481.

[83] Mandal, D., Jarzynski, C., Work and information processing in a solvable model of Maxwell's demon. Proceedings of the National Academy of Sciences Jul (2012), Volume 109, Issue 29, pp 11641 – 11645.

[84] Maršík, F., Dvořák, I., Biotermodynamika, 2nd Edition. Praha, Academia, 1998. [in Czech]

[85] Marenduzzo, D., Working with the Langevin and Fokker-Planck equations [online]. University of Edinburg. [cit. 26th November 2019]

[86] Maxwell, J. M., Theory of heat. Longmans, Green and Co., London, 1872.

[87] McClare, C. W. F., Chemical Machines, Maxwell's demon and Living Organisms. Journal of Theoretical Biology (1971), Volume 30, pp 1 – 34.

[88] Moores, C. A., Milligan, R. A., Lucky 13 – microtubule depolymerisation by kinesin-13 motors. Journal of Cell Science (2006), Volume 119, pp 3905 – 3913.

[89] Motl, L., Zahradník, M. Pěstujeme lineární algebru. Praha, Matematicko-fysikální fakulta UK, 1994. [in Czech]

[90] Nyquist, H., Certain factors affecting telegraph speed. Journal of the American Institute of Electrical Engineers (1924), Volume 43, Issue 2, pp 124 – 130.

[91] O'Connell, C. B., Tyska, M. J., Mooseker, M. S., Myosin at work: Motor adaptations for a variety of cellular functions. Biochimica at Biophysica Acta (2007), Volume 1773, pp 615 – 630.

[92] Oiwa, K., Chaen, S., Kamitsubo, E., Shimmen, T. and Sugi, H. Steady-state force fibres. The Journal of Physiology (1988), Volume 404, pp 301 – 321.

[93] Parondo, J. M. R., Horowitz, J. M., Sagawa, T., Thermodynamics of information. Nature Physics (2015), Volume 11, pp 131 – 139.

[94] Pathria, R. K., Beale P. D., Statistical Mechanics – 3rd Edition. Elsevier, Oxford, 2011.

[95] Pavelka, M., Klika, V., Grmela, M. Multiscale Thermo-Dynamics. Walter de Gruyterm Berlin, Boston, 2018.

[96] Pikin, S., Haase, W., Physics of the ATPas Molecular Motor. Journal of Experimental and Theoretical Physics (2001), Volume 92, Number 1, pp. 174 -– 178.

[97] Plastino, A., Rocca, M. C., Hypergeometric foundations of Fokker-Planck like equations. Physics Letters A (2016), Volume 380, pp 1900 – 1903.

[98] Puglisi, A., Sarracino, A., Vulpiani, A., Temperature in and out of equilibrium: A review of concepts, tools and attempts. Physics Reports (2017), Volume 709–710, pp 1 — 60.

[99] Qian, H., The Mathematical Theory of Molecular Motor Movement and Chemomechanical Energy Transduction. Journal of Mathematical Chemistry (2000), Volume 27, Issue 3, pp 219 – 234.

[100] Rai, A. K. et al., Molecular Adaptations Allow Dynein to Generate Large Collective Forces inside Cells. Cell (2013), Volume 152, pp 172 — 182.

[101] Rayment, I. et al., Structure of the Actin-Myosin Complex and Its Implications for Muscle Contraction. Science (1993), Volume 261, pp 58 – 65.

[102] Reimann, P., Brownian motors: noisy transport far from equilibrium. Physics Reports (2002), Volume 361, pp 557 – 268.

[103] Rex, A., Maxwell's Demon - A Historical Review. Entropy (2017), Volume 19, Issue 6, pp 1 – 13.

[104] Richards, T. A., Cavalier-Smith, T., Myosin Domain Evolution and the Primary Divergence of Eukaryotes. Nature (2005), Volume 436, pp 1113 -– 1118.

[105] Roberts, A. J., Emerging mechanisms of dynein transport in the cytoplasm versus the cilium. Biochemical Society Transactions (2018), Volume 46, pp 967 – 982.

[106] Rosenberg, J., Teoretická mechanika. 2nd Edition. Plzeň, Západočeská univerzita, 2003. [in Czech]

[107] Rosenberg, J., Liška, V., Experimentální chirurgie – nové technologie v medicíně – II. díl: Biomechanika. Univerzita Karlova v Praze, Lékařská fakulta v Plzni, Plzeň, 2013. [in Czech]

[108] Ross, S. M., Introduction to Probability and Statistics for Engineers and Scientists, 3rd edition. Academic Press, Amsterdam, 2004.

[109] Rouhani, H. et al., PID Controller Design for FES Applied to Ankle Muscles in Neuroprosthesis for Standing Balance. Frontier in Neuroscience (2017), Volume 11, Article number 347, pp 1 – 14.

[110] Sagawa, T., Ueda, M., Generalized Jarzynski Equality under Nonequilibrium Feedback Control. Physical Review Letters (2010), Volume 104, Article number 090602, pp 1 – 4.

[111] Sagawa, T., Ueda, M., Nonequilibrium thermodynamics of feedback control. Physical Review E (2012) , Volume 85, Article number 021104, pp 1 – 16.

[112] Sagawa, T., Ueda, M., Role of mutual information in entropy production under information exchanges. New Journal of Physics (2013), Volume 15, Article number 125012, pp 1 – 23.

[113] Sagawa, T., Ueda, M., Second Law of Thermodynamics with Discrete Quantum Feedback Control. Physical Review Letters (2008), Volume 100, Article number 080403, pp 1 – 4.

[114] Sekimoto, K., Stochastic Energetics, Lecture Notes in Physics. Springer, Berlin Heidelberg, 2010.

[115] Serhan, H. J., Nasr, C. G., Henaff, P., Designing a Muscle like System Based on PID Controller and Tuned by Neural Network. International Joint Conference on Neural Networks (2006), Vancouver, BC, Canada.

[116] Sugi, H. et al., Enhancement of Force Generated by Individual Myosin Heads in Skinned Rabbit Psoas Muscle Fibers at Low Ionic Strength. PLoS ONE (2013), Volume 8, Issue 5, e63658.

[117] Sugi, H., Chaen, S., Review: Force–velocity relationships in actin–myosin interactions causing cytoplasmic streaming in algal cells. The Journal of Experimental Biology (2003), Volume 206, pp 1971 – 1976.

[118] Sun, X. et al., Derivation of Fokker-Planck equations for stochastic systems under excitation of multiplicative non-Gaussian white noise. Journal of Mathematical Analysis and Applications (2017), Volume 446, pp 786 – 800.

[119] Tůma, F., Automatické řízení 1 – Lineární spojité dynamické systémy. 2nd Edition. Plzeň, Západočeská univerzita v Plzni, 2003. [in Czech]

[120] Tessarotto, M., Cremaschini, C., Role of Quantum Entropy and Establishment of H-Theorems in the Presence of Graviton Sinks for Manifestly-Covariant Quantum Gravity. Entropy (2019), Volume 21, Issue 418, pp 1 – 25.

[121] The Nobel Foundation, All Nobel Prizes in Chemistry [online]. Stockholm [cit. 29th May 2019]. Available from https:www.nobelprize.orgprizeslistsall-nobel-prizes-in-chemistry.

[122] The Nobel Foundation, The Nobel Prize in Chemistry 2016 – popular science background. How molecules became machines. The Royal Swedish Academy of Sciences, 2016. [cit. 29th May 2019].

[123] The Nobel Foundation, The Nobel Prize in Chemistry 2016 – popular science background. They captured life in atomic detail. The Royal Swedish Academy of Sciences, 2017. [cit. 29th May 2019].

[124] The Nobel Foundation, The Nobel Prize in Chemistry 2017. NobelPrize.org. Nobel Media AB 2019. [cit. 17th July 2019].

[125] Thomson, W., On the Dynamical Theory of Hear, with numerical results deduces from Mr Joule's Equivalent of a Thermal Unit, and M. Regnault's Observation on Steam. Transactions of the Royal Society of Edinburgh (1853), Volume 20, pp 261 – 288.

[126] Toba, S. et al., Overlapping hand-over-hand mechanism of single molecular motility of cytoplasmic dynein. Proceedings of the National Academy of Sciences (2006), Volume 103, pp 5741 – 5745.

[127] Vidrighin, M. D. et al., Photonic Maxwell's Demon. Physical Review Letters (2016), Volume 116, Article number 050401, 1 – 7.

[128] Vilfan, A., Duke, T., Instabilities in the Transient Response of Muscle. Biophysical Journal (2003), Volume 85, pp 818 – 827.

[129] Volkenstein, M. V., Entropy and Information. Birkhäuser Verlag AG, Basel, 2009.

[130] Waite, G. N., Wait, L. R., Applied Cell and Molecular Biology for ENGINEERS. The McGraw-Hill Companies, Inc., USA, 2007.

[131] Wang, H., Convergence of Numerical Method for Solving Discontinuous Fokker-Planck equations. SIAM Journal on Numerical Analysis (2007), Volume 45, Issue 4, pp 1425 -– 1452.

[132] Wang, H., Peskin, C. S.m Elston, T. C., A robust Numerical algorithm for Studying Biomolecular Transport Processes. Journal theoretical Biology (2003), Volume 221, pp 491 – 511.

[133] Wang, H., Several Issues in Modeling Molecular Motors. Journal of Computational and Theoretical Nanoscience (2008), Volume 5, pp 1 – 35.

[134] Wang, Y., Generalized Fokker-Planck equation with generalized interval probability. Mechanical Systems and Signal Processing (2013), Volume 37, pp 92 – 104.

[135] Yang, S. et al., An Approach to Improve the Resolution of Helical Filaments with a Large Axial Rise and Flexible Subunits. Journal of Structural Biology (2016), Volume 193, Issue 1, pp 45 -– 54.

[136] Yin, Y., Guo, Z., Collective mechanism of molecular motors and a dynamic mechanical model for sarcomere. Science China – Technological Sciences (2011), Volume 54, Issue 8, pp 2130 – 2137.

[137] Zimmermann, E., Dynamics and thermodynamics of molecular motor-cargo systems, PhD. thesis. II. Institut für Theoretische Physik der Universität Stuttgart, 2015.

[138] Åström, K.J., Hägglund, T., The future of PID control. International Federation of Automatic Control Proceedings (2000), Volume 33, Issue 4, pp 19 – 30.

[139] Čibera, V., Three filament cross-bridge model of sarcomere. Plzeň, 2016. Dissertation thesis (Ph.D.). University of West Bohemia in Pilsen, Faculty of Applied Sciences.

[140] Štoll, I., Tolar, J., Jex, I. Klasická teoretická fyzika, 1st Edition. Praha, Karolinum Press, 2017. [in Czech]

[141] Štulajter, F., Odhady v náhodných procesoch. Alfa, Bratislava 1990. [in Slovakian]

[142] Čulík, F., Nooga, M., Úvod do štatistickej fyziky a termodynamiky, 1st Edition. Alfa Bratislava, 1982. [in Slovakian]

Part VI

Appendix

Appendix A

Termodynamic potentials

A.1 Entropy

The most complex parameter in thermodynamics is for sure the system entropy S. It is defined by the second law of thermodynamics [142] as follows

1. S is single-valued function of the system state
2. S is additive
3. The entropy differential $\mathrm{d}S$ has to obey relationship

$$\mathrm{d}S \geq \frac{\delta Q}{T}, \tag{A.1}$$

where δQ is the received heat to the system. The sign of equality is applied only for reversible processes. For a thermally insulated system, $\delta Q = 0$,

$$\mathrm{d}S \geq 0. \tag{A.2}$$

So the entropy of an insulated system cannot decrease. It increases at irreversible processes and it is a constant at reversible processes.

In statistical physics, the entropy is usually expressed by the Boltzmann formula

$$S = -k_B \log \Omega, \tag{A.3}$$

where Ω is the actual number of all possible microstates and k_B is Boltzmann constant. Although the formula carries Boltzmann's name, the first one who derivated it was Planck [94].

There is also one important relationship for the entropy. It is

$$S = -k_B \langle \log p \rangle. \tag{A.4}$$

About its importance is written in [94]: "It shows that the entropy of a physical system is solely and completely determined by the probability value p." It is also a good relation to a derivation of the other thermodynamic potentials.

A.2 Internal energy

In the statistical equilibrium point of view is the internal energy U the same as the mean energy of the system $\langle E \rangle$. It means the internal energy can be evaluated in relation to expected value (see equation (3.11)), i.e.

$$U = \langle E \rangle = Z^{-1} \sum_r E_r \exp(-\beta E_r). \tag{A.5}$$

This can be also simply modified to receive the internal energy directly from the partition function

$$U = -\frac{\partial}{\partial \beta} \ln Z. \tag{A.6}$$

A.3 Enthalpy

If volume $\mathcal{V}$ is a constant during a process, it is useful to define a kind of energy called the enthalpy H as

$$H = U + P\mathcal{V}, \tag{A.7}$$

where P is a pressure. In that case, a differential of enthalpy $\mathrm{d}H$ is equal to an amount of a received heat δQ.

This thermodynamic potential cannot be simply (and generally) expressed by the partition function. The term PV is dependent on a state equation, but it has to be determined according to which one of the system behaves, i.e. the ideal gas state equation, the van der Waals equation and so on.

A.4 Helmholtz free energy

The work made by external forces during an isothermal reversible process is the Helmholtz free energy F_H defined in thermodynamics as

$$F_H = U - TS, \tag{A.8}$$

which can be rewritten with help of equations (A.4) and (A.6) to a statistical relation

$$F_H = -k_B T \ln Z. \tag{A.9}$$

A.5 Free enthalpy

As the name suggests, it has something in common with the Helmholtz free energy and with the enthalpy. It is very simply shown by its definition

$$G = H - TS, \tag{A.10}$$

where G is free enthalpy. It is formally the same relation as equation (A.8).

The Free enthalpy, also known as the Gibbs potential, cannot be rewritten in a statistical mean due to its dependency to the enthalpy, see above to section A.3.

Appendix B

Balance

Balance is used in many fields. Here, it is important for a better understanding of algorithms which are used in statistical physics. However, the concept of balance is used even for studying social behaviour. Such an example serves article [7]. They use the balance for studying alliances in online computer games and compare it with the real political network during the cold war.

The definition of balance between two nodes is intuitive – what is going from one node to the second one must be equal to the amount going from the second node to the first one.

This fact can be extended for a system with three nodes. The flux among these nodes going "clockwise" must be equal to "anti-clockwise" flux.

Moreover, if the balance can be found between every pair of nodes, the system is in detailed balance [32]. This condition is very important in molecular dynamics, especially, in Monte Carlo simulations. In this model, there is a used algorithm (the WPE algorithm, see Chapter 6) which holds the condition of the detail balance [132].

The mathematical definition of the detail balance is as follows

$$\frac{k_{j\to j+1}(x)}{k_{j+1\to j}} = \exp\left(\frac{G_j(x) - G_{j+1}(x)}{k_B T}\right), \quad 1 \le j \le N-1 \tag{B.1}$$

$$\frac{k_{N\to 1}(x)}{k_{1\to N}} = \exp\left(\frac{G_N(x) - (G_1(x) + \Delta G)}{k_B T}\right), \quad j = N\,. \tag{B.2}$$

The property of fulfilling detail balance is very important for systems in thermodynamic equilibrium. If this condition is not obeyed in the algorithm itself, it produces artificial velocities [132].

Conditions of detailed balance are similar to conditions which constrain transition rates for molecular motors [133].

In Ref. [66], the detail balance is disobeyed.

Appendix C

Potentials

In this thesis, 6 different potentials are used as an input parameters to the model. They are described in Table 11.1. However, sometimes it is more useful to see graphs instead of mathematical formulas. Each section in this chapter contains a graph and its formula. The shortcut FS still refers to

$$FS(\Delta G, x) = \Delta G \left(\sin \frac{2\pi x}{L} - 0.5 \sin \frac{4\pi x}{L} + 0.3 \sin \frac{6\pi x}{L} \right) , \tag{11.3}$$

C.1 Case 1

This case is generated by zero function for the unbound state, $FS(\Delta G, x)$ for the weakly-bound state and by $FS(-\Delta G, x)$ for the post-power stroke state.

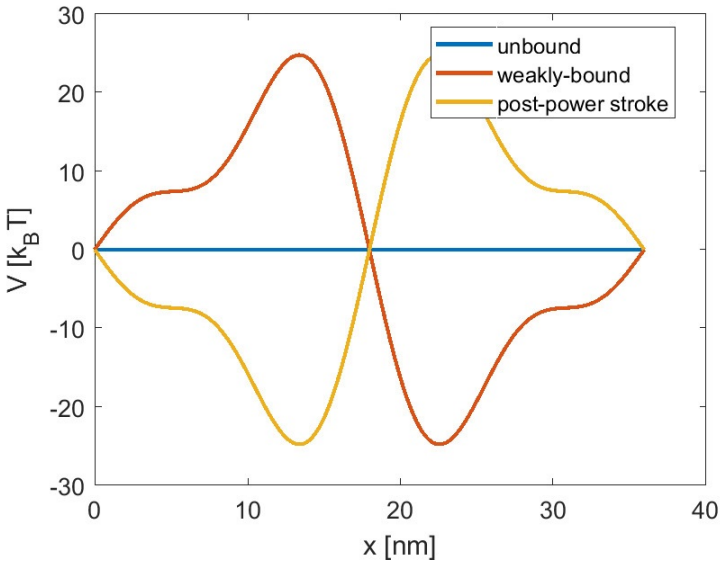

Figure C.1: Case 1

C.2 Case 2

This case is generated by E_m for the unbound state, $FS(\Delta G, x) + E_m$ for the weakly-bound state and by $FS(-\Delta G, x) + E_m$ for the post-power stroke state.

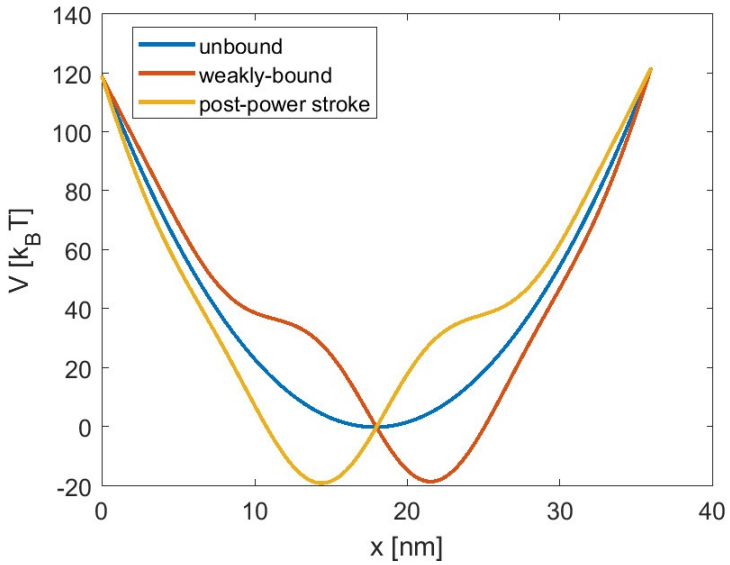

Figure C.2: Case 2

C.3 Case 3

This case is generated by zero function for the unbound state, $FS(\Delta G, x) + E_m$ for the weakly-bound state and by $FS(-\Delta G, x) + E_m$ for the post-power stroke state.

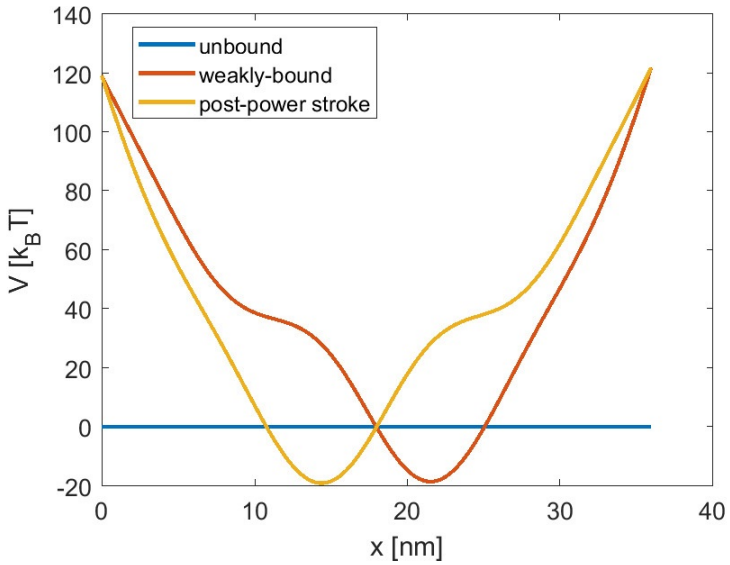

Figure C.3: Case 3

C.4 Case 4

This case is generated by zero function for the unbound state, $FS(\Delta G, x)$ for the weakly-bound state and by $FS(\Delta G, x + d)$ for the post-power stroke state.

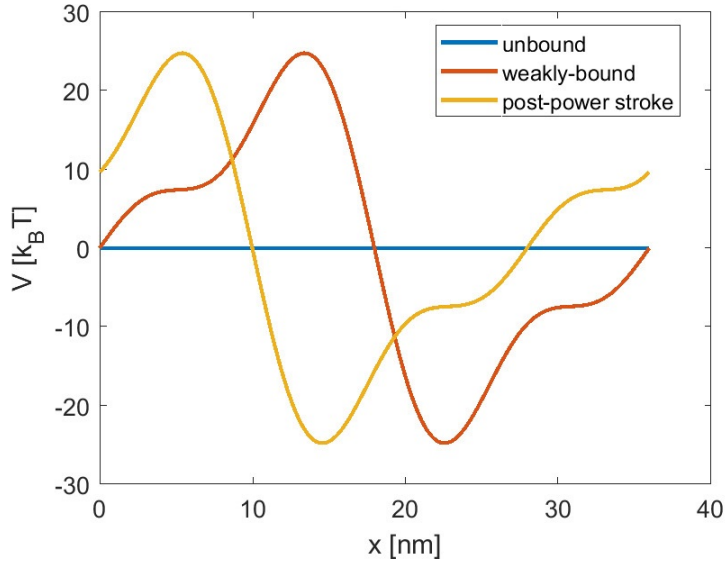

Figure C.4: Case 3

C.5 Case 5

This case is generated by E_m for the unbound state, $FS(\Delta G, x) + E_m$ for the weakly-bound state and by $FS(\Delta G, x + d) + E_m$ for the post-power stroke state.

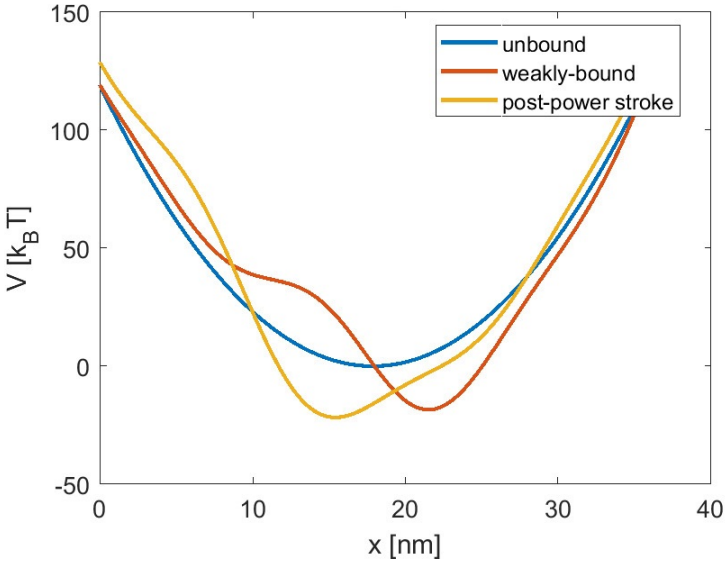

Figure C.5: Case 5

C.6 Case 6

This case is generated by zero function for the unbound state, $FS(\Delta G, x) + E_m$ for the weakly-bound state and by $FS(\Delta G, x + d) + E_m$ for the post-power stroke state.

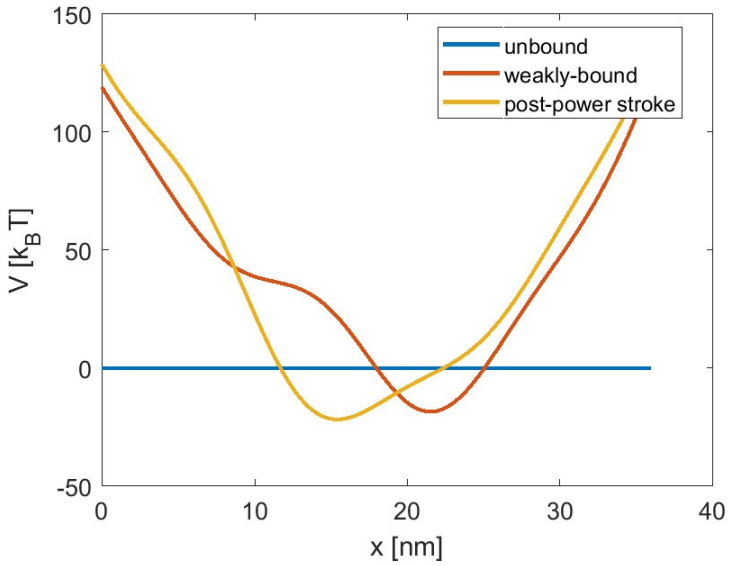

Figure C.6: Case 6